

The metallicity signature of evolved stars with planets ★,★☆

J. Maldonado¹, E. Villaver¹, and C. Eiroa¹

Universidad Autónoma de Madrid, Dpto. Física Teórica, Módulo 15, Facultad de Ciencias, Campus de Cantoblanco, E-28049 Madrid, Spain

Received 11 January 2013; accepted 12 March 2013

ABSTRACT

Aims. We aim to test whether the well established correlation between the metallicity of the star and the presence of giant planets found for main sequence stars still holds for the evolved and generally more massive giant and subgiant stars. Although several attempts have been made so far, the results are not conclusive since they are based on small or inhomogeneous samples.

Methods. We determine in a homogeneous way the metallicity and individual abundances of a large sample of evolved stars, with and without known planetary companions, and discuss their metallicity distribution and trends. Our methodology is based on the analysis of high-resolution échelle spectra ($R \geq 67000$) from 2-3 meter class telescopes.

Results. The metallicity distributions show that giant stars hosting planets are not preferentially metal-rich having similar abundance patterns to giant stars without known planetary companions. We have found, however, a very strong relation between the metallicity distribution and the stellar mass within this sample. We show that the less massive giant stars with planets ($M \leq 1.5 M_{\odot}$) are not metal rich, but, the metallicity of the sample of massive ($M > 1.5 M_{\odot}$), young (age < 2 Gyr) giant stars with planets is higher than that of a similar sample of stars without planets. Regarding other chemical elements, giant stars with and without planets in the mass domain $M \leq 1.5 M_{\odot}$ show similar abundance patterns. However, planet and non-planet hosts with masses $M > 1.5 M_{\odot}$ show differences in the abundances of some elements, specially Na, Co, and Ni. In addition, we find the sample of subgiant stars with planets to be metal rich showing similar metallicities to main-sequence planet hosts.

Conclusions. The fact that giant planet hosts in the mass domain $M_{\star} \leq 1.5 M_{\odot}$ do not show metal-enrichment is difficult to explain. Given that these stars have similar stellar parameters to subgiants and main-sequence planet hosts, the lack of the metal-rich signature in low-mass giants could be explained if originated from a pollution scenario in the main sequence that gets erased as the star become fully convective. However, there is no physical reason why it should play a role for giants with masses $M_{\star} \leq 1.5 M_{\odot}$ but is not observed for giants with $M_{\star} > 1.5 M_{\odot}$.

Key words. techniques: spectroscopic - stars: abundances -stars: late-type -stars: planetary systems

1. Introduction

Understanding the origin and evolution of planets and planetary systems is one of the major goals of modern Astrophysics. Twenty years after the discovery of the first exoplanets (Wolszczan & Frail 1992; Mayor & Queloz 1995), we are still far from understanding which stellar properties influence (and how) planet formation the most. Excluding the well established correlation between the stellar metallicity and the probability that the star hosts a gas-giant planet (e.g. Santos et al. 2004; Fischer & Valenti 2005), any other claim of a chemical trend in planet hosting stars has been so far disputed. For instance, the evidence of a higher depletion of lithium in planet host stars has been the subject of an intense discussion (e.g. Israeli et al. 2009; Baumann et al. 2010; Ghezzi et al. 2010c; Sousa et al. 2010, and references therein), as well as whether stars with planets (specially solar analogs) show or not different trends on the abundance-condensation temperature (see Ramírez et al.

2010; González Hernández et al. 2010, 2013; Gonzalez 2011; Schuler et al. 2011, and references therein).

The planet-metallicity correlation itself has revealed to be more complex than initially thought, as stars with orbiting low-mass planets ($M_p \sin i < 30 M_{\oplus}$) do not seem to be preferentially metal rich (Ghezzi et al. 2010b; Mayor et al. 2011; Sousa et al. 2011, and references therein). This observational result explained within the framework of core-accretion models (e.g. Pollack et al. 1996; Rice & Armitage 2003; Alibert et al. 2004; Mordasini et al. 2012), assumes that the timescale needed to form an icy/rocky core is largely dependent on the metal content of the protostellar cloud. In this way, in low-metal environments, the gas has already been depleted from the disc by the time the cores are massive enough to start a runaway accretion of gas and, therefore, only low-mass planets can be formed. The metallicity patterns found in stars hosting dusty debris discs also agree with the predictions of this scenario of planet formation (see Maldonado et al. 2012, and references therein).

Observations of solar-type (FGK dwarfs) Main Sequence (MS) planet hosts point towards a metal rich nature of the MS stars throughout their interiors, and therefore, to a primordial nature of the metallicity enhancement (e.g. Santos et al. 2004; Fischer & Valenti 2005). Alternative scenarios in which the metal enhancement results from the late-stage accretion of H and He-depleted material onto the convective zone of the star (Gonzalez 1997; Laughlin & Adams 1997) were rapidly ruled-out. With our current understanding, and given its primordial

Send offprint requests to: J. Maldonado
e-mail: jesus.maldonado@uam.es

* Based on observations made with the Mercator Telescope, operated on the island of La Palma by the Flemish Community; and observations made with the Nordic Optical Telescope, operated on the island of La Palma jointly by Denmark, Finland, Iceland, Norway, and Sweden.

** Tables 2, 3, 5, and 7 are only available in the electronic version of the paper or at the CDS via anonymous ftp to cdsarc.u-strasbg.fr (130.79.128.5) or via <http://cdsweb.u-strasbg.fr/cgi-bin/qcat?J/A+A/>

nature, the observed correlation between the metallicity of the star and the presence of planets should also hold for Red Giants and Subgiant stars that, having left the MS when they exhaust the hydrogen in the core, have larger radii, cooler photospheres, and are convective for the most part.

The opportunity of testing how well-founded the planet-metallicity relation is with a statistically sound sample of evolved stars, has become possible recently provided by the large number of planets found by the different successful surveys. Some examples include the Lick K-giant Survey (Frink et al. 2002), the Okayama Planet Search (Sato et al. 2003), the Retired A stars and Their Companions (Johnson et al. 2007), or the Pennsylvania-Toruń Planet Search (Niedzielski et al. 2007).

The first conclusions regarding the metallicity of giant stars hosting planets were based on the analysis of small or inhomogeneous samples obtained from the different surveys available: Sadakane et al. (2005, with 4 planet-hosting stars analyzed), Schuler et al. (2005, 1 star), Pasquini et al. (2007, 10 stars). These studies suggested that, unlike their MS counterparts, G and K giants stars with planets do not have a tendency to show metal-enrichment. An attempt to expand the sample size, setting stellar metallicities from the literature in a common spectroscopic scale, is made by Hekker & Meléndez (2007, with a total of 20 planet hosts analyzed) where they find evidence that the giant planet metallicity correlation might also hold for giants stars. More recently, studies based on the analysis of high-resolution spectra, Takeda et al. (2008, 10 stars), and Ghezzi et al. (16 stars, 2010a), point again towards a lack of a planet-metallicity relation for giant stars. This latter study also included 15 subgiants with planets which are found to have, on average, the same metallicity distribution that a sample of dwarf stars with planets.

Evidence that subgiant stars with planets might follow the planet-metallicity correlation were previously reported by Fischer & Valenti (2005) who analyzed 9 subgiant stars with planets from a total of 1040 stars observed as part of the California & Carnegie, and the Anglo-Australian planet search projects. The metallicity distribution of the planet-host subgiant stars appeared to be consistent with that of MS stars with planets, being more metal-rich than their counterparts without detected planets. A recent analysis of the California Planet Survey targets is presented in Johnson et al. (2010) who analyzed a sample of 1266 stars including a broad range of stellar masses, from late-K and M stars to subgiants with masses up to $1.9 M_{\odot}$. The authors found evidence of a planet-metallicity correlation for all stellar masses, even when the sample was restricted to subgiant stars with masses in the range $M_{\star} > 1.4 M_{\odot}$ (including 36 planet hosts). The occurrence of gas-giant planets was found to be not only dependent on the stellar metallicity, but it also scales with the stellar mass (see also Johnson et al. 2011).

Several explanations have been put forward to explain the observed metallicity distribution of giant planet hosts. For instance, that planets around intermediate-mass stars are formed preferentially by instabilities, and thus are not dependent on the metallicity of the primordial disk (see discussion in Pasquini et al. 2007), or by late-stage accretion of depleted material onto the convective zone of the star (Gonzalez 1997; Laughlin & Adams 1997). Moreover, recent simulations of planet population synthesis (Alibert et al. 2011; Mordasini et al. 2012) based on the core-accretion model of planet formation, have shown that the stellar mass can play a role in planet formation by scaling the mass of the protoplanetary disk. In this scenario, a high-mass protoplanetary disk might compen-

sate (at least up to certain point) for a low-metallicity environment, allowing the formation of giant-planets even around low-metallicity stars. The positive correlation found between the presence of gas-giant planets with both stellar metallicity and stellar mass (e.g. Johnson et al. 2010) could be then explained by assuming that higher mass stars are likely to form with more massive protoplanetary disks.

We believe that the analysis of an homogeneous and large sample of evolved stars hosting planets is needed before an explanation to the apparent nature of the metallicity correlation for evolved stars is invoked. This is precisely the goal of this paper, in which we present an homogeneous analysis of a large sample of evolved stars based on high resolution and high S/N ratio échelle spectra.

The paper is organised as follows: Section 2 describes the stellar samples analysed in this work, the spectroscopic observations, and how stellar parameters and abundances are obtained. In order to explore the presence of any possible bias that could affect our analysis, the samples are compared in terms of age, distance, and kinematics, the parameters that most likely might affect the metallicity content of a star. Possible non-LTE effects are also discussed. The metallicity distributions are presented in Section 3, together with an exploration of the parameters that could explain the results, and the properties of the planets orbiting around evolved stars. The results are discussed at length in Section 4. Our conclusions follow in Section 5 .

2. Observations

2.1. The stellar sample

Our sample contains 142 evolved stars from which 70 are known to host at least one planetary companion according to the available data at the Extrasolar Planets Encyclopaedia¹. The selection criteria of the sample was very simple, from the list of evolved stars with confirmed planetary companions we have kept those stars for which a high S/N spectra (at least 100) could be taken with the combination of instruments and telescopes used. The control sample was drawn from the Massarotti et al. (2008) list of Hipparcos giants within 100 pc from the Sun, to cover similar stellar parameters as the stars with detected planets.

Figure 1 shows the HR diagram of the observed stars. They are classified as red giants (blue triangles, giants from now on), subgiants (red squares), and late MS (green asterisks). The classification among the different luminosity classes is somehow uncertain for those stars which are in the boundary between two classes. In order to distinguish between subgiants and red giants, a limit in $M_{\text{bol}} = 2.82$ mag (as in Ghezzi et al. 2010a) was set, although some stars brighter than 2.82 mag which have not yet started their ascent into the RGB (Red Giant Branch) have been kept as subgiants. In addition, 11 stars which are above the MS tracks on the HR diagram, but still have not moved towards the red have been denoted as late MS stars. According to their luminosity class and taken into account the presence (or absence) of planetary companions, our sample is divided into: 43 giant stars with known planets (hereafter, GWPs), 67 giant stars without planets (GWOPs), 16 subgiants hosting planets (SGWPs), 5 subgiants without planets (SGWOPs), and 11 late MS stars harbouring planets (LMSWPs). The sample of subgiant stars has been supplemented with data from the literature (see Section 2.6).

¹ <http://exoplanet.eu/>

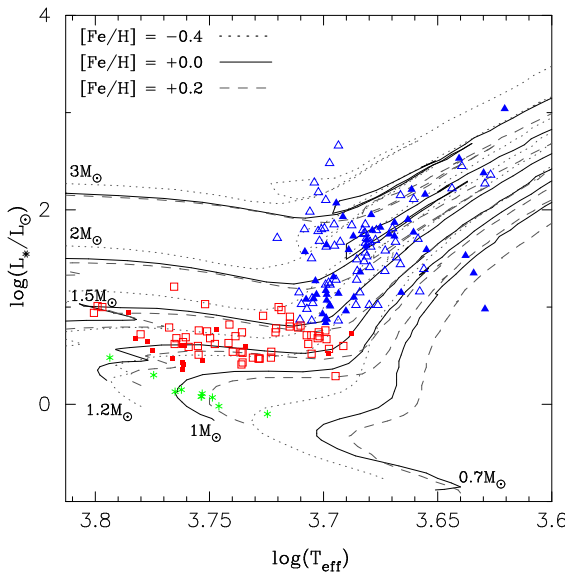


Fig. 1. Luminosity versus T_{eff} diagram for the observed stars. Giants are plotted with blue triangles, subgiants with red squares, and late main-sequence stars with green asterisks. Filled symbols indicate planet hosts. Some evolutionary tracks ranging from 0.7 to 3.0 solar masses from Girardi et al. (2000) are overplotted. For each mass, three tracks are plotted, corresponding to $Z=0.008$ ($[\text{Fe}/\text{H}]=-0.4$ dex, dotted lines), $Z=0.019$ ($[\text{Fe}/\text{H}]=+0.0$ dex, solid lines), and $Z=0.030$ ($[\text{Fe}/\text{H}]=+0.20$ dex, dashed lines).

2.2. Spectroscopic observations

High-resolution spectra of the stars were obtained at La Palma observatory (Canary Islands, Spain) during four observing runs (two at the MERCATOR telescope and two at the Nordic Optical Telescope) between February and August 2011. At the MERCATOR telescope (1.2 m) 28 stars were observed with the HERMES spectrograph (Raskin et al. 2011). HERMES spectra have a resolution of $R \sim 85000$ and cover the spectral range $\lambda\lambda 3800-9000 \text{ \AA}$. HERMES spectra were automatically reduced by a detailed data reduction pipeline available at the telescope². The rest of the data, 114 stars, was obtained with the FIES instrument (Frandsen & Lindberg 1999) at the Nordic Optical Telescope (2.56 m). FIES spectra cover a slightly shorter wavelength range, from 3640 to 7360 \AA , with a resolution of $R \approx 67000$. FIES spectra were reduced using the *advanced* option of the automatic data reduction tool *FIEStool*³. Both pipelines implement the typical corrections involved in échelle spectra reduction, i.e., bias level, flat-fielding, scattered light correction, removing of the blazeshape, order extraction, wavelength calibration, and merge of individual orders. HERMES spectra has S/N values between 90 and 340, with an average of $\sim 150/160$ in the spectral range around the H_{α} line. In the same spectral range, FIES spectra has a S/N of roughly 75 in the worst cases, but up to 480 in the best ones. The average value is around 225. The log of the observations is given in Table 1.

The spectra were corrected from radial velocity shifts by using the IRAF⁴ task *dopcor*. Radial velocities were previously measured by cross-correlating the spectra of our program stars

² See <http://www.mercator.iac.es/instruments/hermes/> for details.

³ See <http://www.not.iac.es/instruments/fies/fiestool/FIEStool.html> for details.

⁴ IRAF is distributed by the National Optical Astronomy Observatory, which is operated by the Association of Universities

Table 1. Observing runs performed on 2011.

Date	Telescope & Instrument	N stars
Feb. 14-15	HERMES/MERCATOR	15
May 17-18	HERMES/MERCATOR	13
May 26-28	NOT/FIES	49
Aug. 16-18	NOT/FIES	65

with spectra of radial velocity standard stars of similar spectral types obtained during the observations.

2.3. Analysis

The basic stellar parameters T_{eff} , $\log g$, microturbulent velocity (ξ_t), and $[\text{Fe}/\text{H}]$, are determined using the code *TGVIT*⁵ (Takeda et al. 2005), which is based on iron-ionization and excitation equilibrium conditions.

Iron abundances are computed for a well-defined set of 302 Fe I and 28 Fe II lines. Basically, the stellar parameters are adjusted until: i) no dependence is found between the abundances derived from Fe I lines and the lower excitation potential of the lines; ii) no dependence is found between the abundances derived from the Fe I lines and their equivalent widths; and iii) the derived mean Fe I and Fe II abundances are the same. The line list as well as the adopted parameters (excitation potential, $\log(gf)$ values, solar EWs) can be found in Y. Takeda's web page. This code makes use of ATLAS9, plane-parallel, LTE atmosphere models (Kurucz 1993). The assumed solar Fe abundance is $A_{\odot} = 7.50$ as in Takeda et al. (2005). Uncertainties in the stellar parameters are computed by progressively changing each stellar parameter from the converged solution to a value in where any of the aforementioned conditions i), ii), iii) is not longer fulfilled. Uncertainties in the iron abundances are computed by propagating the errors in T_{eff} , $\log g$, and ξ_t . We are aware that this procedure only evaluates "statistical" errors. However, other systematic sources of uncertainties such as the choice of the atmosphere model, the adopted atomic parameters, or the list lines used are difficult to estimate (see for details, Takeda et al. 2002a,b).

In order to avoid errors due to uncertainties in the damping parameters, only lines with $\text{EW} < 120 \text{ m}\text{\AA}$ were considered (e.g. Takeda et al. 2008). Stellar EWs are measured using the automatic code *ARES* (Sousa et al. 2007). In order to test the quality of the EWs measured by *ARES*, we selected four representative stars of our sample, covering the whole space of parameters, namely HIP 118319 (5989 K), HIP 50887 (5001 K), HIP 42527 (4516 K), HIP 100587 (4259 K) and measured the EWs of iron lines "manually" by using the IRAF-task *splot*. Median differences between the measured EWs are: $\langle \text{EW}_{\text{ARES}} - \text{EW}_{\text{IRAF}} \rangle = -0.39 \pm 2.1 \text{ m}\text{\AA}$, $-0.34 \pm 2.1 \text{ m}\text{\AA}$, $-0.48 \pm 2.6 \text{ m}\text{\AA}$, and $-0.74 \pm 4.1 \text{ m}\text{\AA}$ for HIP 118319, HIP 50887, HIP 42527, HIP 118319, respectively. We do not find any significant difference between *ARES* equivalent widths and the "manual" measurements. The estimated stellar parameters and iron abundances are given in Table 2.

for Research in Astronomy, Inc., under contract with the National Science Foundation.

⁵ <http://optik2.mtk.nao.ac.jp/takeda/tgv/>

Table 2. Spectroscopic parameters with uncertainties for the stars measured in this work. Columns 7 and 9 give the mean iron abundance derived from Fe I and Fe II lines, respectively, while columns 8 and 10 give the corresponding number of lines. The rest of the columns are self-explanatory. Only the first five lines are shown here; the full version of the table is available online.

HIP	HD	T _{eff} (K)	log g (cm s ⁻²)	ξ_t (km s ⁻¹)	[Fe/H] dex	$\langle A(\text{Fe I}) \rangle$	n _I	$\langle A(\text{Fe II}) \rangle$	n _{II}	Spec. [†]
(1)	(2)	(3)	(4)	(5)	(6)	(7)	(8)	(9)	(10)	(11)
Giants with planets										
1692	1690	4343 ± 20	2.06 ± 0.08	1.56 ± 0.14	-0.23 ± 0.04	7.27 ± 0.05	197	7.27 ± 0.07	17	2
4297	5319	4900 ± 25	3.35 ± 0.09	1.10 ± 0.10	0.05 ± 0.04	7.55 ± 0.04	234	7.55 ± 0.06	18	2
10085	13189	4175 ± 33	1.62 ± 0.13	1.49 ± 0.17	-0.37 ± 0.06	7.13 ± 0.07	229	7.13 ± 0.10	20	1
12247	16400	4864 ± 25	2.65 ± 0.08	1.42 ± 0.10	-0.03 ± 0.03	7.47 ± 0.04	217	7.47 ± 0.06	17	2
	17092	4634 ± 28	2.48 ± 0.10	1.31 ± 0.13	0.11 ± 0.05	7.61 ± 0.05	237	7.61 ± 0.08	21	1

[†]Spectrograph: (1) MERCATOR/HERMES; (2) NOT/FIES

2.4. Photometric parameters and comparison with previous works

Photometric effective temperatures are derived from the *Hipparcos* ($B - V$) colours (Perryman & ESA 1997) by using the calibration provided by Casagrande et al. (2010, Table 4). Uncertainties in the photometric temperatures are estimated by taking into account the standard deviation of the calibration (~ 73 K), the uncertainty in the zero point of the temperature scale (which is, according to the authors, of the order of 15-20 K), and the propagation of the errors associated with colours and metallicities. These three sources of uncertainty have been added quadratically. Although this calibration was built using dwarfs and subgiants stars, we find that it also reproduces the spectroscopic temperatures obtained for our sample of giants.

Since our sample contains stars up to roughly 0.5 kpc, colours are de-reddened before we compute the photometric temperatures. Visual extinction, A_V , and colour excesses, $E_{(B-V)}$ ⁶, are computed as a function of the stellar distance and the galactic coordinates (l, b) by interpolating in the tables given by Arenou et al. (1992). Distances are obtained from the revised parallaxes provided by van Leeuwen (2007) from a new reduction of the *Hipparcos*'s raw data. For the five stars with planets that do not have *Hipparcos*'s data the parallaxes have been taken from the papers in which the discovery of the corresponding planets were announced. The comparison between the temperature values obtained by both procedures, spectroscopic and photometric, is illustrated in Figure 2 where we do not find any sound systematic difference between them, being the mean value of ΔT_{eff} ~ -16 K, with a standard deviation of only 96 K. We have also computed photometric temperatures using the calibration provided by González Hernández & Bonifacio (2009, Table 5), since this relationship was build using giant stars. We note that the temperatures obtained with this relationship tend to be slightly cooler than the ones obtained by using the relationship provided by Casagrande et al. (2010) (and therefore slightly cooler than our spectroscopic values). Nevertheless, the difference ΔT_{eff} is small, ~ 71 K, with a standard deviation of 88 K. The small offset between both calibrations may be related to the different absolute calibration and zero points adopted for Vega (González Hernández & Bonifacio 2009; Casagrande et al. 2010).

Values of the stellar luminosities ($\log L_{\star}/L_{\odot}$) are estimated from the absolute magnitudes and bolometric corrections using the measurements by Flower (1996, Table 3). Uncertainties

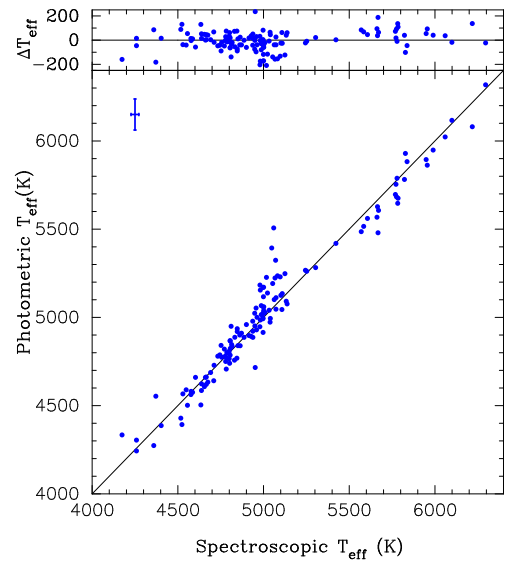


Fig. 2. Comparison between our spectroscopic-derived T_{eff} and those obtained from ($B - V$) colours. The upper panel shows the differences between the spectroscopic and the photometric values. Mean uncertainties in the derived temperatures are also shown.

in the stellar luminosities have been computed by propagating the errors associated with the V magnitudes, visual extinction, parallaxes, and effective temperatures. Estimates of the uncertainty in the visual extinction are already given in the tables by Arenou et al. (1992), while typical uncertainties in V are ± 0.01 mag (Perryman & ESA 1997). Bolometric corrections have been derived as a function of T_{eff} . For the error computations, the uncertainty due to the propagation of the errors in T_{eff} , and the sigma of the calibration BC- T_{eff} have been added quadratically. The values of visual extinction, photometric temperatures and luminosities are shown in Table 3.

Evolutionary values of gravities are computed from *Hipparcos* V magnitudes and parallaxes using L. Girardi's code *PARAM*⁷ (da Silva et al. 2006), which is based on the use of Bayesian methods. Our derived spectroscopic T_{eff} and metallicities are used as inputs for *PARAM*. The code also estimates the stellar evolutionary parameters, age, mass, and radius. These quantities are also given in Table 3, while a comparison between the spectroscopic and evolutionary $\log g$ values is shown in Figure 3. It is clear from the figure that spectroscopic $\log g$

⁶ The usual relationship $A_V = 3.10 \times E_{(B-V)}$ is assumed (e.g. Savage & Mathis 1979).

⁷ http://stev.oapd.inaf.it/cgi-bin/param_1.1

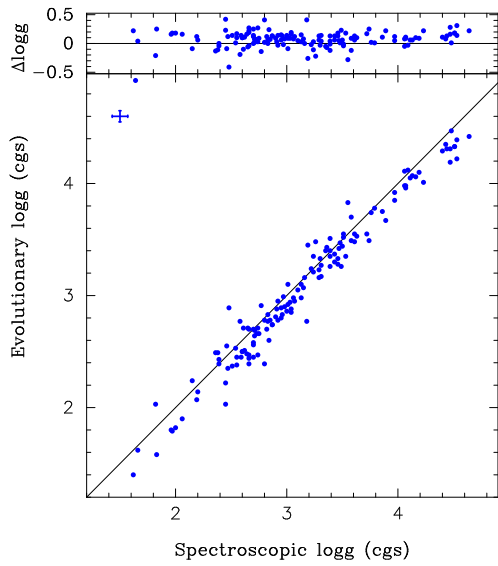


Fig. 3. Spectroscopic-derived $\log g$ values versus $\log g$ estimates based on *Hipparcos* parallaxes. The upper panel shows the differences between the spectroscopic and the *Hipparcos* values. Mean uncertainties in $\log g$ values are also shown.

values tend to be systematically larger than the evolutionary estimates. Specifically, spectroscopic values are ~ 0.09 larger (in median) than the evolutionary estimates with a standard deviation of 0.13. Such a trend of larger spectroscopic $\log g$ values has already been reported and discussed by several authors (e.g. da Silva et al. 2006, and references therein) pointing towards non-LTE effects on Fe I abundances or thermal inhomogeneities as possible causes. We note, however, that the standard deviation of the distribution $\log g_{\text{spec}} - \log g_{\text{evol}}$ is 0.13, which is of the same order of magnitude of the uncertainties in the spectroscopic derived $\log g$ values. Therefore, we may state that our spectroscopic values are in agreement (within the uncertainties) with the evolutionary estimates, ruling out significant departures from LTE conditions (see discussion in Section 2.7).

There is one outlier, namely BD+20 2457 (left upper corner in Figure 3); but this is due to its largely undetermined parallax, $\pi = 5.0 \pm 26.0$ mas (Niedzielski et al. 2009).

We finally compare our metallicities with those already reported in the literature. Values for the comparison are taken from the Extrasolar Planets Encyclopaedia⁸ (and references therein) as well as from Hekker & Meléndez (2007), Luck & Heiter (2007), Takeda et al. (2008), and Ghezzi et al. (2010a), where we were able to find literature metallicities for roughly 70% of our program stars. The comparison is shown in Figure 4. The agreement is in overall good, with $\langle [\text{Fe}/\text{H}]_{\text{this work}} - [\text{Fe}/\text{H}]_{\text{other works}} \rangle = +0.00$ dex and a standard deviation of 0.08 dex.

2.5. Abundance computation

Chemical abundances of individual elements (Na, Mg, Al, Si, Ca, Sc, Ti I, Ti II, Mn, Cr I, Cr II, V, Co, Ni, Zn) are obtained by using the *WIDTH9* program (Castelli 2005) together with ATLAS9 atmosphere models (Kurucz 1993), updated to work under Linux by Sbordone et al. (2004) and Sbordone (2005).

The measured equivalent widths of a list of narrow, non-blended lines for each of the aforementioned ions are used as

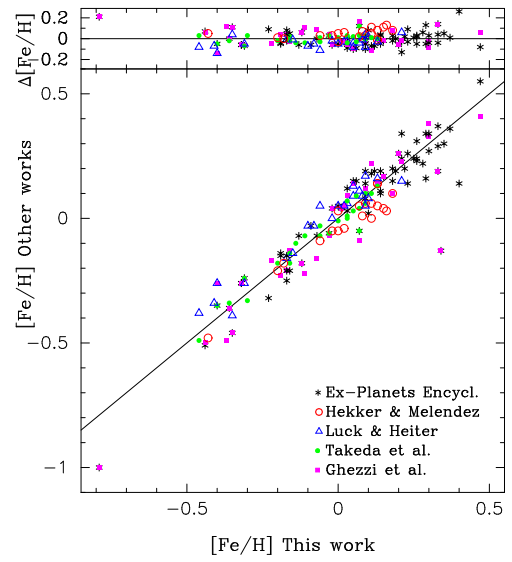


Fig. 4. $[\text{Fe}/\text{H}]$ values, this work, versus literature estimates. The upper panel shows the differences between the metallicities derived in this work and the values given in the literature.

inputs for *WIDTH9*. The selected lines are mainly taken from the list provided by Neves et al. (2009, Table 2), although we keep the parameters of the lines (excitation potential, oscillator strength) as given in Kurucz's lists of lines. For Zn abundances, the lines at 4810.54 and 6362.34 Å were considered.

The abundances obtained are given in Table 5. They are expressed relative to the solar values provided by Asplund et al. (2009). We have used the four representative stars mentioned in Section 2.3 in order to provide an estimate on how the uncertainties in the atmospheric parameters propagate into the abundance calculation. Abundances for each of these four stars have been recomputed using $T_{\text{eff}} + \Delta T_{\text{eff}}$, $T_{\text{eff}} - \Delta T_{\text{eff}}$, and similarly for $\log g$ and ξ_t . Results are given in Table 4. As final uncertainties for the derived abundances we give the quadratically sum of the uncertainties due to the propagation of the errors in the stellar parameters, plus the line-to-line scatter errors (computed as σ / \sqrt{N} , where σ is the standard deviation of the derived individual abundances from the N lines). We would like to point out here that even these uncertainties should be considered as lower limits, given that the errors in the stellar parameters are only statistical (as explained in Section 2.3), and the abundance estimates are affected by systematics which are not taken into account in line-to-line errors (i.e. atomic data, or uncertainties in the atmosphere models).

A comparison of our derived abundances with those previously reported in the literature is shown in Figure 5. Derived abundances of Na, Al, Ti, and Ni agree reasonable well with previously reported values, with the σ of the distribution $[\text{X}/\text{H}]_{\text{(this work)}} - [\text{X}/\text{H}]_{\text{(other work)}}$ ranging from ~ 0.03 to 0.08 dex, although our abundances seem to be slightly shifted towards higher values (maximum mean differences $\leq \sim 0.08$ dex). In the cases of Si and Ca, our abundances are in median a bit larger (~ 0.1 dex) than those given in Gilli et al. (2006) and Valenti & Fischer (2005), but in agreement with Luck & Heiter (2007); Takeda (2007); Takeda et al. (2008). For Mg, our abundances are on average a bit lower (within 0.1 dex) than those given by Valenti & Fischer (2005) and Gilli et al. (2006), although in excellent agreement with Takeda (2007). Abundances of Cr, and Co are slightly lower than those previously reported,

⁸ <http://exoplanet.eu/>

Table 3. Photometric and evolutionary parameters for the stars measured in this work (see text for details). Only the first five lines are shown here; the full version of the table is available online. Each quantity is accompanied by its corresponding uncertainty.

HIP/ Other name (1)	A _V (mag) (2)	L _★ /L _⊙ (log) (3)	T _{eff} ^{phot} (K) (4)	log g _{evol} (cms ⁻²) (5)	Age (Gyr) (6)	Mass (M _⊙) (7)	Radius (R _⊙) (8)
Giants with planets							
1692	0.10 ± 0.04	1.53 ± 0.39	-	1.90 ± 0.10	6.72 ± 3.18	1.11 ± 0.15	18.80 ± 2.77
4297	0.10 ± 0.03	0.96 ± 0.09	4960 ± 86	3.40 ± 0.07	3.45 ± 0.66	1.37 ± 0.08	3.72 ± 0.36
10085	0.82 ± 0.50	3.04 ± 0.41	4334 ± 168	1.40 ± 0.11	4.56 ± 2.97	1.19 ± 0.25	34.60 ± 6.28
12247	0.08 ± 0.06	1.73 ± 0.04	4839 ± 86	2.71 ± 0.05	1.38 ± 0.18	1.90 ± 0.12	9.67 ± 0.40
HD 17092	0.20 ± 0.05	1.15 ± 0.44	4504 ± 86	2.89 ± 0.28	5.60 ± 3.17	1.20 ± 0.20	6.34 ± 2.18

specially in the case of Co, but still mean differences are within ± 0.1 dex. The largest dispersion are found for Sc, V, and Mn, probably due to the small number of lines used for these elements or uncertainties in the atomic parameters. It is well known that some lines of Sc, V, Mn (and also Co) split into different subcomponents due to electron-nucleus interactions showing a significant hyperfine structure, (e.g. Schuler et al. 2011). Hyperfine structure (hfs) has not been considered in our analysis and, as a consequence the abundances of these elements may be overestimated. We note, however, that the differences between hfs synthesis abundances and EW-based abundances derived by Schuler et al. (2011) are small, ≤ 0.04 dex, in 8 out of the 10 late-F and G type analysed stars. In addition, we do not expect hfs effects to bias the results of the comparisons performed in this work (see Section 3.4) between samples of stars with and without planets, given that they have otherwise similar properties.

Finally, considering Zn, only Takeda et al. (2008) give abundances for this element. Despite the small number of stars in common the agreement is quite clear, as shown in Figure 5.

2.6. Expanding the SGWOP sample

Given the small number of stars observed classified as SGWOPs, we have expanded the sample with data from the literature in order to make a proper comparison between the properties of subgiants with and without planetary companions. We have added to the SGWOP sample those stars given in Valenti & Fischer (2005, hereafter VF05) which fulfilled our criteria for being classified as subgiants (Section 2.1). These stars have been monitored for planets on the Keck, Lick, and Anglo-Australian Telescope planet search programs, discarding the presence of planetary companions with radial velocity semiamplitudes $K > 30 \text{ m s}^{-1}$ and orbital periods shorter than 4 yr (Fischer & Valenti 2005). Those stars already observed by us, as well as stars with recently discovered planets, were discarded. The final number of stars added to the SGWOP sample amounts to 50.

In order to keep the analysis as homogeneous as possible, VF05 metallicities were set into our own metallicity scale by using the stars in common. A linear fit was made, obtaining the following linear transformation: [Fe/H](our scale) = (0.96±0.11)×[Fe/H](VF05) - (0.04±0.03), (RMS=0.07, $\chi^2_r \sim 10.4$). Effective temperatures provided by VF05 were also set into our own temperature scale by using the linear relationship: T_{eff}(our scale) = (1.02±0.03)×T_{eff}(VF05) - (140±179), (RMS=42, $\chi^2_r \sim 5.25$). Considering log g values, we get the following transformation: log g(our scale) = (1.17±0.06)×log g(VF05) - (0.79±0.26), (RMS=0.009, $\chi^2_r \sim 2.2$).

Table 4. Abundance sensitivities.

Ion	HIP 118319			HIP 50887		
	ΔT_{eff} ±25 (K)	$\Delta \log g$ ±0.05 (cms ⁻²)	$\Delta \xi_t$ ±0.14 (kms ⁻¹)	ΔT_{eff} ±10 (K)	$\Delta \log g$ ±0.04 (cms ⁻²)	$\Delta \xi_t$ ±0.06 (kms ⁻¹)
	Na	0.01	0.01	0.05	<0.01	<0.01
Mg	0.01	0.01	0.13	<0.01	<0.01	0.01
Al	0.01	<0.01	0.03	0.01	<0.01	0.01
Si	0.01	<0.01	0.02	<0.01	<0.01	<0.01
Ca	0.01	0.01	0.16	0.01	<0.01	0.03
Sc	0.03	<0.01	0.05	0.01	<0.01	0.01
T I	0.02	<0.01	0.03	0.02	<0.01	0.02
Ti II	<0.01	0.02	0.05	<0.01	0.02	0.02
V	0.02	<0.01	0.15	0.01	<0.01	0.02
Cr I	0.03	0.01	0.11	0.01	<0.01	0.02
Cr II	<0.01	0.02	0.20	0.01	0.02	0.02
Mn	0.02	<0.01	0.21	0.01	<0.01	0.03
Co	0.02	<0.01	0.05	0.01	0.01	0.02
Ni	0.01	<0.01	0.08	0.01	0.01	0.01
Zn	0.01	<0.01	0.28	<0.01	0.01	0.02
Ion	HIP 42527			HIP 100587		
	ΔT_{eff} ±18 (K)	$\Delta \log g$ ±0.07 (cms ⁻²)	$\Delta \xi_t$ ±0.09 (kms ⁻¹)	ΔT_{eff} ±35 (K)	$\Delta \log g$ ±0.13 (cms ⁻²)	$\Delta \xi_t$ ±0.15 (kms ⁻¹)
	Na	0.01	0.01	0.03	0.03	0.02
Mg	0.01	0.01	0.02	0.01	0.01	0.04
Al	0.01	<0.01	0.02	0.02	<0.01	0.04
Si	0.01	0.01	0.01	0.04	0.04	0.03
Ca	0.02	0.01	0.05	0.03	0.01	0.09
Sc	0.02	<0.01	0.03	0.04	<0.01	0.11
T I	0.03	<0.01	0.06	0.05	0.01	0.12
Ti II	<0.01	0.03	0.05	0.01	0.06	0.08
V	0.03	0.01	0.08	0.04	0.01	0.17
Cr I	0.02	<0.01	0.04	0.03	<0.01	0.08
Cr II	0.02	0.03	0.03	0.03	0.06	0.05
Mn	0.01	<0.01	0.07	0.01	<0.01	0.13
Co	0.01	0.01	0.04	<0.01	0.04	0.08
Ni	<0.01	0.02	0.03	0.01	0.04	0.07
Zn	0.02	0.02	0.04	0.03	0.03	0.04

Stellar ages, masses and radius for these stars were recomputed following the same procedure that the one used for the stars analyzed in this work (Section 2.4), and are also listed in Table 3.

2.7. Possible biases

Before we proceed further in the comparison between the different samples it is due an exploration of the possible sources of bias that could mimic metallicity differences. Metallicity reflects the enrichment history of the ISM (see e.g. Timmes et al. 1995). It is, therefore, important to determine whether the different samples have randomly selected stellar hosts in terms of age, distance, and kinematics, which are the parameters most likely to reflect the original metal content of the molecular cloud where

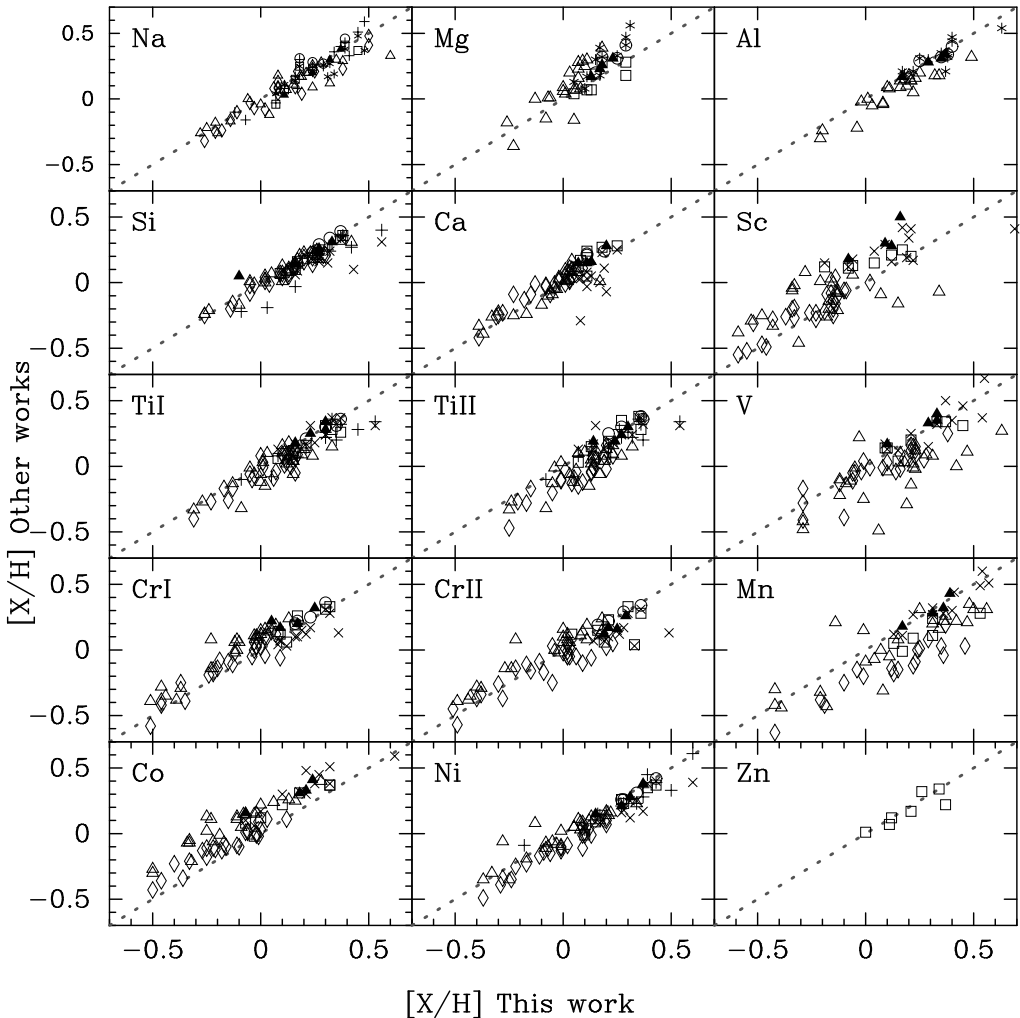


Fig. 5. Comparison of our abundances to those of Beirão et al. (2005)(*), Bensby et al. (2005) (open circles), Valenti & Fischer (2005)(+), Gilli et al. (2006)(\times), Luck & Heiter (2007) (open triangles), Takeda (2007) (open squares), Takeda et al. (2008) (diamonds), and Neves et al. (2009) (filled triangles).

Table 5. Derived abundances of Na, Mg, Al, Si, Ca, Sc, Ti I, Ti II, V, Cr I, Cr II, Mn, Co, Ni, and Zn. Only the first five lines are shown here; the full version of the table is available online.

HIP/Other	[Na/H]	[Mg/H]	[Al/H]	[Si/H]	[Ca/H]	[Sc/H]	[Ti I/H]	[Ti II/H]	[V/H]	[Cr I/H]	[Cr II/H]	[Mn/H]	[Co/H]	[Ni/H]	[Zn/H]
Giants with planets															
1692	-0.12 ± 0.11	-0.17 ± 0.06	0.10 ± 0.06	0.07 ± 0.04	-0.34 ± 0.12	-0.11 ± 0.27	0.12 ± 0.15	0.12 ± 0.22	0.23 ± 0.24	-0.30 ± 0.10	-0.20 ± 0.13	0.05 ± 0.18	-0.20 ± 0.17	-0.12 ± 0.09	-0.22 ± 0.29
4297	0.13 ± 0.06	0.05 ± 0.06	0.24 ± 0.03	0.15 ± 0.03	-0.01 ± 0.06	-0.05 ± 0.10	0.15 ± 0.13	0.09 ± 0.04	0.32 ± 0.09	-0.02 ± 0.15	0.01 ± 0.04	0.33 ± 0.14	0.02 ± 0.11	0.12 ± 0.04	0.12 ± 0.20
10085	-0.11 ± 0.09	-0.21 ± 0.10	-0.07 ± 0.12	-0.01 ± 0.09	-0.36 ± 0.12	-0.09 ± 0.27	0.15 ± 0.16	-0.17 ± 0.16	0.35 ± 0.24	-0.20 ± 0.12	-0.40 ± 0.14	-0.05 ± 0.23	-0.29 ± 0.16	-0.19 ± 0.09	-0.56 ± 0.21
12247	0.16 ± 0.06	0.05 ± 0.11	0.11 ± 0.03	0.13 ± 0.06	-0.04 ± 0.10	-0.23 ± 0.12	0.06 ± 0.04	0.04 ± 0.10	0.08 ± 0.10	-0.08 ± 0.04	-0.15 ± 0.06	0.22 ± 0.12	-0.16 ± 0.11	-0.01 ± 0.04	0.02 ± 0.06
HD 17092	0.42 ± 0.22	0.11 ± 0.06	0.33 ± 0.04	0.34 ± 0.08	0.08 ± 0.10	0.05 ± 0.20	0.14 ± 0.09	0.15 ± 0.19	0.43 ± 0.18	0.05 ± 0.06	0.05 ± 0.09	0.46 ± 0.22	0.11 ± 0.14	0.25 ± 0.06	0.69 ± 0.13

the stars were born. The properties of the stars obtained with the procedure explained in the previous subsections, are summarised for the different samples in Table 6.

The comparison of the stellar properties among the different samples show that planet hosts tend to be systematically at larger distances than the stars without known planetary companions. This is no unexpected since we selected the control sample from stars within 100 pc, while the sample of stars with planets is not volume limited. In order to check whether there

is a systematic trend in the metallicity due to the distance, the [Fe/H]-distance space is shown in Figure 6. It can be seen from the figure that GWPs and GWOPs located within ~ 100 pc are well-mixed in the [Fe/H]-distance plane showing a similar behaviour. At slightly larger distances and up to 200 pc the GWP sample covers approximately the same range in [Fe/H] as the sample within ~ 100 pc. However, the four GWPs located beyond 200 pc have very small negative metallicities, specially BD+20 2457 (already mentioned in Section 2.4). We consider

Table 6. Comparison between the properties of the different samples studied in this work.

	GWOPs			GWP		
	Range	Mean	Median	Range	Mean	Median
V (mag)	2.8/7.8	5.5	5.5	1.1/9.8	6.2	6.1
Distance (pc)	18.5/107.2	75.4	78.1	10.4/561.8	112.3	96.9
Age (Gyr)	0.2/9.8	2.6	1.9	0.4/10.5	3.0	2.4
T _{eff} (K)	4235/5252	4850	4847	4175/5107	4779	4861
M (M _⊙)	0.9/3.8	1.8	1.6	0.9/2.9	1.6	1.5
SpType (%)	36 (G); 64 (K)			33 (G); 67 (K)		
D/TD [†] (%)	84 (D); 1 (TD); 15 (R)			79 (D); 5 (TD); 16 (R)		
	SGWOPs			SGWP		
	Range	Mean	Median	Range	Mean	Median
V (mag)	3.5/8.6	6.6	6.6	4.5/10.5	7.4	8.0
Distance (pc)	9.0/112	51.4	50.0	25.3/320.5	77.3	65.5
Age (Gyr)	1.9/11.7	5.3	4.3	0.9/7.6	4.8	4.9
T _{eff} (K)	4913/6318	5431	5382	4873/6566	5745	5779
M (M _⊙)	1.0/1.6	1.2	1.2	1.1/1.5	1.2	1.2
SpType (%)	5.5 (F); 74.5 (G); 20 (K)			12.5 (F); 75 (G); 12.5 (K)		
D/TD [†] (%)	62 (D); 5 (TD); 33 (R)			56 (D); 6 (TD); 38 (R)		
	LMSWP					
	Range	Mean	Median			
V (mag)	5.5/12.2	8.0	7.9			
Distance (pc)	15.6/480.8	91.5	42.3			
Age (Gyr)	0.5/10.6	4.7	4.7			
T _{eff} (K)	5304/6597	5805	5671			
M (M _⊙)	0.9/1.4	1.1	1.0			
SpType (%)	9 (F); 82 (G); 9 (K)					
D/TD [†] (%)	82 (D); 18 (R)					

[†] D: Thin disc, TD: Thick disc, R: Transition

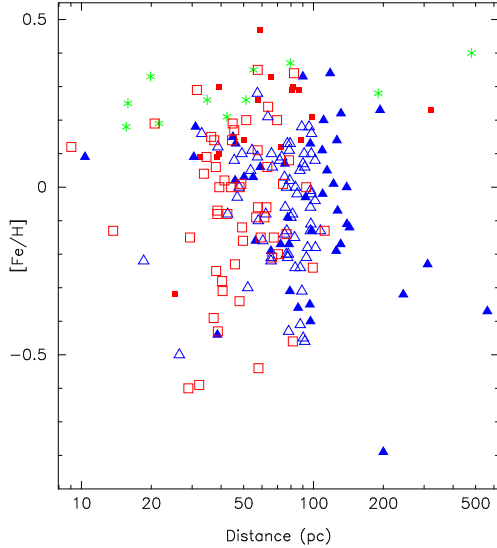


Fig. 6. [Fe/H] as a function of the stellar distance. Colours and symbols are as in Figure 1.

this figure (four stars, $\sim 9\%$ of the whole GWP sample) too-low to bias the metallicity distribution of the GWP sample, so we do not expect any significant chemical difference between the GWP and GWOP samples introduced by their distances from the Sun. Nevertheless, we have checked whether this is indeed the case in Section 3.2.

Thick disc stars are expected to be relatively old (e.g. Bensby et al. 2005), metal-poor, and to show α -enhancement (e.g. Fuhrmann 1998; Haywood 2008b; Adibekyan et al. 2011). We have checked if there are differences between the different

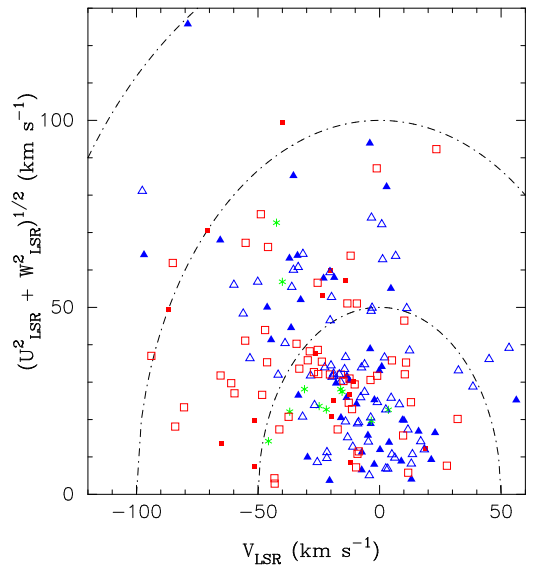


Fig. 7. Toomre diagram of the observed stars. Colours and symbols are as in Figure 1. Dash-dot lines indicate constant total velocities, $V_{\text{Total}} = \sqrt{U_{\text{LSR}}^2 + V_{\text{LSR}}^2 + W_{\text{LSR}}^2} = 50, 100$, and 150 km s^{-1} .

samples in terms of membership to the thin/thick disc. The procedure involves measuring radial velocities by cross-correlating the spectra of the stars with spectra of radial velocity standard stars of similar spectral types. For the SGWOPs stars taken from the literature, the radial velocities values have been mainly taken from the compilation by Kharchenko et al. (2007).

Galactic spatial-velocity components (U, V, W) are computed from the radial velocities, together with *Hipparcos* parallaxes (van Leeuwen 2007), and *Tycho-2* proper motions (Høg et al. 2000), following the procedure described in Montes et al. (2001), and Maldonado et al. (2010).

For stars in known binary systems the radial velocity of the centre of mass of the system is used. Finally, stars have been classified as belonging to the thin/thick disc applying the methodology described in Bensby et al. (2003, 2005). Figure 7 shows the Toomre diagram for the observed stars, while the derived velocities are given in Table 7. This type of diagram constitutes a useful way to discriminate stellar populations in velocity space, since it plots the energy versus the angular momentum properties of the stars (e.g. Fuhrmann 2004). We find that roughly $\sim 80\%$ of the stars belong to the thin disc and we do not find any difference in the distribution of the different samples; in particular, there are no differences between planet host and stars without planets. It is worth mention that while our classification of thin/thick disc stars is based only on kinematical criteria, a complete description of the thin/thick disc populations would require the combination of kinematics, metallicities, and stellar ages (e.g. Fuhrmann 1998). Nevertheless, the methodology used is sufficient to discard the presence of a significant fraction of thick disc stars within any of our samples.

We note that the two GWP stars possible members of the thick disk have low metallicities ($[{\text{Fe}}/{\text{H}}] < -0.3$ dex) and $\sim 43\%$ of the GWP stars classified as transition stars have also metallicities below -0.3 dex. Haywood (2008a) argued that at metallicities $[{\text{Fe}}/{\text{H}}] < -0.3$ dex, giant planets seem to favour thick disk stars. Statistics of thick disk stars are too small in our sample, but they do not contradict Haywood (2008a) idea.

Table 7. Radial velocities and Galactic spatial-velocity components for the observed stars. Only the first five lines are shown here; the full version of the table is available online. The assumed solar motion with respect to the LSR is $(U_\odot, V_\odot, W_\odot) = (10.0, 5.25, 7.17) \text{ km s}^{-1}$ (Dehnen & Binney 1998).

HIP/ Other (1)	V_r^* (km s $^{-1}$) (2)	U_{LSR} (km s $^{-1}$) (3)	V_{LSR} (km s $^{-1}$) (4)	W_{LSR} (km s $^{-1}$) (5)	C † (6)
Giants with planets					
1692	17.58 ± 0.25	-8.80 ± 8.15	3.94 ± 3.75	-10.75 ± 0.94	D
4297	-0.21 ± 0.31	25.28 ± 1.68	-13.56 ± 2.00	-5.40 ± 1.33	D
10085	25.36 ± 0.46	-13.81 ± 3.55	22.85 ± 3.10	8.97 ± 6.33	D
12247	8.60 ± 0.31	3.65 ± 0.49	-20.57 ± 1.33	-0.63 ± 0.41	D
HD17092	5.56 ± 0.31	-7.50 ± 6.73	-7.26 ± 8.17	8.42 ± 1.49	D

* For those stars in binary systems we have considered the radial velocity of the centre of mass of the system.

† Thin/thick disc classification, D: Thin disc, TD: Thick disc, R: Transition

Both samples of giant stars, with and without planets, cover a wider stellar mass range and represent on average a younger population of stars than the subgiant or late main sequence samples. The metallicity biases possibly hidden in the age and mass of the different samples are rather complicated to discuss at length at this point, we refer their full examination to Section 3.

2.8. Non-LTE effects

Non-LTE (Local Thermodynamic Equilibrium) effects, if present, should not constitute a bias in the comparison between groups of stars at the same evolutionary stage, provided that the samples are composed of a statistically significant number of stars, showing similar properties (see previous section). Another issue, however, is whether non-LTE effects might bias the comparison of samples of stars at different stages on their evolution (dwarf/subgiant/giant), by affecting in bulk the abundances determination within a group of stars.

Non-LTE corrections to the abundance determination increase with decreasing [Fe/H] and $\log g$, showing a strong dependence on the effective temperature in dwarf stars (e.g. Bergemann et al. 2011). For the giant stars considered in this work, non-LTE corrections would be $\lesssim 0.1$ dex, while for the hottest (i.e., the “worst” case) subgiants and late main-sequence stars, non-LTE corrections could be up to ~ 0.1 dex (Bergemann et al. 2011, Figure 3). Mashonkina et al. (2011) also analyzes LTE and non-LTE iron abundances for five stars covering a wide range of stellar parameters (T_{eff} : 4600 - 6400 K, $\log g$: 1.60 - 4.5 dex, [Fe/H]: -2.7 to +0.10 dex). The authors find that departures from LTE do not exceed 0.1 dex for stars with solar metallicity and mildly metal-deficient stars.

When significant departures from LTE populations in Fe I and Fe II are present, an LTE analysis produces systematically underestimated gravities and metallicities (e.g. Lind et al. 2012). Therefore, the comparison of $\log g_{\text{spec}}$ and $\log g_{\text{evol}}$ provides a mechanism to investigate whether non-LTE effects are significant or not. As discussed in Section 2.4, the standard deviation of the distribution $\log g_{\text{spec}} - \log g_{\text{evol}}$ is of the same order of magnitude of the uncertainties in the spectroscopic $\log g$ values. In addition, a linear fit of $(\log g_{\text{spec}} - \log g_{\text{evol}})$ with T_{eff} gives a slope consistent with zero ($\sim 10^{-7}$ dex/K). The dependence with the stellar metallicity is more evident, although still the slope is consistent with zero (~ 0.05 dex/dex)⁹. In other words, the good agreement between $\log g_{\text{spec}}$ and $\log g_{\text{evol}}$ values over the range

⁹ Excluding the metal-poor star BD+20 2457

Table 8. [Fe/H] statistics of the stellar samples.

Sample	Mean	Median	Deviation	Min	Max	N
GWOPs	-0.06	-0.03	0.18	-0.50	+0.28	67
GWP	-0.06	-0.02	0.23	-0.79	+0.34	43
SGWOPs	-0.06	-0.06	0.22	-0.60	+0.35	55
SGWP	+0.19	+0.23	0.17	-0.32	+0.47	16
LMSWPs	+0.28	+0.26	0.07	+0.18	+0.40	11

of T_{eff} and [Fe/H] analysed in this work suggests that there are not significant departures from LTE.

Considering other elements (Na, Mg, Si, ...) the only comparisons performed through this paper are between GWPs and GWOPs (Section 3.4). Although abundances for individual stars may be affected by non-LTE effects, those effects, if present, should not bias the comparison GWPs/GWOPs.

3. Results

3.1. Analysis of the Metallicity Distributions of the Different Samples of Stars

As mentioned before, our observations contain 67 giant stars without known planets and 43 giant stars with planets. Some statistical diagnostics for the GWOP and GWP samples are summarised in Table 8 and their normalised metallicity distributions are shown in Figure 8 (left). We find that both samples show similar distributions and statistical diagnostics. However, in order to assess if both distributions are equal from a statistical point of view, the standard two-sample Kolmogorov-Smirnov (K-S) test was performed. The maximum difference between the GWOPs and GWPs cumulative distribution functions is ~ 0.11 , and the statistical probability of both distributions to be drawn from the same parent distribution is significantly high, 87% ($n_{\text{eff}} \sim 26$). Therefore, we find that giant stars harbouring planets do not seem to follow the planet-metallicity correlation of MS stars. We find that giant stars with planets are not more metal rich than the giant stars without them. Other authors have reached the same conclusions before based on smaller samples of stars, Sadakane et al. (2005), Pasquini et al. (2007), and Takeda et al. (2008).

Figure 8, right panel, shows the normalised metallicity distribution of the SGWP sample and of its corresponding comparison sample (SGWOPs). The data suggest that the metallicity distribution of the SGWP sample is significantly shifted towards higher metallicities with respect to the SGWOP sample, a behaviour which resembles the well known giant-planet metallicity correlation found in main-sequence stars (e.g. Santos et al. 2004; Fischer & Valenti 2005). A two sample K-S test confirms that both distributions are different from a statistical point of view (p -value $\sim 10^{-5}$, $D \sim 0.66$, $n_{\text{eff}} \sim 12.4$).

With the aim of completeness, a sample of main-sequence planet hosts (MSWPs) has been added to the discussion of the results that follows. We have selected those stars hosting exclusively giant planets with available metallicities in VF05, where we have removed stars with retracted or not confirmed exoplanets, as well as, those stars already included in our SGWP or LMSWP samples. In order to keep the analysis as homogeneous as possible we proceeded as in Section 2.6 to set the VF05 metallicities into our own metallicity scale.

The cumulative metallicity distributions of all samples, Figure 9, allow us to get an overall picture of the metallicity trends. There are a few interesting facts to be taken from these distributions and their statistical tests: i) there is not difference in

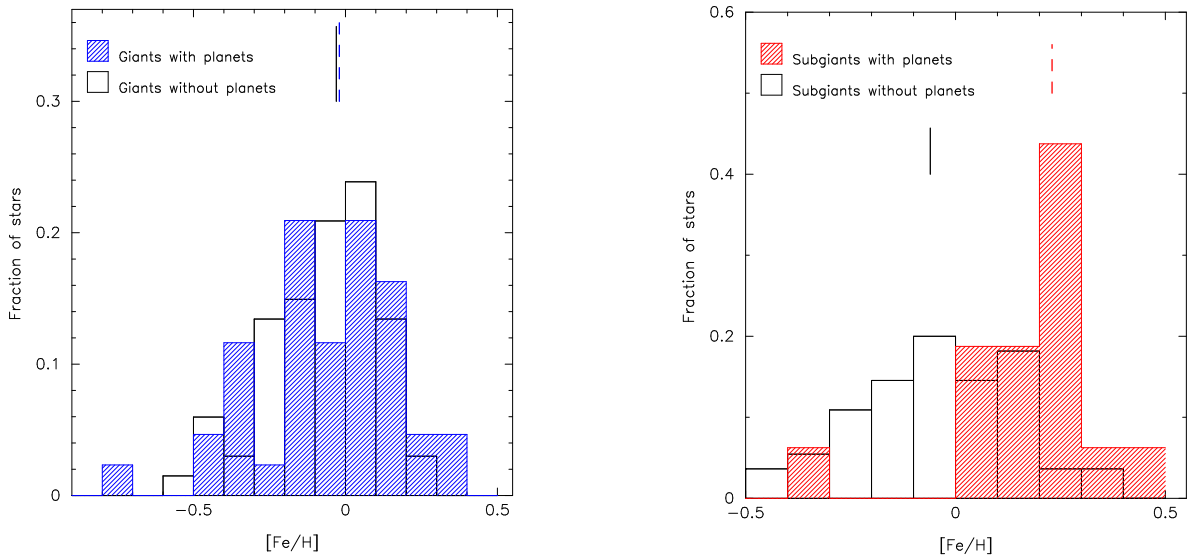


Fig. 8. Left: Normalised metallicity distribution of the GWP sample (blue histogram) versus giant stars without known planets. Right: Normalised metallicity distribution of the SGWP sample (red histogram) versus subgiant stars without known planets. Median values of the distributions are shown with vertical lines.

the metallicities for giant stars regarding the presence or absence of planets; ii) the distribution of subgiant stars with planets is clearly separated from that of subgiants without planets; iii) the distribution of subgiant stars without planets follows a similar trend than giant stars (with and without planets); and iv) more interestingly, the metallicity distribution of subgiant stars with planets is different from that of giant stars, but similar to the one of MS stars with planets.

We note that the metallicity distribution of SGWPs seems also to be slightly shifted towards lower metallicities with respect to the LMSWP sample. Nevertheless, their median metallicities are quite similar (see Table 8), and both consistent with the known trends for main-sequence stars hosting giant-planets (see below).

The K-S test comparing the SGWP/GWP and LMSWP/GWP samples, confirms that the distributions are different within a 98% confidence level¹⁰. The K-S test reveals that the probability of LMSWPs and SGWPs to be drawn from the same parent distribution is low, around 0.12 ($D=0.44$, $n_{\text{eff}} \sim 6.5$), although we cannot rule out this possibility. There is a clear outlier in the SGWP sample, namely HIP 36795, which is the only star in the SGWPs sample with a [Fe/H] below the solar value. We note that even if we do not take into account this star, the K-S probability is still low, of the order of 0.20. Therefore, we conclude that from an statistical point of view, we cannot state a difference between the SGWP and LMSWP samples, whilst we can affirm that, with the data at hand, the metal distributions of subgiant stars with planets are similar to the ones of late and MS stars with planets and that differ from those of giant stars with planets.

3.2. Metallicity as a Function of the Stellar Mass

The metallicity distribution of the different samples presented in Figure 9 suggest that the metal-rich nature of the planet host stars tend to disappear as the star evolves. This could be a remarkable result that needs to be analyzed very carefully as there

¹⁰ p -value of $\sim 10^{-5}$ for the SGWPs/GWPs comparison, and $\sim 10^{-6}$ for the LMSWPs/GWPs comparison

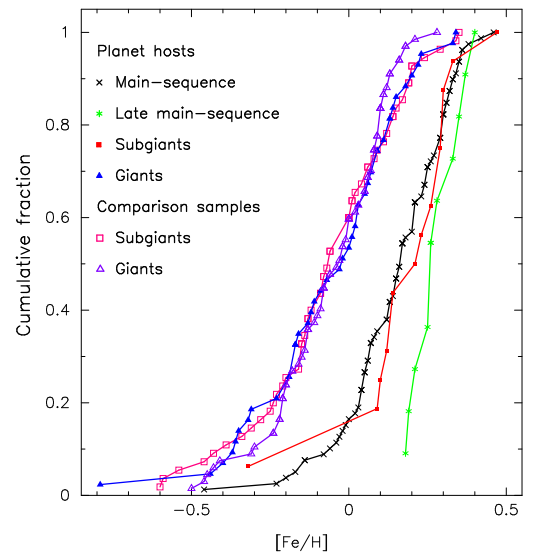


Fig. 9. Histogram of cumulative frequencies for the different samples studied in this work.

are obvious differences between the samples in terms of mass and age. Therefore, the data has been examined for correlations between mass and metallicity given that mass is the parameter which significantly varies between the giants (covering the mass range $\sim 1-3.8 M_{\odot}$) and the SGWP and LMSWP samples (restricted to the mass range $1-1.5 M_{\odot}$) (see also Table 6) and the MS samples. Figure 10 shows the [Fe/H]-Mass diagram of the stars analysed in this work, where the mass has been determined as explained in Section 2.4. A similar plot covering the $0.8-1.2 M_{\odot}$ mass range was presented by Fischer & Valenti (2005). Our data allow us to extend the plot up to $3.8 M_{\odot}$. A hint of a possible dependency of metallicity with stellar mass seems to appear in Figure 10 that could hinder the differences found for the giant stars with and without planets. Note that for stellar masses up to $\sim 1.6 M_{\odot}$ giant stars with and without planets are mixed showing a lot of scatter in the graph and covering the whole range of metallicities. However, a clear segregation in metallicity appears

Table 9. [Fe/H] statistics of the sample of giant stars separated in two ranges of mass.

Sample	Mean	Median	Deviation	Min	Max	N
$M_{\star} \leq 1.5 M_{\odot}$						
GWOPs	-0.12	-0.15	0.22	-0.50	+0.28	28
GWP	-0.19	-0.16	0.22	-0.79	+0.18	22
$M_{\star} > 1.5 M_{\odot}$						
GWOPs	-0.01	+0.00	0.11	-0.21	+0.21	39
GWP	+0.07	+0.09	0.15	-0.19	+0.34	21

above the $\sim 1.6 M_{\odot}$ stellar mass, the scatter in the metallicity axis is smaller and the giant stars with planets are located systematically on the metal rich part of the plot.

So, we find that for giant stars as a whole there is no correlation between the presence of giant planets and the metallicity of the star, but within the lack of correlation there seems to be hidden a dependency with the stellar mass. In the light of Figure 10 we have studied the metallicity distribution of the giant stars in the sample separated according to their mass, those under $1.5 M_{\odot}$ and those with larger masses. The $1.5 M_{\odot}$ mass value has been chosen so that a subsample of the giants cover the same mass range as the subgiant sample. The histograms of the distributions are shown in Figure 11, while some statistic diagnostics are given in Table 9. We find that the GWP and GWOP samples are clearly separated in metallicity when only stars with $M > 1.5 M_{\odot}$ are considered. A K-S test shows that the probability of GWP and GWOP to be drawn from the same parent population is p -value ~ 0.70 when considering only stars with $M_{\star} \leq 1.5 M_{\odot}$ ($D \sim 0.19$, $n_{\text{eff}} \sim 12.3$), while when considering the giants with masses larger than $1.5 M_{\odot}$, the K-S test probability diminishes significantly, p -value ~ 0.05 ($D \sim 0.35$, $n_{\text{eff}} \sim 13.7$).

As explained in Section 2.7, there are four GWP located further than 200 pc with significant negative metallicities, while there are no similar comparison stars beyond this distance. We note that these four stars fall in the mass domain $M_{\star} \leq 1.5 M_{\odot}$. It is important to check if these low-metallicity stars are biasing our GWP sample in such a way that they are preventing us to reproduce a planet-metallicity correlation in giants with $M_{\star} \leq 1.5 M_{\odot}$. If it was the case, removing these four stars should shift the GWP sample towards higher metallicities. If we repeat the K-S test for the GWP/GWOP samples within this mass domain, but removing these four stars, the p -value increases up to roughly 80% ($D \sim 0.19$, $n_{\text{eff}} \sim 11$). So even excluding these four low-metallicity stars, GWP and GWOP in the mass domain $M_{\star} \leq 1.5 M_{\odot}$ show a similar metallicity distribution. Therefore, the lack of a planet-metallicity correlation in this mass-domain is not related to the inclusion of GWP with low-metallicities located at larger distances.

A search for a correlation between [Fe/H] and stellar mass has been performed for the GWP sample. For the giant hosts with $M_{\star} > 1.5 M_{\odot}$ a Spearman's correlation test gives a probability of correlation of the order of 99%. A linear fit to the data has been done and it is shown in Figure 10 (continuous line). For the giant hosts with masses below $1.5 M_{\odot}$ there seems to be no correlation between metallicity and stellar mass, the probability of a non-correlation is around 0.24, in other words, the correlation is not significantly different from zero.

Fischer & Valenti (2005) found a correlation between metallicity and stellar mass in the $0.8-1.2 M_{\odot}$ mass domain. The authors, however, note that such trend does not seem to be real (i.e., it is not related to the properties of the stars) but instead "artificial", i. e. consequence of stellar evolution and the colour

and magnitude cuts used in planet search programs for targets selection. Johnson et al. (2010) also notices an artificial mass-metallicity correlation in a sample of 246 subgiants with stellar masses between $1.4-2.0 M_{\odot}$. It is difficult to firmly establish if a similar effect could be the reason for the metallicity-mass relationship found for GWP in the mass domain $M_{\star} > 1.5 M_{\odot}$, since the GWP sample is composed of stars selected in different planet search programmes with (probably) different criteria, sampling different regions of the HR diagram. The GWOP sample does not help since it is drawn from another source, the Massarotti et al. (2008) compilation. Nevertheless, most planet search programmes apply cuts in colours and magnitudes (see e.g. Johnson et al. 2006, Figure 1), so we cannot rule out the possibility that the mass-metallicity relation in $M_{\star} > 1.5 M_{\odot}$ could be related to selection effects.

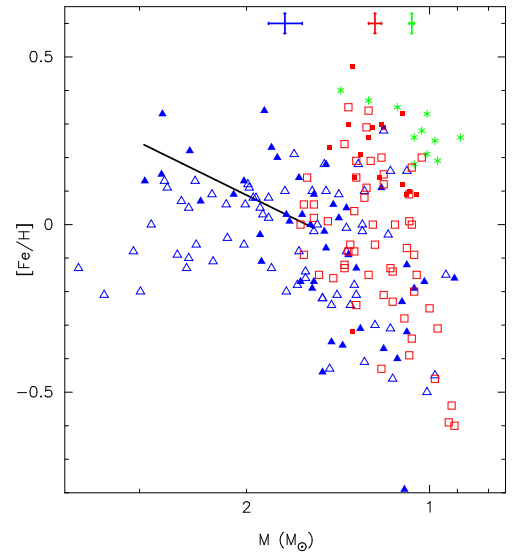


Fig. 10. Stellar metallicity, [Fe/H], as a function of the stellar mass. A linear fit to the data is shown to GWP with $M_{\star} > 1.5 M_{\odot}$ (continuous line). Typical uncertainties in metallicities and stellar masses are also shown. Colours and symbols are the same as in previous figures.

3.3. Metallicity as a function of the Stellar Radius

In subgiant stars, the envelope is still cooling and expanding, in part at the expense of the energy being supplied by the hydrogen burning-shell, and they do not become fully convective until they reach the base of the red giant branch ascending track on the HR diagram. Giant stars, on the other hand, have fully convective envelopes. Therefore they both offer an unique opportunity to test the pollution hypothesis of planet formation. Within this scenario, high stellar metallicity of planet hosts is simply produced as a consequence of the accretion of gas depleted material on the convective zone of the star (Gonzalez 1997; Laughlin & Adams 1997). Given that in this framework the metallicity would be confined to the convective zone in MS stars, only the external layers are affected. It is thus expected that the metallicity signature would be lost as the star evolves and the external metal-rich layers are gradually diluted when the convective zone penetrates the envelope. So late-stage accretion of material would produce several observables and a tendency to systematically lower metallicities would be expected as the

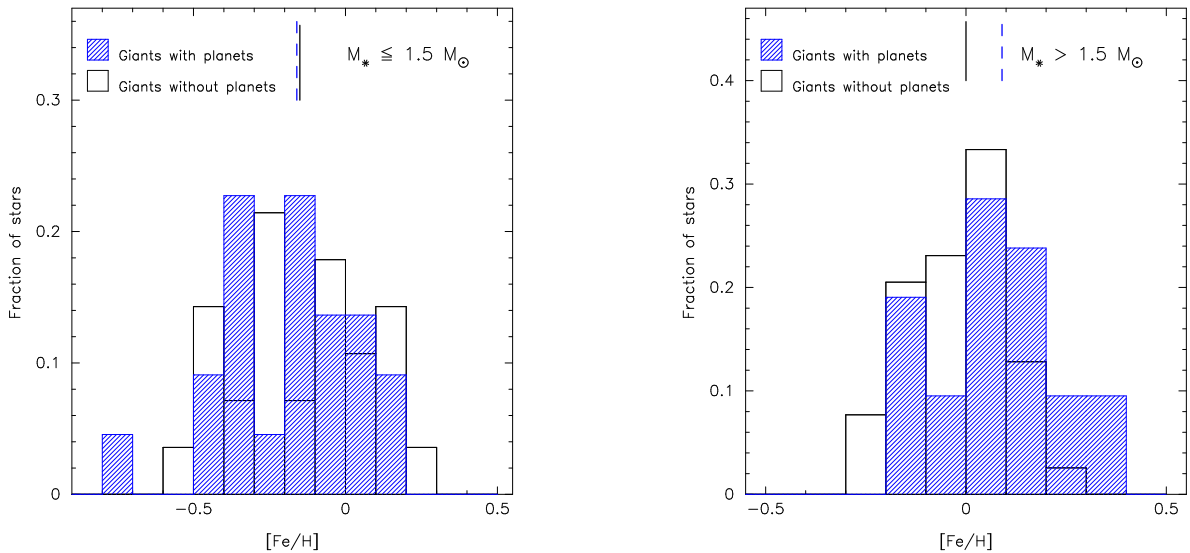


Fig. 11. Left: Normalised metallicity distribution of the GWP sample (blue histogram) versus giant stars without known planets for stars with $M_* \leq 1.5 M_\odot$. Right: Normalised metallicity distribution of the GWP sample (blue histogram) versus giant stars without known planets for stars with $M_* > 1.5 M_\odot$. Median values of the distributions are shown with vertical lines.

star evolves from the main sequence to the subgiant stage and finally up the red giant phase. A way to disentangle the metallicity signature with evolution is exploring if there is any dependency with the radius of the star.

The stellar metallicity as a function of the stellar radius for the GWP and GWOP samples is shown in Figure 12. The stellar radius have been computed as explained in Section 2.4. Different colours and symbols are used for stars with masses lower than $1.5 M_\odot$ and stars with masses greater than $1.5 M_\odot$. Besides the expected trend towards larger radius as the stellar sample considered is more evolved, no other obvious trend is apparent in Figure 12. A very mild trend of decreasing metallicities with increasing stellar radius for GWPs with $M_* \leq 1.5 M_\odot$ is doubtful as it disappears if we remove the 3 stars with the largest radius (94% and 95% Pearson and Spearman tests respectively).

When considering the GWPs with masses greater than $1.5 M_\odot$ only, no correlation between metallicity and radius is found. The probabilities of non-correlation are ~ 0.26 (Pearson's test), ~ 0.14 (Spearman's test).

3.4. Other Chemical Signatures

In order to try to disclose differences in the abundances of other chemical elements besides Iron we show in Figure 13 the cumulative distribution $[X/Fe]$ comparing the abundances $[X/Fe]$ (where X represents Na, Mg, Al, Si, Ca, Sc, Ti I, Ti II, V, Cr I, Cr II, Mn, Co, Ni, and Zn), between GWPs and GWOPs. On the left panel the distributions for giants with masses $M_* \leq 1.5 M_\odot$ are shown, while on the right panel we show the giants with masses $M_* > 1.5 M_\odot$. Some statistic diagnostics are shown in Table 10, where the results of a K-S test for each ion are also listed.

For giants in the mass domain $M_* \leq 1.5 M_\odot$ a similar behaviour between planets hosts and stars without planets is found. From the 15 chemical species analysed, in eight the K-S probabilities are considerably high ($\geq 70\%$), specially when considering Na, Ni, and Ca. In the rest, although the probabilities are not high, they are not significant low to state a difference between GWPs and GWOPs. The only remarkable exception is Si,

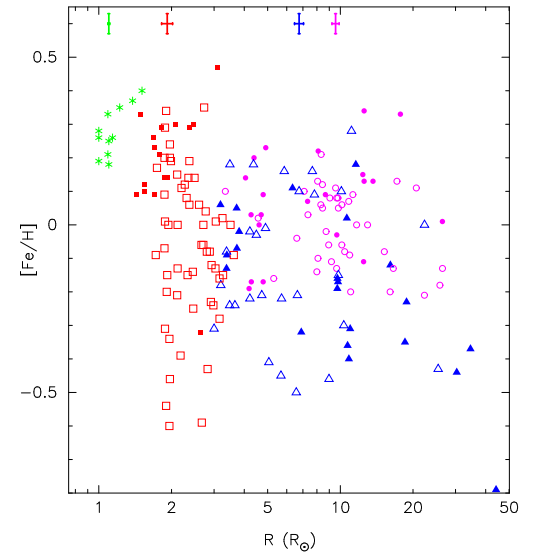


Fig. 12. Stellar metallicity, $[Fe/H]$, as a function of the stellar radius. Colours and symbols are the same as in previous figures for LMSWP, SGWP, and SGWOP samples. Giants with $M_* \leq 1.5 M_\odot$ are plotted in blue triangles, while giants with $M_* > 1.5 M_\odot$ are shown with purple circles. In both cases filled symbols indicate planet hosts. Typical uncertainties in metallicities and stellar radius are also shown.

for which the GWPs distribution seems to be slightly shifted towards higher abundances.

For stars with $M_* > 1.5 M_\odot$, there are significant differences between planets hosts and stars without planets in three species namely, Na (GWPs showing slightly lower abundances) and Co and Ni where abundances of GWPs seem to be higher than the ones of GWOPs. However, GWPs and GWOPs show very similar behaviours in Cr I and Al.

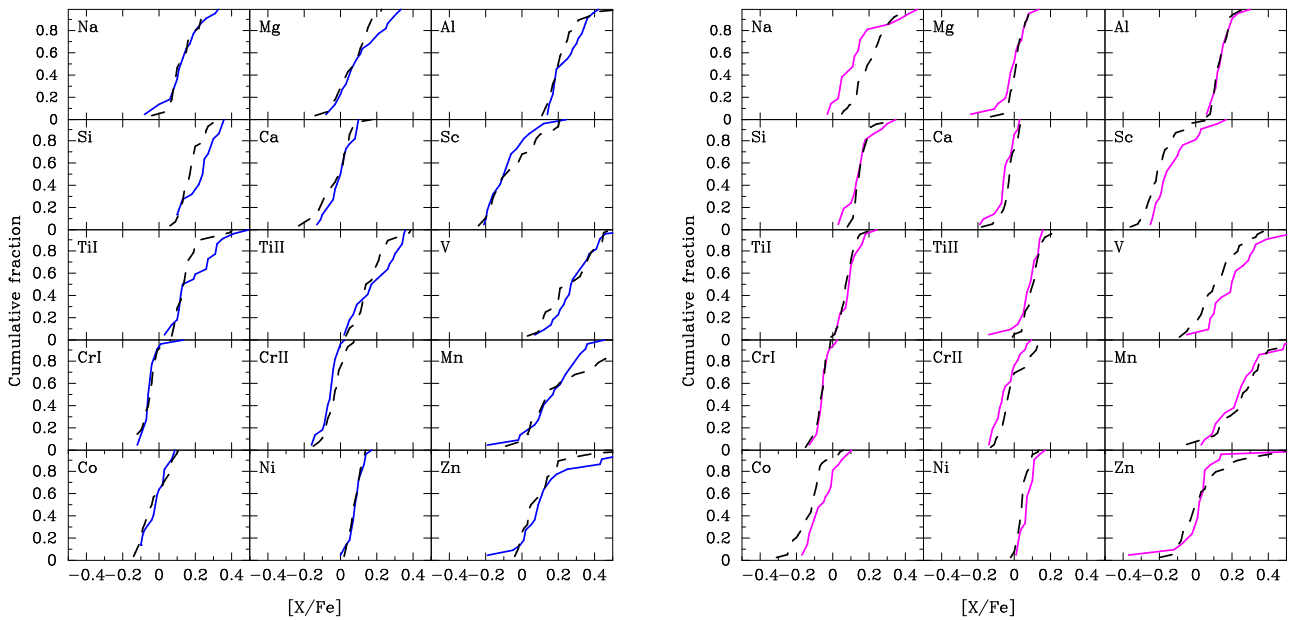


Fig. 13. $[X/Fe]$ cumulative fraction of GWPs and GWOPs. Left: Stars with $M_\star \leq 1.5 M_\odot$, GWPs (blue continuous line) against GWOPs (black dashed line). Right: Stars with $M_\star > 1.5 M_\odot$, GWPs (purple continuous line) against GWOPs (black dashed line).

The question of whether main-sequence planet hosts show (or not) over-abundances of refractory elements¹¹ is still open (see e.g. Adibekyan et al. 2012, and references therein). An overabundance of refractory elements with respect to volatiles in main-sequence planet hosts is considered as a possible sign of late-stage accretion, a tendency that is expected to disappear during the star evolution towards the red-giant phase.

We find that GWPs show similar abundance patterns in all the elements analysed to that of GWOPs in the mass domain $M_\star \leq 1.5 M_\odot$. We do not know whether this is due to *i*) mixing processes which diluted the refractory enrichment previously suffered by the stars' progenitors; or because *ii*) pollution played a rather little role, so the GWPs progenitors never showed overabundance of refractory elements. On the other hand, for masses larger than $1.5 M_\odot$, GWPs and GWOPs show differences in some elements, specially Na, Co, and Ni.

3.5. Age-Metallicity Relation

In the light of the metallicity trends with stellar mass found within the giant stars sample it is reasonable to explore a possible age-metallicity relation. In Figure 14 we show the stellar age versus its metallicity of the different samples analyzed in this work. For comparison, main-sequence hosts from VF05 are overplotted with VF05 $[Fe/H]$ values set into our metallicity scale as explained in Section 2.6. In addition, the stellar ages of these stars have been recomputed using the methodology followed in this work (Section 2.4). Two clear trends can be identified in Figure 14. To the left of the plot are located the giant stars with masses $M_\star > 1.5 M_\odot$ stars, and to the right of the plot all the other stars studied. The plot shows the expected trend in metallicity with stellar ages. As the population is older the metallicity have a tendency to show a larger spread in values.

Table 10. Comparison between the elemental abundances of GWPs and GWOPs.

$[X/Fe]$	$M_\star \leq 1.5 M_\odot$					
	GWPs		GWOPs		K-S test [†]	
	Median	Deviation	Median	Deviation	p-value	D
Na	0.12	0.10	0.12	0.08	0.96	0.14
Mg	0.09	0.12	0.09	0.09	0.39	0.25
Al	0.24	0.09	0.21	0.10	0.42	0.24
Si	0.25	0.09	0.18	0.06	0.04	0.39
Ca	0.00	0.07	0.01	0.09	0.90	0.16
Sc	-0.10	0.12	-0.07	0.14	0.75	0.19
Ti I	0.16	0.13	0.14	0.08	0.17	0.30
Ti II	0.19	0.12	0.16	0.09	0.30	0.27
V	0.28	0.14	0.29	0.14	0.71	0.19
Cr I	-0.06	0.06	-0.05	0.05	0.86	0.17
Cr II	-0.05	0.05	-0.03	0.05	0.18	0.30
Mn	0.18	0.15	0.14	0.20	0.26	0.28
Co	-0.02	0.06	-0.04	0.08	0.87	0.16
Ni	0.09	0.04	0.09	0.03	0.96	0.14
Zn	0.10	0.20	0.07	0.17	0.71	0.19

[†] $n_{\text{eff}} \sim 12.3$

$[X/Fe]$	$M_\star > 1.5 M_\odot$					
	GWPs		GWOPs		K-S test [‡]	
	Median	Deviation	Median	Deviation	p-value	D
Na	0.12	0.14	0.21	0.09	0.01	0.42
Mg	0.00	0.08	0.02	0.05	0.73	0.18
Al	0.14	0.06	0.13	0.05	0.95	0.14
Si	0.15	0.08	0.15	0.05	0.66	0.19
Ca	-0.05	0.06	-0.02	0.05	0.06	0.34
Sc	-0.16	0.12	-0.21	0.10	0.11	0.32
Ti I	0.09	0.06	0.08	0.05	0.59	0.20
Ti II	0.09	0.07	0.11	0.05	0.70	0.18
V	0.20	0.15	0.11	0.12	0.04	0.36
Cr I	-0.05	0.03	-0.06	0.03	0.98	0.12
Cr II	-0.06	0.07	-0.03	0.08	0.24	0.27
Mn	0.24	0.15	0.26	0.15	0.84	0.16
Co	-0.05	0.08	-0.11	0.08	0.02	0.40
Ni	0.07	0.04	0.05	0.04	0.01	0.41
Zn	0.02	0.22	0.02	0.16	0.49	0.22

[‡] $n_{\text{eff}} \sim 13.7$

¹¹ Elements with condensation temperatures near or above the condensation temperature of iron.

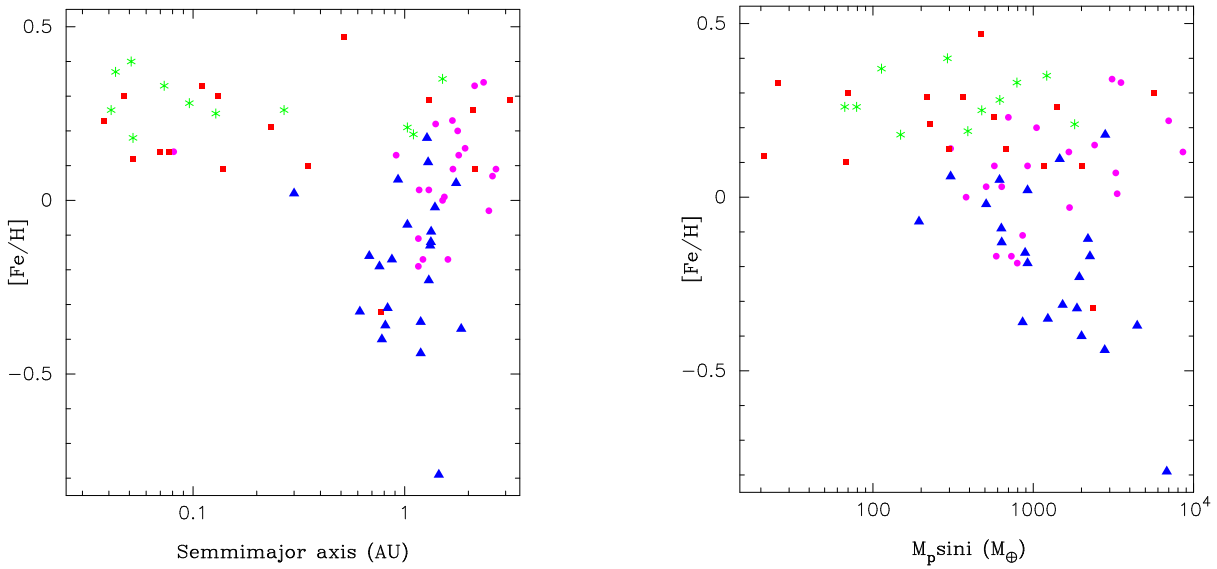


Fig. 15. Left: Stellar metallicity as a function of the semimajor axis of the innermost planet. Right: Stellar metallicity as a function of the mass of the most massive planet. GWPs with $M_\star > 1.5 M_\odot$ are plotted with purple circles, GWPs less massive than $1.5 M_\odot$ in blue triangles, SGWPs as red squares, while LMSWPs are plotted as green asterisks.

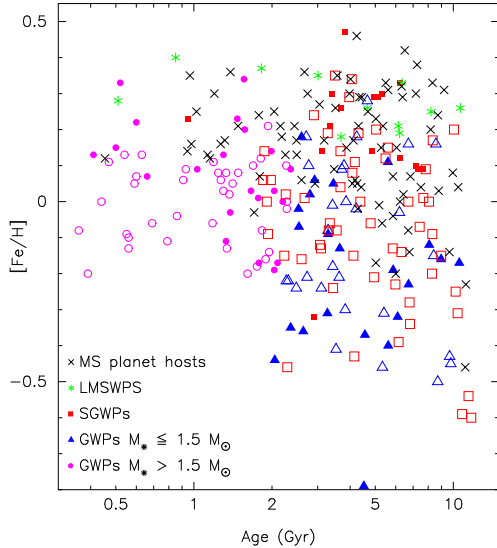


Fig. 14. Age-metallicity relation for the different samples studied in this work. Open symbols indicate the corresponding comparison samples.

3.6. Trends with the planetary properties

Studies around MS stars have revealed that the metal signature on the star seems to influence the maximum mass of the planet that can be formed (Mayor et al. 2011). It has been shown that the planet deficiency at small orbital distances found around red giant stars (see also Johnson et al. 2007; Sato et al. 2008; Wright et al. 2009) can be explained by tidal interactions in the star-planet system as the star evolves off the main-sequence, which can lead to variations in the planetary orbits and to the engulfment of close-in planets (Villaver & Livio 2009). The planet accretion process can lead to a transfer of angular momentum to the stellar envelope which ultimately can spin up the star and even indirectly modify its chemical abundances. Possible evidence of this process has been recently found (see e.g. Adamów et al. 2012). Furthermore, Carlberg et al. (2012)

analysed a sample of slow and rapid RGB rotators and found lithium enrichment on the rapid rotators consistent with planet accretion onto the stellar envelope.

In order to disclose any possible trends on the planet properties among the stellar samples studied in this work we show on the left panel of Figure 15 the stellar metallicity versus the orbital distance of the planet and on the right panel the stellar metallicity as a function of the mass of the more massive planet¹². The planets on our sample follow the general trend mentioned above, that is, nearly all planets orbiting GWPs are cool distant ($a > 0.5$ AU) gaseous jupiters, with the only exception of HIP 57820 (which hosts a close-in Jupiter at a ~ 0.08 AU) and HIP 114855 ($a = 0.3$ AU). Regarding the planet-mass metallicity relation (right panel) there seems to be a trend of decreasing metallicities as we move towards higher planetary masses. A Spearman correlation test provides a likelihood of correlation of 96%. This appears to be in contradiction with the known trends of main-sequence FGK hosts in which a positive correlation between the metallicity of the host star and the mass of its most massive planets is found (Mayor et al. 2011; Sousa et al. 2011). A closer inspection of the metallicity-planetary mass plane reveals that this general tendency is due to the GWPs stars less massive than $1.5 M_\odot$. Considering only these stars, the likelihood of a correlation is $\sim 99\%$ (Spearman's test). On the other hand, there is no obvious correlation when considering the other samples. The behaviour of LMSWPs and SGWPs is more or less flat, while for GWPs with $M_\star > 1.5 M_\odot$ there seems to be a hint of increasing metallicities with increasing planetary masses (a Spearman's test gives a probability of correlation of $\sim 91\%$). In other words, subgiants and high-mass giants reproduce the known trends for main-sequence hosts, while giants in the low-mass domain show a behaviour which is hard to understand.

Next, we explore the planet properties among the different samples. It has been suggested that giant stars host more-massive planets than main-sequence hosts (e.g. Johnson et al. 2007; Lovis & Mayor 2007). A comparison of the cumulative

¹² $M_p \sin i$, with the exceptions of the planets orbiting around the stars GSC 2883 -01687, HIP 80838, TrES-4, and HAT-P-7, detected by transits.

frequency of planet mass¹³ between our sample of GWP s and main-sequence stars from VF05 hosting exclusively giant planets reveals that the distribution of the former is clearly shifted towards higher masses. While main-sequence hosts spread a planetary mass range from 0.1 to 18 M_{Jup} with a median value of 1.9 M_{Jup} , our sample of GWP s covers from 0.6 to 22 M_{Jup} with a median value of 3.3 M_{Jup} . A K-S test shows that both distributions are statistically different within a confidence level of 98% (p -value $\sim 10^{-3}$). This result should be interpreted very carefully, since the larger levels of jitter in evolved stars might prevent the detection of lower mass planets shifting the planet mass distribution towards larger values. No obvious segregation either in mass nor in orbital distance is found among the planets orbiting giant stars with different masses.

Regarding multiplicity, we find a rate of multi-planet systems in GWP s of the order of 12% which is in agreement with the 14% multiple confirmed planetary systems given by Wright et al. (2009) although it could be 28% or higher if those cases with significant evidence of being multiple are included. Finally, no correlation between the stellar metallicity and the planet's eccentricity was found, although as pointed out by Johnson et al. (2008) we note that the eccentricity distribution of GWP s seems to be shifted towards lower values than the eccentricity distribution of main-sequence hosts. While the median eccentricity in GWP s is 0.15, in main-sequence hosts is around 0.25. A K-S test reveals both distributions to be different (p -value $\sim 10^{-3}$).

Planets in the SGWP sample are predominantly cool, although around 30% of the stars host a hot-Jupiter at a distance closer than 0.1 AU. In addition, two of our stars in the SGWP sample host low-mass planets ($M_p < 30 M_{\oplus}$), namely HIP 94256, and HIP 115100. When considering the LMSWP sample, roughly 50% of the stars harbour at least one hot-Jupiter, while the other 50% only host cool distant planets. HIP 98767 hosts two planets, being the innermost one a low-mass planet.

4. Discussion

As pointed out in Section 3.1, we find that the metal distribution of subgiant stars with planets is clearly separated from that of subgiants without planets, and that it is similar to the one of MS stars with planets. Considering the whole sample of giant stars (i.e. without mass segregation) we do not find a difference in the metal distribution of giant stars that host planets when compared with giant stars where no planetary systems have been detected. While the metallicity distribution of the subgiants fit well within the current paradigm of planet formation, the giant stars results are harder to understand within this context.

One could argue that the metallicity signature of planet formation disappears at the moment the star evolves into red giant branch. The M_{bol} criterion chosen to separate the subgiant from the giant sample physically reflects the time at which the star becomes fully convective. At this point, three lines of arguments could be followed: i) there was not metal difference between the stars bearing planets and stars with no planets in this sample of giant stars, ii) there was a different metallicity but has been lost, iii) the sample is biased in such a way that prevent us from seeing any metallicity difference.

¹³ We take as reference the innermost planet in multiple systems since radial velocity surveys are more sensitive to close-in, massive planets.

Can massive proto-planetary disks explain the observed trends?

Lets explore the first possibility, i. e. that the giant stars represent a different stellar population in which a metal rich environment is not required for planet formation. The red giant stars that constitute our GWP sample are the result of the evolution of early-type main-sequence dwarfs. If we go back in time on the evolutionary tracks, the stars in the GWP sample are the result of the evolution of main-sequence dwarfs with effective temperatures in the range 5500 - 12000 K, (spectral-types G5V-B8V, and stellar masses between 0.9 and 4 M_{\odot}). On the other hand, SGWP s come mainly from G5V-F0V (M_{\star} between 0.9 and 1.6 M_{\odot}), while stars in the LMSWP sample come from less massive stars with spectral types in the range K2V-F2V. It is therefore natural to ask whether the observed differences in the metallicity distribution of the different samples are related to the different mass distributions of the star's progenitors in the main-sequence (e.g. Ghezzi et al. 2010a). In principle, high-mass stars are likely to harbour more massive protoplanetary disks (e.g. Natta et al. 2000, see also Fig. 5 in Williams & Cieza 2011). Observations of H_{α} EWs in young, low-mass objects suggest that the mass accretion rate scales approximately with the square of the stellar mass (Muñoz et al. 2003; Natta et al. 2004; Mendigutía et al. 2011, 2012), a result which can be reproduced assuming that a relationship between the disk mass and the central star mass on the form $M_{\text{disk}} \propto M_{\star}^{1.2}$ holds (Alibert et al. 2011).

According to recent simulations of planet population synthesis (Alibert et al. 2011; Mordasini et al. 2012), protoplanetary disk masses play a significant role in planet formation. In particular, it is shown that giant planet formation can occur in low-metallicity (low dust-to gas ratio) but high-mass protoplanetary disks. The metallicity effect depends on the mass of the disc, being the minimum metallicity required to form a massive planet correspondingly lower for massive stars than for low-mass stars. In this scenario, the fact that GWP s do not show the metal-rich signature, could be explained by the more massive protoplanetary disks of their progenitors. However, several difficulties arise.

One of the consequences of the protoplanetary disk mass on planet formation is that planets orbiting massive giant stars should be more massive than planets around dwarf stars. However, as already mentioned in Section 3.6, one should be careful in the comparison between planets around giants and MS stars, given that the detections are affected from biases introduced by the star. The samples of giant stars with different masses are however suitable for this comparison and we find that there is not obvious difference on the minimum mass of the planet found between the low mass and the high mass giant stars.

Second, core-accretion models are not able to predict the presence of very massive companions around very-low metallicity stars, and moreover around stars that did not suppose to have a massive disk to begin with (giants with $M_{\star} \leq 1.5 M_{\odot}$). Although those planets are rare, we note that there are some of them in our GWP sample, such as the two companions around BD+20 2457 ([Fe/H]=-0.79 dex, planets of 21.4 M_{Jup} at 1.5 AU, and 12.5 M_{Jup} at 2.0 AU), the planet around γ^1 Leo ([Fe/H]=-0.44 dex, planet of $\sim 8 M_{\text{Jup}}$ at 1.2 AU), or the one orbiting HD 13189 ([Fe/H]=-0.37 dex, planet of $\sim 14 M_{\text{Jup}}$ at 2 AU). This is because the time needed to form a core big enough to start a runaway accretion of gas is so long that by that time the gas has already been significantly depleted.

But the most intriguing point is the mass-segregation found for GWP s (Section 3.2). While the metallicity distribution of GWP s in the mass-domain $M_{\star} > 1.5 M_{\odot}$ is shifted towards

higher metallicities with respect to a similar sample of giants without planets, GWP in the mass range $M_\star \leq 1.5 M_\odot$ do not show the metal signature of the presence of planets. This is a puzzling result, at least in two ways. First, if planet formation can occur in low-metal, but high protoplanetary disk masses environments, a population of massive giant stars with low metallicities hosting planets might be expected. Our observations show somehow the opposite, massive ($M_\star > 1.5 M_\odot$) giant stars with planets show high-metallicities.

Second, it is worth to note that the sample of less massive ($M_\star \leq 1.5 M_\odot$) giant stars with planets covers the same mass range as the MS progenitors and subgiant stars where the metal signature has been observed. In other words, the protoplanetary disks of GWPs and $M_\star \leq 1.5 M_\odot$ are not massive, and thus, there is nothing to help planet formation at low metallicities. Furthermore, there is no age difference between this sample of stars and the MS or subgiants stars. Thus, the fact that giant stars with $M_\star \leq 1.5 M_\odot$ and planets are not more metal rich is hard to understand as it is in apparent contradiction with the trademark of the core-accretion model.

Can the metallicity signature be erased as the star evolves?

If we accept the possibility that giant stars do not favour the existence of a metal poor environment for planet formation, then we have to explore the option that the metallicity signature was present at the time the planet was formed but then disappeared as a consequence of the evolution of the star. Gonzalez (1997, see also Lin et al. 1996) explain the metal content of planet host stars as a consequence of the accretion of gas depleted material in the stellar surface, the so-called pollution scenario. In this scenario, only the external layers of the stars are affected, and as the star evolves, the external metal-rich layers are gradually diluted as the convective zone of the star grows.

Our data does not support evidence of pollution. If the metal-rich signature was limited to the convective envelope of the stars, subgiants with planets should show lower metallicities than main-sequence hosts. We find the opposite, with SGWP and main-sequence planet host samples showing the same chemical signature (Section 3.1). Furthermore, the different metallicity behaviour of GWPs depending on their masses is again difficult to understand in the pollution scenario. There is no physical reason why the metal-rich nature of the star would be lost due to convection only for giant stars with $M_\star \leq 1.5 M_\odot$, remaining for giants with $M_\star > 1.5 M_\odot$. The metallicity-stellar radius relation does not shed any light into this issue as $M_\star \leq 1.5 M_\odot$ giant stars cover the same range on stellar radius as the $M_\star > 1.5 M_\odot$ stars.

Is our sample biased?

Other lines of arguments such as the one suggested by Haywood (2009) in which the observed correlation between the presence of gas-giant planets and enhanced stellar metallicity observed in main-sequence planet hosts, might be related to a possible inner disk origin of these stars does not fit the data either. In this scenario, the observed metallicity distribution of GWPs would be shifted towards lower metallicities with respect to the one of main-sequence hosts, just simply because the GWP sample contains stars younger than the dwarf sample and, therefore, less contaminated by radial mixing. Nevertheless, according to this scenario, giant stars with planets and high-masses ($M_\star > 1.5 M_\odot$) should not be metal-rich.

The possible biases affecting our sample have been explored in the paper. We have found no biases in age, mass, population, or distance that could explain our results. However, an option that we cannot exclude is the risk of the sample size being small. To fix this issue we will have to wait for more planet discoveries to take place.

4.1. Mass segregation and previous results

We should finally discuss how the mass-segregation found for GWPs in this work compares with previous results on evolved stars with planets. It is worth to note that most of the stars included in previous works are in the mass-domain $M_\star \leq 1.5 M_\odot$, where the metal-rich signature of planet hosts is lost. Specifically, the number of low-mass giants in each work are: 2 out the 4 stars analyzed in Sadakane et al. (2005); 1/1 in Schuler et al. (2005); 7/10 in Pasquini et al. (2007); and 7/16 in Ghezzi et al. (2010a). However, among the 20 giants included in Hekker & Meléndez (2007), 11 are high-mass ($M_\star > 1.5 M_\odot$) giants. The fact that GWPs in the high-mass domain show metal enrichment, while less-massive giants do not, could explain the disagreement between Hekker & Meléndez (2007) and other works. We note, however, that Takeda et al. (2008) do not found metal-enrichment in GWPs, despite the fact of 7 out of the 10 stars analyzed in that work are in the high-mass domain.

5. Conclusions

Evolved stars (subgiants and red giants) with planets constitute valuable tools to set constraints into our understanding on how planetary systems do form and evolve. Nowadays, an increasing effort is being applied in searching for planetary companions around this kind of stars. In addition, the properties of evolved stars with planets, and also the properties of the planets found around these stars seem to be different from which we already know for main-sequence planet hosts. In this work, we perform an analysis of the stellar properties and elemental abundances of a large sample of evolved stars. Although data from the literature has been used to expand the SGWOP sample, our analysis has, to our best knowledge, the best combination between homogeneity and sample size discussed so far. In addition, a detailed analysis of the stellar samples properties is performed in order to avoid any bias which could affect our results.

We find that, unlike the case of main-sequence hosts, planets around giant stars are not preferentially found around metal-rich stars when the whole sample of giant stars is analyzed. The metallicity distribution of GWPs is clearly shifted towards lower values in comparison with SGWPs and LMSWPs. Taken into account the homogeneous procedure followed in this work, and the fact that we are mainly dealing with solar-type stars, we state that the differences in the metallicity distributions are real and not due to non-LTE effects.

Subgiant stars show the same metal trends with planets as MS stars and also have a similar mass range. In an attempt to understand if the more massive stars within the giant sample are shifting the metal distribution of the GWP towards lower metallicities, we segregated the giant stars in two mass bins, $M_\star \leq 1.5 M_\odot$ and $M_\star > 1.5 M_\odot$. It is shown for the first time that the metallicity distribution of the more massive giant stars with planets is shifted towards higher metallicities, as it is the one for the MS and subgiant stars.

The metal signature of the presence of planets is lost, however, for stars in the $M_\star \leq 1.5 M_\odot$ range, a fact which is difficult to understand with current models of planet formation.

These stars show a similar range of stellar parameters than subgiant and main-sequence planet hosts but, do not show the metal-enrichment signature. In particular, giants with $M_{\star} \leq 1.5 M_{\odot}$ show a similar age distribution than subgiants and main-sequence hosts, ruling out radial mixing as a possible explanation of their metallicity distribution. Since they also show similar masses, a planet formation scenario in which low-metallicity environments are compensated by higher-mass protoplanetary disks, can be also discarded. Taken into account that no bias that could affect the metallicity distribution of low-mass giant hosts has been identified, the only explanation points towards a non-primordial origin of the metallicity-gas giant planet relationship. We have, however, not found clear evidence of pollution and furthermore, what is more intriguing, why convection should play a role erasing the metal signature for giants in the mass domain $M_{\star} \leq 1.5 M_{\odot}$, and not for giants with $M_{\star} > 1.5 M_{\odot}$?

Additional differences between giants with masses $\leq 1.5 M_{\odot}$ and more massive giants have been found when analysing the abundance patterns of different elements. While in the case of the less-massive giants, planet hosts and non-planet hosts show similar abundance patters, in the more massive stars there are differences in some elements between stars hosting planets and stars without known planets, specially in the cases of Na, Co, and Ni abundances.

Finally, we note that planets around evolved stars show some peculiarities with respect to the planets orbiting around main-sequence stars, like a lack of close-in planets or higher masses and eccentricities. The data also suggest a decreasing trend between the stellar metallicity and the mass of the most massive planet.

Acknowledgements. This work was supported by the Spanish Ministerio de Ciencia e Innovación (MICINN), Plan Nacional de Astronomía y Astrofísica, under grant AYA2010-20630 and AYA2011-26202. J.M. acknowledges support from the Universidad Autónoma de Madrid (Department of Theoretical Physics). E. V. also acknowledges the support provided by the Marie Curie grant *FPT-People-RG268111*. The authors would like to thank Robert. L. Kurucz, Sergio Sousa, Yoichi Takeda, and Léo Girardi, for making their codes publicly available. Jean Schneider is also acknowledged for maintaining the Extrasolar Planets Encyclopedia. We sincerely appreciate the careful reading of the manuscript and the constructive comments of an anonymous referee.

References

- Adamów, M., Niedzielski, A., Villaver, E., Nowak, G., & Wolszczan, A. 2012, ApJ, 754, L15
- Adibekyan, V. Z., Santos, N. C., Sousa, S. G., & Israelián, G. 2011, A&A, 535, L11
- Adibekyan, V. Z., Santos, N. C., Sousa, S. G., et al. 2012, A&A, 543, A89
- Alibert, Y., Mordasini, C., & Benz, W. 2004, A&A, 417, L25
- Alibert, Y., Mordasini, C., & Benz, W. 2011, A&A, 526, A63
- Arenou, F., Grenon, M., & Gomez, A. 1992, A&A, 258, 104
- Asplund, M., Grevesse, N., Sauval, A. J., & Scott, P. 2009, ARA&A, 47, 481
- Baumann, P., Ramírez, I., Meléndez, J., Asplund, M., & Lind, K. 2010, A&A, 519, A87
- Beirão, P., Santos, N. C., Israelián, G., & Mayor, M. 2005, A&A, 438, 251
- Bensby, T., Feltzing, S., & Lundström, I. 2003, A&A, 410, 527
- Bensby, T., Feltzing, S., Lundström, I., & Ilyin, I. 2005, A&A, 433, 185
- Bergemann, M., Lind, K., Collet, R., & Asplund, M. 2011, Journal of Physics Conference Series, 328, 012002
- Carlberg, J. K., Cunha, K., Smith, V. V., & Majewski, S. R. 2012, ApJ, 757, 109
- Casagrande, L., Ramírez, I., Meléndez, J., Bessell, M., & Asplund, M. 2010, A&A, 512, A54
- Castelli, F. 2005, Memorie della Società Astronomica Italiana Supplementi, 8, 44
- da Silva, L., Girardi, L., Pasquini, L., et al. 2006, A&A, 458, 609
- Dehnen, W. & Binney, J. J. 1998, MNRAS, 298, 387
- Fischer, D. A. & Valenti, J. 2005, ApJ, 622, 1102
- Flower, P. J. 1996, ApJ, 469, 355
- Frandsen, S. & Lindberg, B. 1999, in Astrophysics with the NOT, ed. H. Karttunen & V. Piironen, 71
- Frink, S., Mitchell, D. S., Quirrenbach, A., et al. 2002, ApJ, 576, 478
- Fuhrmann, K. 1998, A&A, 338, 161
- Fuhrmann, K. 2004, Astronomische Nachrichten, 325, 3
- Ghezzi, L., Cunha, K., Schuler, S. C., & Smith, V. V. 2010a, ApJ, 725, 721
- Ghezzi, L., Cunha, K., Smith, V. V., et al. 2010b, ApJ, 720, 1290
- Ghezzi, L., Cunha, K., Smith, V. V., & de la Reza, R. 2010c, ApJ, 724, 154
- Gilli, G., Israelián, G., Ecuvillon, A., Santos, N. C., & Mayor, M. 2006, A&A, 449, 723
- Girardi, L., Bressan, A., Bertelli, G., & Chiosi, C. 2000, A&AS, 141, 371
- Gonzalez, G. 1997, MNRAS, 285, 403
- Gonzalez, G. 2011, MNRAS, 416, L80
- González Hernández, J. I. & Bonifacio, P. 2009, A&A, 497, 497
- González Hernández, J. I., Delgado-Mena, E., Sousa, S. G., et al. 2013, ArXiv e-prints
- González Hernández, J. I., Israelián, G., Santos, N. C., et al. 2010, ApJ, 720, 1592
- Haywood, M. 2008a, A&A, 482, 673
- Haywood, M. 2008b, MNRAS, 388, 1175
- Haywood, M. 2009, ApJ, 698, L1
- Hekker, S. & Meléndez, J. 2007, A&A, 475, 1003
- Høg, E., Fabricius, C., Makarov, V. V., et al. 2000, A&A, 355, L27
- Israelián, G., Delgado Mena, E., Santos, N. C., et al. 2009, Nature, 462, 189
- Johnson, J. A., Aller, K. M., Howard, A. W., & Crepp, J. R. 2010, PASP, 122, 905
- Johnson, J. A., Clanton, C., Howard, A. W., et al. 2011, ApJS, 197, 26
- Johnson, J. A., Fischer, D. A., Marcy, G. W., et al. 2007, ApJ, 665, 785
- Johnson, J. A., Marcy, G. W., Fischer, D. A., et al. 2006, ApJ, 652, 1724
- Johnson, J. A., Marcy, G. W., Fischer, D. A., et al. 2008, ApJ, 675, 784
- Kharchenko, N. V., Scholz, R.-D., Piskunov, A. E., Röser, S., & Schilbach, E. 2007, Astronomische Nachrichten, 328, 889
- Kurucz, R. 1993, ATLAS9 Stellar Atmosphere Programs and 2 km/s grid. Kurucz CD-ROM No. 13. Cambridge, Mass.: Smithsonian Astrophysical Observatory, 1993., 13
- Laughlin, G. & Adams, F. C. 1997, ApJ, 491, L51
- Lin, D. N. C., Bodenheimer, P., & Richardson, D. C. 1996, Nature, 380, 606
- Lind, K., Bergemann, M., & Asplund, M. 2012, MNRAS, 427, 50
- Lovis, C. & Mayor, M. 2007, A&A, 472, 657
- Luck, R. E. & Heiter, U. 2007, AJ, 133, 2464
- Maldonado, J., Eiroa, C., Villaver, E., Montesinos, B., & Mora, A. 2012, A&A, 541, A40
- Maldonado, J., Martínez-Arnáiz, R. M., Eiroa, C., Montes, D., & Montesinos, B. 2010, A&A, 521, A12
- Mashonkina, L., Gehren, T., Shi, J.-R., Korn, A. J., & Grupp, F. 2011, A&A, 528, A87
- Massarotti, A., Latham, D. W., Stefanik, R. P., & Fogel, J. 2008, AJ, 135, 209
- Mayor, M., Marmier, M., Lovis, C., et al. 2011, ArXiv e-prints
- Mayor, M. & Queloz, D. 1995, Nature, 378, 355
- Mendigutía, I., Calvet, N., Montesinos, B., et al. 2011, A&A, 535, A99
- Mendigutía, I., Mora, A., Montesinos, B., et al. 2012, A&A, 543, A59
- Montes, D., López-Santiago, J., Gálvez, M. C., et al. 2001, MNRAS, 328, 45
- Mordasini, C., Alibert, Y., Benz, W., Klahr, H., & Henning, T. 2012, A&A, 541, A97
- Muzerolle, J., Hillenbrand, L., Calvet, N., Briceño, C., & Hartmann, L. 2003, ApJ, 592, 266
- Natta, A., Grinin, V., & Mannings, V. 2000, Protostars and Planets IV, 559
- Natta, A., Testi, L., Muzerolle, J., et al. 2004, A&A, 424, 603
- Neves, V., Santos, N. C., Sousa, S. G., Correia, A. C. M., & Israelián, G. 2009, A&A, 497, 563
- Niedzielski, A., Konacki, M., Wolszczan, A., et al. 2007, ApJ, 669, 1354
- Niedzielski, A., Nowak, G., Adamów, M., & Wolszczan, A. 2009, ApJ, 707, 768
- Pasquini, L., Döllinger, M. P., Weiss, A., et al. 2007, A&A, 473, 979
- Perryman, M. A. C. & ESA, eds. 1997, ESA Special Publication, Vol. 1200, The HIPPARCOS and TYCHO catalogues. Astrometric and photometric star catalogues derived from the ESA HIPPARCOS Space Astrometry Mission
- Pollack, J. B., Hubickyj, O., Bodenheimer, P., et al. 1996, Icarus, 124, 62
- Ramírez, I., Asplund, M., Baumann, P., Meléndez, J., & Bensby, T. 2010, A&A, 521, A33
- Raskin, G., van Winckel, H., Hensberge, H., et al. 2011, A&A, 526, A69
- Rice, W. K. M. & Armitage, P. J. 2003, ApJ, 598, L55
- Sadakane, K., Ohnishi, T., Ohkubo, M., & Takeda, Y. 2005, PASJ, 57, 127
- Santos, N. C., Israelián, G., & Mayor, M. 2004, A&A, 415, 1153
- Sato, B., Ando, H., Kambe, E., et al. 2003, ApJ, 597, L157
- Sato, B., Toyota, E., Omiya, M., et al. 2008, PASJ, 60, 1317
- Savage, B. D. & Mathis, J. S. 1979, ARA&A, 17, 73
- Sbordone, L. 2005, Memorie della Società Astronomica Italiana Supplementi, 8, 61
- Sbordone, L., Bonifacio, P., Castelli, F., & Kurucz, R. L. 2004, Memorie della Società Astronomica Italiana Supplementi, 5, 93

- Schuler, S. C., Flateau, D., Cunha, K., et al. 2011, ApJ, 732, 55
Schuler, S. C., Kim, J. H., Tinker, Jr., M. C., et al. 2005, ApJ, 632, L131
Sousa, S. G., Fernandes, J., Israelián, G., & Santos, N. C. 2010, A&A, 512, L5
Sousa, S. G., Santos, N. C., Israelián, G., Mayor, M., & Monteiro, M. J. P. F. G. 2007, A&A, 469, 783
Sousa, S. G., Santos, N. C., Israelián, G., Mayor, M., & Udry, S. 2011, A&A, 533, A141
Takeda, Y. 2007, PASJ, 59, 335
Takeda, Y., Ohkubo, M., & Sadakane, K. 2002a, PASJ, 54, 451
Takeda, Y., Ohkubo, M., Sato, B., Kambe, E., & Sadakane, K. 2005, PASJ, 57, 27
Takeda, Y., Sato, B., Kambe, E., Sadakane, K., & Ohkubo, M. 2002b, PASJ, 54, 1041
Takeda, Y., Sato, B., & Murata, D. 2008, PASJ, 60, 781
Timmes, F. X., Woosley, S. E., & Weaver, T. A. 1995, ApJS, 98, 617
Valenti, J. A. & Fischer, D. A. 2005, ApJS, 159, 141
van Leeuwen, F. v. 2007, Hipparchos, the New Reduction of the Raw Data (XXXII, 449 p., Hardcover, ISBN: 978-1-4020-6341-1: Astrophysics and Space Science Library , Vol. 350)
Villaver, E. & Livio, M. 2009, ApJ, 705, L81
Williams, J. P. & Cieza, L. A. 2011, ARA&A, 49, 67
Wolszczan, A. & Frail, D. A. 1992, Nature, 355, 145
Wright, J. T., Upadhyay, S., Marcy, G. W., et al. 2009, ApJ, 693, 1084

Online material

Results produced in the framework of this work are only available in the electronic version of the corresponding paper or at the CDS via anonymous ftp to cdsarc.u-strasbg.fr (130.79.128.5) or via <http://cdsweb.u-strasbg.fr/cgi-bin/qcat?J/A+A/>

Table 2 contains: HIP number (column 1); HD number (column 2); effective temperature in Kelvins (column 3); logarithm of the surface gravity in cm s^{-2} (column 5); microturbulent velocity in km s^{-1} (column 5); final metallicity in dex (column 6); mean iron abundance derived from Fe I lines (column 7) in the usual scale ($A(Fe) = \log[(N_{Fe}/N_H) + 12]$); number of Fe I lines used (column 8); mean iron abundance derived from Fe II lines (column 9); number of Fe II lines used (column 10); and spectrograph (column 11). Each measured quantity is accompanied by its corresponding uncertainty.

Table 3 gives: HIP number (column 1); visual extinction in magnitudes (column 2); $\log(L_*/L_\odot)$ (column 3); photometric effective temperature in Kelvins (column 4); evolutionary values of the logarithm of the surface gravity in cm s^{-2} (column 5); stellar age in Gyr (column 6); stellar mass in solar units (column 7); and stellar radius in solar units (column 8). Each quantity is accompanied by its corresponding uncertainty.

Table 5 gives the abundances of Na, Mg, Al, Si, Ca, Ti I, Ti II, V, Cr I, Cr II Mn, Co, Ni, and Zn (Table 10). They are expressed relative to the solar value, i.e., $[X/H] = \log(N_X/N_H) - \log(N_X/N_H)_\odot$.

Finally, in Table 7 radial velocities and Galactic spatial-velocity components for the observed stars with respect to the LSR are presented. The assumed solar motion with respect to the LSR is $(U_\odot, V_\odot, W_\odot) = (10.0, 5.25, 7.17) \text{ km s}^{-1}$ (Dehnen & Binney 1998).

Table 2 Basic physical parameters and metallicities for the stars measured in this work.

HIP/ Other name (1)	HD (2)	T _{eff} (K) (3)	log g (cms ⁻²) (4)	ξ_t (kms ⁻¹) (5)	[Fe/H] dex (6)	$\langle A(\text{Fe I}) \rangle$ (7)	n _I (8)	$\langle A(\text{Fe II}) \rangle$ (9)	n _{II} (10)	Spec. [†] (11)
Giants with planets										
1692	1690	4343 ± 20	2.06 ± 0.08	1.56 ± 0.14	-0.23 ± 0.04	7.27 ± 0.05	197	7.27 ± 0.07	17	2
4297	5319	4900 ± 25	3.35 ± 0.09	1.10 ± 0.10	0.05 ± 0.04	7.55 ± 0.04	234	7.55 ± 0.06	18	2
10085	13189	4175 ± 33	1.62 ± 0.13	1.49 ± 0.17	-0.37 ± 0.06	7.13 ± 0.07	229	7.13 ± 0.10	20	1
12247	16400	4864 ± 25	2.65 ± 0.08	1.42 ± 0.10	-0.03 ± 0.03	7.47 ± 0.04	217	7.47 ± 0.06	17	2
	17092	4634 ± 28	2.48 ± 0.10	1.31 ± 0.13	0.11 ± 0.05	7.61 ± 0.05	237	7.61 ± 0.08	21	1
20889	28305	4915 ± 25	2.75 ± 0.08	1.40 ± 0.13	0.15 ± 0.04	7.65 ± 0.05	234	7.65 ± 0.06	23	1
36616	59686	4666 ± 20	2.62 ± 0.07	1.31 ± 0.11	0.13 ± 0.04	7.63 ± 0.05	234	7.63 ± 0.06	21	1
37826	62509	4886 ± 18	3.00 ± 0.06	1.22 ± 0.10	0.09 ± 0.03	7.59 ± 0.04	254	7.59 ± 0.04	23	1
42527	73108	4518 ± 18	2.39 ± 0.07	1.31 ± 0.09	-0.17 ± 0.03	7.33 ± 0.04	244	7.33 ± 0.05	21	1
46471	81688	4771 ± 13	2.38 ± 0.05	1.41 ± 0.08	-0.36 ± 0.02	7.14 ± 0.03	255	7.14 ± 0.03	22	1
BD+20 2457		4258 ± 13	1.64 ± 0.07	1.63 ± 0.08	-0.79 ± 0.02	6.71 ± 0.02	207	6.71 ± 0.04	20	2
γ^1 Leo		4372 ± 15	1.66 ± 0.06	1.43 ± 0.09	-0.44 ± 0.03	7.06 ± 0.03	239	7.06 ± 0.05	21	1
50887	90043	5001 ± 10	3.26 ± 0.04	1.10 ± 0.06	-0.09 ± 0.02	7.41 ± 0.02	276	7.41 ± 0.02	23	1
53666	95089	4937 ± 15	3.31 ± 0.05	1.08 ± 0.08	0.00 ± 0.02	7.50 ± 0.03	271	7.50 ± 0.03	22	1
57428	102272	4830 ± 23	2.58 ± 0.08	1.38 ± 0.14	-0.32 ± 0.04	7.18 ± 0.04	257	7.18 ± 0.06	24	1
57820	102956	4979 ± 28	3.39 ± 0.09	1.13 ± 0.12	0.14 ± 0.04	7.64 ± 0.04	230	7.64 ± 0.06	19	2
58952	104985	4666 ± 15	2.39 ± 0.06	1.38 ± 0.08	-0.40 ± 0.02	7.10 ± 0.03	251	7.10 ± 0.04	22	1
61740	110014	4586 ± 40	2.47 ± 0.14	1.37 ± 0.19	0.33 ± 0.07	7.83 ± 0.08	209	7.84 ± 0.11	22	1
74793	136726	4265 ± 33	1.97 ± 0.13	1.43 ± 0.16	0.01 ± 0.06	7.51 ± 0.07	224	7.51 ± 0.10	18	1
74961	136418	4999 ± 13	3.48 ± 0.05	1.04 ± 0.08	-0.13 ± 0.02	7.37 ± 0.02	273	7.37 ± 0.03	25	1
75458	137759	4577 ± 30	2.70 ± 0.10	1.20 ± 0.13	0.18 ± 0.05	7.68 ± 0.06	236	7.68 ± 0.08	21	1
76311	139357	4603 ± 30	2.64 ± 0.10	1.24 ± 0.14	0.34 ± 0.05	7.84 ± 0.06	227	7.84 ± 0.08	24	1
77655	142091	4861 ± 13	3.29 ± 0.05	1.05 ± 0.09	0.09 ± 0.02	7.59 ± 0.03	258	7.59 ± 0.03	22	1
79219	145457	4802 ± 20	2.55 ± 0.06	1.35 ± 0.09	-0.19 ± 0.03	7.31 ± 0.03	251	7.31 ± 0.04	22	1
80687	148427	5017 ± 20	3.51 ± 0.06	1.09 ± 0.10	0.06 ± 0.03	7.57 ± 0.03	229	7.56 ± 0.04	16	2
88048	163917	4948 ± 20	2.84 ± 0.08	1.54 ± 0.14	0.13 ± 0.04	7.63 ± 0.05	216	7.63 ± 0.06	18	2
89047	167042	4981 ± 10	3.53 ± 0.04	1.10 ± 0.08	0.03 ± 0.02	7.53 ± 0.03	238	7.53 ± 0.03	16	2
90344	170693	4524 ± 15	2.45 ± 0.06	1.39 ± 0.10	-0.35 ± 0.03	7.15 ± 0.03	213	7.15 ± 0.05	16	2
91852	173416	4777 ± 28	2.36 ± 0.10	1.37 ± 0.12	-0.11 ± 0.04	7.39 ± 0.05	213	7.39 ± 0.07	22	2
92895	175541	5048 ± 35	3.36 ± 0.11	1.08 ± 0.15	-0.07 ± 0.04	7.43 ± 0.05	239	7.43 ± 0.07	19	2
94576	180314	4997 ± 30	3.06 ± 0.10	1.27 ± 0.15	0.22 ± 0.04	7.72 ± 0.05	215	7.72 ± 0.07	20	2
94951	180902	4996 ± 15	3.47 ± 0.05	1.11 ± 0.10	-0.02 ± 0.03	7.48 ± 0.03	234	7.48 ± 0.04	17	2
95124	181342	5001 ± 15	3.43 ± 0.05	1.14 ± 0.11	0.20 ± 0.03	7.70 ± 0.04	226	7.70 ± 0.04	19	2
97938	188310	4798 ± 30	2.66 ± 0.10	1.45 ± 0.15	-0.16 ± 0.05	7.34 ± 0.05	214	7.34 ± 0.08	17	2
99894	192699	5101 ± 25	3.24 ± 0.08	1.08 ± 0.11	-0.19 ± 0.03	7.31 ± 0.04	237	7.31 ± 0.05	19	2
103527	199665	5107 ± 30	3.10 ± 0.09	1.34 ± 0.13	0.07 ± 0.04	7.58 ± 0.05	230	7.58 ± 0.07	19	2
104202	200964	5062 ± 15	3.30 ± 0.05	1.11 ± 0.09	-0.17 ± 0.02	7.33 ± 0.03	241	7.33 ± 0.03	19	2
107251	206610	4962 ± 45	3.46 ± 0.14	1.00 ± 0.20	0.23 ± 0.06	7.73 ± 0.07	229	7.73 ± 0.10	21	2
109577	210702	4996 ± 15	3.43 ± 0.05	1.14 ± 0.08	0.03 ± 0.02	7.53 ± 0.03	234	7.52 ± 0.04	18	2
110813	212771	5053 ± 15	3.49 ± 0.05	1.12 ± 0.08	-0.17 ± 0.02	7.33 ± 0.02	238	7.33 ± 0.03	19	2
	240210	4308 ± 33	1.82 ± 0.13	1.50 ± 0.16	-0.12 ± 0.06	7.38 ± 0.06	194	7.38 ± 0.10	19	2
114855	219449	4691 ± 23	2.60 ± 0.08	1.40 ± 0.12	0.02 ± 0.04	7.52 ± 0.05	206	7.52 ± 0.06	18	2
116076	221345	4733 ± 15	2.66 ± 0.06	1.47 ± 0.10	-0.31 ± 0.03	7.19 ± 0.03	218	7.19 ± 0.05	19	2
Giants without planets										
729	448	4814 ± 23	2.70 ± 0.08	1.39 ± 0.12	0.05 ± 0.04	7.55 ± 0.04	219	7.55 ± 0.06	21	2
873	645	4847 ± 15	3.07 ± 0.05	1.20 ± 0.08	0.03 ± 0.02	7.53 ± 0.03	227	7.53 ± 0.04	19	2
6682	8594	4832 ± 15	3.16 ± 0.05	1.14 ± 0.08	-0.01 ± 0.03	7.50 ± 0.03	231	7.49 ± 0.04	17	2
6999	9057	4959 ± 23	2.87 ± 0.08	1.44 ± 0.11	0.07 ± 0.03	7.57 ± 0.04	215	7.57 ± 0.05	22	2
7097	9270	4937 ± 40	2.20 ± 0.14	1.76 ± 0.24	-0.13 ± 0.06	7.38 ± 0.07	207	7.37 ± 0.10	18	2
7607	9927	4403 ± 38	2.19 ± 0.14	1.46 ± 0.16	0.11 ± 0.07	7.61 ± 0.07	190	7.61 ± 0.11	19	2
7719	10072	5109 ± 15	2.83 ± 0.05	1.33 ± 0.08	-0.13 ± 0.02	7.37 ± 0.02	234	7.37 ± 0.03	17	2
9222	11949	4806 ± 10	2.95 ± 0.04	1.21 ± 0.08	-0.14 ± 0.02	7.36 ± 0.03	230	7.35 ± 0.03	16	2
13531	17878	5059 ± 23	2.66 ± 0.06	1.25 ± 0.12	-0.20 ± 0.03	7.30 ± 0.04	238	7.29 ± 0.05	17	2
19038	25604	4805 ± 25	2.73 ± 0.09	1.39 ± 0.12	0.09 ± 0.04	7.59 ± 0.05	212	7.59 ± 0.07	20	2
42528	73764	5138 ± 23	3.39 ± 0.08	1.22 ± 0.12	0.02 ± 0.03	7.52 ± 0.04	237	7.52 ± 0.05	20	2
59285	105639	4638 ± 33	2.83 ± 0.13	1.22 ± 0.15	0.09 ± 0.05	7.59 ± 0.06	215	7.59 ± 0.09	18	2
59646	106314	5133 ± 23	3.61 ± 0.06	1.13 ± 0.12	0.10 ± 0.03	7.60 ± 0.04	235	7.60 ± 0.05	18	2
59847	106714	4871 ± 20	2.46 ± 0.08	1.40 ± 0.10	-0.20 ± 0.03	7.30 ± 0.03	226	7.30 ± 0.05	22	2
59856	106760	4576 ± 25	2.45 ± 0.10	1.39 ± 0.15	-0.13 ± 0.05	7.37 ± 0.05	213	7.37 ± 0.07	17	2
68904	123351	4851 ± 20	3.39 ± 0.07	1.59 ± 0.13	-0.02 ± 0.03	7.48 ± 0.04	210	7.48 ± 0.05	15	2
69185	123929	5067 ± 10	3.39 ± 0.04	1.08 ± 0.06	-0.31 ± 0.01	7.19 ± 0.02	239	7.19 ± 0.02	19	2
69427	124294	4235 ± 20	1.83 ± 0.08	1.48 ± 0.11	-0.43 ± 0.04	7.07 ± 0.04	203	7.07 ± 0.06	17	2
69612	124679	4806 ± 23	2.70 ± 0.08	1.38 ± 0.11	-0.08 ± 0.03	7.42 ± 0.04	218	7.42 ± 0.05	21	2
70027	125560	4556 ± 45	2.55 ± 0.16	1.35 ± 0.19	0.28 ± 0.07	7.78 ± 0.09	200	7.78 ± 0.12	18	2
70038	125490	5073 ± 23	3.01 ± 0.07	1.20 ± 0.09	-0.04 ± 0.03	7.46 ± 0.03	237	7.46 ± 0.05	17	2
80816	148856	5038 ± 17	2.54 ± 0.05	1.51 ± 0.08	-0.08 ± 0.02	7.42 ± 0.03	220	7.42 ± 0.04	19	2
84975	157261	4979 ± 20	3.24 ± 0.06	1.17 ± 0.08	-0.21 ± 0.02	7.29 ± 0.03	236	7.29 ± 0.04	18	2
88765	165760	5001 ± 15	2.71 ± 0.05	1.48 ± 0.10	0.00 ± 0.03	7.50 ± 0.03	218	7.50 ± 0.04	20	2
88836	166229	4655 ± 33	2.85 ± 0.12	1.23 ± 0.16	0.21 ± 0.06	7.71 ± 0.07	213	7.71 ± 0.09	18	2
89826	168775	4638 ± 28	2.51 ± 0.10	1.48 ± 0.16	0.13 ± 0.05	7.63 ± 0.06	196	7.63 ± 0.08	18	2
89918	168656	5081 ± 18	2.87 ± 0.06	1.39 ± 0.08	-0.09 ± 0.02	7.41 ± 0.03	229	7.41 ± 0.04	18	2

Table 2 Continued

HIP/ Other name (1)	HD (2)	T _{eff} (K) (3)	log g (cm s ⁻²) (4)	ξ_t (km s ⁻¹) (5)	[Fe/H] dex (6)	$\langle A(\text{Fe I}) \rangle$ (7)	n _I (8)	$\langle A(\text{Fe II}) \rangle$ (9)	n _{II} (10)	Spec. [†] (11)
89962	168723	4949 ± 20	3.15 ± 0.06	1.21 ± 0.08	-0.22 ± 0.02	7.28 ± 0.03	232	7.28 ± 0.04	18	2
95822	183492	4817 ± 25	2.71 ± 0.09	1.36 ± 0.10	0.06 ± 0.04	7.57 ± 0.04	209	7.56 ± 0.06	19	2
95926	183756	4999 ± 15	3.61 ± 0.05	1.04 ± 0.08	-0.08 ± 0.02	7.43 ± 0.02	240	7.42 ± 0.03	17	2
96016	184010	4987 ± 10	3.29 ± 0.04	1.15 ± 0.06	-0.16 ± 0.02	7.34 ± 0.02	235	7.34 ± 0.03	18	2
96229	184406	4530 ± 35	2.82 ± 0.12	1.15 ± 0.16	0.16 ± 0.06	7.66 ± 0.07	220	7.66 ± 0.09	18	2
98210	188844	4811 ± 18	3.04 ± 0.06	1.22 ± 0.10	-0.21 ± 0.03	7.30 ± 0.03	231	7.29 ± 0.04	18	2
98314	189186	5002 ± 10	3.13 ± 0.04	1.21 ± 0.07	-0.41 ± 0.02	7.09 ± 0.02	234	7.09 ± 0.03	19	2
98845	190571	5097 ± 28	3.19 ± 0.09	1.08 ± 0.15	-0.24 ± 0.04	7.25 ± 0.05	236	7.26 ± 0.06	21	2
98920	190608	4784 ± 30	3.03 ± 0.10	1.16 ± 0.13	0.10 ± 0.04	7.60 ± 0.05	222	7.60 ± 0.07	19	2
99171	191067	4786 ± 20	3.31 ± 0.07	1.06 ± 0.09	-0.03 ± 0.03	7.47 ± 0.03	225	7.47 ± 0.05	17	2
99841	192787	5023 ± 15	2.96 ± 0.05	1.32 ± 0.07	-0.11 ± 0.02	7.39 ± 0.03	232	7.39 ± 0.03	17	2
99913	192836	4805 ± 15	2.92 ± 0.06	1.25 ± 0.10	0.08 ± 0.03	7.58 ± 0.04	217	7.58 ± 0.04	19	2
100022	193343	4938 ± 28	3.58 ± 0.09	1.05 ± 0.12	0.18 ± 0.04	7.68 ± 0.04	229	7.68 ± 0.06	17	2
100503	194110	5125 ± 10	3.50 ± 0.04	1.10 ± 0.06	-0.24 ± 0.01	7.26 ± 0.02	235	7.26 ± 0.02	20	2
100541	194013	4928 ± 18	2.90 ± 0.06	1.38 ± 0.09	-0.06 ± 0.03	7.44 ± 0.03	223	7.44 ± 0.04	19	2
100587	194317	4259 ± 35	2.00 ± 0.13	1.42 ± 0.15	0.00 ± 0.06	7.50 ± 0.07	193	7.50 ± 0.10	18	2
101848	196645	5072 ± 15	3.51 ± 0.05	1.08 ± 0.07	-0.18 ± 0.02	7.32 ± 0.02	235	7.32 ± 0.03	20	2
101936	196758	4800 ± 33	2.74 ± 0.11	1.40 ± 0.14	0.08 ± 0.05	7.58 ± 0.05	214	7.58 ± 0.08	18	2
102532	197964	4798 ± 20	3.04 ± 0.06	1.22 ± 0.09	0.12 ± 0.03	7.62 ± 0.04	216	7.62 ± 0.05	18	2
103004	198809	5252 ± 18	2.97 ± 0.05	1.43 ± 0.10	-0.10 ± 0.02	7.40 ± 0.03	233	7.40 ± 0.04	19	2
103519	199870	4999 ± 20	3.13 ± 0.06	1.28 ± 0.11	0.13 ± 0.03	7.62 ± 0.04	227	7.63 ± 0.05	20	2
105390	203358	5070 ± 18	3.46 ± 0.05	1.05 ± 0.08	-0.22 ± 0.02	7.28 ± 0.02	230	7.27 ± 0.03	19	2
105411	203344	4782 ± 25	2.80 ± 0.09	1.45 ± 0.13	-0.15 ± 0.04	7.35 ± 0.04	210	7.35 ± 0.06	20	2
105502	203504	4675 ± 20	2.59 ± 0.06	1.43 ± 0.11	0.00 ± 0.03	7.50 ± 0.04	210	7.50 ± 0.06	19	2
106081	204642	4711 ± 25	3.01 ± 0.09	1.14 ± 0.11	0.10 ± 0.04	7.60 ± 0.05	215	7.60 ± 0.07	18	2
106093	204771	4957 ± 20	2.98 ± 0.07	1.33 ± 0.10	0.06 ± 0.03	7.56 ± 0.04	226	7.56 ± 0.05	18	2
110538	212496	4752 ± 13	2.74 ± 0.05	1.26 ± 0.08	-0.30 ± 0.02	7.20 ± 0.03	232	7.20 ± 0.04	18	2
111944	214868	4360 ± 25	1.96 ± 0.10	1.54 ± 0.15	-0.18 ± 0.05	7.32 ± 0.06	201	7.32 ± 0.08	19	2
112041	215030	4779 ± 8	2.70 ± 0.03	1.29 ± 0.07	-0.46 ± 0.02	7.04 ± 0.02	232	7.04 ± 0.03	17	2
112067	214995	4709 ± 28	2.61 ± 0.10	1.39 ± 0.16	-0.02 ± 0.05	7.49 ± 0.06	205	7.48 ± 0.08	18	2
112158	215182	4981 ± 20	2.15 ± 0.06	1.57 ± 0.11	-0.21 ± 0.03	7.29 ± 0.03	222	7.29 ± 0.05	17	2
112242	215373	5040 ± 20	2.91 ± 0.07	1.44 ± 0.12	0.11 ± 0.03	7.61 ± 0.04	223	7.61 ± 0.05	16	2
115696	220807	4847 ± 10	2.95 ± 0.04	1.20 ± 0.06	-0.45 ± 0.02	7.05 ± 0.02	231	7.05 ± 0.03	15	2
115830	220954	4756 ± 25	2.66 ± 0.09	1.35 ± 0.12	0.08 ± 0.04	7.58 ± 0.05	214	7.58 ± 0.07	20	2
115919	221115	5032 ± 15	2.92 ± 0.05	1.37 ± 0.10	0.05 ± 0.03	7.55 ± 0.03	220	7.55 ± 0.04	18	2
116584	222107	4844 ± 30	3.18 ± 0.10	1.44 ± 0.16	-0.50 ± 0.04	7.00 ± 0.04	221	7.00 ± 0.06	16	2
116823	222455	4549 ± 38	2.77 ± 0.14	1.17 ± 0.15	0.16 ± 0.06	7.66 ± 0.07	210	7.66 ± 0.10	18	2
117375	223252	5008 ± 23	2.80 ± 0.08	1.40 ± 0.10	-0.06 ± 0.03	7.44 ± 0.04	226	7.44 ± 0.05	20	2
117411	223301	4745 ± 25	3.22 ± 0.09	1.09 ± 0.12	0.18 ± 0.04	7.68 ± 0.05	220	7.68 ± 0.06	18	2
117541	223524	4661 ± 30	2.60 ± 0.11	1.36 ± 0.13	0.10 ± 0.05	7.60 ± 0.05	200	7.60 ± 0.08	19	2

Subgiants with planets

8159	10697	5662 ± 15	4.07 ± 0.04	1.20 ± 0.10	0.09 ± 0.02	7.60 ± 0.02	234	7.59 ± 0.03	23	2
12048	16141	5773 ± 15	4.16 ± 0.04	1.18 ± 0.09	0.10 ± 0.02	7.60 ± 0.02	224	7.60 ± 0.03	23	2
12191	16175	5955 ± 18	4.11 ± 0.04	1.27 ± 0.11	0.26 ± 0.02	7.76 ± 0.02	258	7.76 ± 0.03	25	1
27253	38529	5584 ± 18	3.86 ± 0.05	1.19 ± 0.09	0.30 ± 0.02	7.80 ± 0.03	274	7.80 ± 0.03	24	1
36795	60532	6099 ± 23	3.58 ± 0.05	1.94 ± 0.16	-0.32 ± 0.02	7.18 ± 0.02	208	7.18 ± 0.03	25	1
42446	73534	4987 ± 43	3.76 ± 0.13	0.87 ± 0.27	0.29 ± 0.06	7.79 ± 0.08	204	7.79 ± 0.10	19	2
49813	88133	5422 ± 13	3.97 ± 0.04	1.02 ± 0.08	0.30 ± 0.02	7.80 ± 0.02	270	7.80 ± 0.03	22	1
54195	96167	5769 ± 15	4.07 ± 0.04	1.22 ± 0.09	0.29 ± 0.02	7.79 ± 0.02	269	7.79 ± 0.03	24	1
66192	118203	5783 ± 20	3.97 ± 0.05	1.25 ± 0.10	0.14 ± 0.02	7.64 ± 0.03	258	7.64 ± 0.03	23	1
93746	177830	4873 ± 40	3.72 ± 0.12	0.95 ± 0.19	0.47 ± 0.05	7.97 ± 0.07	215	7.97 ± 0.09	20	2
94256	179079	5776 ± 30	4.19 ± 0.08	1.21 ± 0.18	0.33 ± 0.04	7.83 ± 0.05	237	7.83 ± 0.06	23	2
HAT-P-7		6566 ± 40	4.06 ± 0.06	1.87 ± 0.22	0.23 ± 0.03	7.73 ± 0.03	204	7.73 ± 0.05	22	2
96507	185269	6060 ± 40	4.06 ± 0.08	1.54 ± 0.22	0.14 ± 0.04	7.64 ± 0.05	220	7.64 ± 0.07	21	2
100970	195019	5779 ± 25	4.09 ± 0.05	1.09 ± 0.14	0.09 ± 0.03	7.59 ± 0.03	229	7.59 ± 0.04	23	2
115100	219828	5838 ± 13	4.13 ± 0.03	1.26 ± 0.10	0.12 ± 0.02	7.62 ± 0.02	231	7.62 ± 0.03	23	2
118319	224693	5989 ± 25	4.23 ± 0.05	1.37 ± 0.14	0.21 ± 0.03	7.71 ± 0.03	228	7.71 ± 0.04	22	2

Late main-sequence with planets

6512	8375	5244 ± 15	3.74 ± 0.04	1.10 ± 0.06	-0.09 ± 0.02	7.41 ± 0.02	236	7.41 ± 0.03	21	2
60585	108103	4952 ± 38	3.55 ± 0.12	1.03 ± 0.20	0.20 ± 0.05	7.70 ± 0.07	233	7.70 ± 0.08	20	2
70616	126647	4997 ± 43	3.89 ± 0.13	0.99 ± 0.23	0.35 ± 0.06	7.86 ± 0.07	228	7.85 ± 0.09	20	2
98138	188993	5828 ± 25	3.63 ± 0.06	1.66 ± 0.12	0.00 ± 0.02	7.50 ± 0.03	212	7.50 ± 0.04	21	2
102531	197963	6295 ± 25	3.79 ± 0.05	1.62 ± 0.10	0.06 ± 0.02	7.56 ± 0.02	206	7.56 ± 0.03	22	2
GSC 02883-01687		5668 ± 30	4.48 ± 0.08	1.03 ± 0.16	0.28 ± 0.03	7.78 ± 0.04	239	7.78 ± 0.05	21	2
20723	28185	5665 ± 13	4.51 ± 0.03	0.92 ± 0.09	0.21 ± 0.01	7.71 ± 0.02	262	7.71 ± 0.02	26	1
31246	46375	5304 ± 18	4.64 ± 0.05	0.77 ± 0.17	0.26 ± 0.02	7.76 ± 0.03	265	7.75 ± 0.03	22	1
60081	107148	5785 ± 13	4.47 ± 0.03	1.04 ± 0.06	0.26 ± 0.01	7.76 ± 0.02	276	7.76 ± 0.02	26	1
80838	149026	6218 ± 45	4.53 ± 0.09	1.54 ± 0.31	0.37 ± 0.05	7.87 ± 0.06	219	7.87 ± 0.08	19	2
TrES-4		6597 ± 75	4.47 ± 0.13	2.09 ± 0.39	0.40 ± 0.05	7.90 ± 0.06	181	7.89 ± 0.08	19	2

Table 2 Continued

HIP/ Other name (1)	HD (2)	T _{eff} (K) (3)	log g (cms ⁻²) (4)	ξ_t (kms ⁻¹) (5)	[Fe/H] dex (6)	$\langle A(\text{Fe I}) \rangle$ (7)	n _I (8)	$\langle A(\text{Fe II}) \rangle$ (9)	n _{II} (10)	Spec. [†] (11)
95740	183263	5949 ± 30	4.40 ± 0.08	1.11 ± 0.17	0.35 ± 0.03	7.85 ± 0.04	237	7.85 ± 0.05	21	2
98767	190360	5606 ± 19	4.44 ± 0.05	0.98 ± 0.11	0.25 ± 0.02	7.74 ± 0.03	239	7.74 ± 0.03	22	2
109378	210277	5570 ± 15	4.53 ± 0.04	0.99 ± 0.11	0.19 ± 0.02	7.69 ± 0.02	237	7.69 ± 0.03	20	2
113357	217014	5822 ± 15	4.43 ± 0.04	1.14 ± 0.09	0.18 ± 0.02	7.68 ± 0.02	226	7.68 ± 0.02	22	2
113421	217107	5671 ± 23	4.51 ± 0.05	1.08 ± 0.10	0.33 ± 0.02	7.83 ± 0.03	235	7.83 ± 0.03	21	2

[†]Spectrograph: (1) MERCATOR/HERMES; (2) NOT/FIES

Table 3 Photometric and evolutionary parameters.

HIP/ Other name (1)	A _V (mag) (2)	L _★ /L _⊙ (log) (3)	T _{eff} ^{phot} (K) (4)	log g _{evol} (cm s ⁻²) (5)	Age (Gyr) (6)	Mass (M _⊙) (7)	Radius (R _⊙) (8)
Giants with planets							
1692	0.10 ± 0.04	1.53 ± 0.39	-	1.90 ± 0.10	6.72 ± 3.18	1.11 ± 0.15	18.80 ± 2.77
4297	0.10 ± 0.03	0.96 ± 0.09	4960 ± 86	3.40 ± 0.07	3.45 ± 0.66	1.37 ± 0.08	3.72 ± 0.36
10085	0.82 ± 0.50	3.04 ± 0.41	4334 ± 168	1.40 ± 0.11	4.56 ± 2.97	1.19 ± 0.25	34.60 ± 6.28
12247	0.08 ± 0.06	1.73 ± 0.04	4839 ± 86	2.71 ± 0.05	1.38 ± 0.18	1.90 ± 0.12	9.67 ± 0.40
HD 17092	0.20 ± 0.05	1.15 ± 0.44	4504 ± 86	2.89 ± 0.28	5.60 ± 3.17	1.20 ± 0.20	6.34 ± 2.18
20889	0.06 ± 0.03	1.93 ± 0.02	4897 ± 80	2.66 ± 0.02	0.50 ± 0.06	2.76 ± 0.08	12.39 ± 0.28
36616	0.00 ± 0.00	1.87 ± 0.02	4621 ± 78	2.51 ± 0.04	1.30 ± 0.32	2.02 ± 0.16	12.55 ± 0.40
37826	0.00 ± 0.00	1.59 ± 0.01	4887 ± 77	2.86 ± 0.02	1.03 ± 0.15	2.10 ± 0.08	8.67 ± 0.12
42527	0.00 ± 0.00	1.59 ± 0.02	4429 ± 76	2.43 ± 0.03	10.54 ± 1.01	1.02 ± 0.03	9.78 ± 0.27
46471	0.10 ± 0.10	1.79 ± 0.05	4820 ± 103	2.49 ± 0.09	2.64 ± 1.20	1.39 ± 0.24	10.72 ± 0.38
BD+20 2457	0.19 ± 0.03	0.98 ± 4.52	4243 ± 182	4.92 ± 0.08	4.52 ± 4.06	1.10 ± 0.25	44.15 ± 7.89
γ ¹ Leo	0.01 ± 0.00	2.53 ± 0.03	4554 ± 77	1.62 ± 0.04	2.05 ± 0.52	1.50 ± 0.15	30.34 ± 1.11
50887	0.03 ± 0.02	0.84 ± 0.03	5022 ± 86	3.48 ± 0.02	3.29 ± 0.23	1.36 ± 0.03	3.39 ± 0.11
53666	0.02 ± 0.00	1.14 ± 0.10	4979 ± 85	3.27 ± 0.08	2.20 ± 0.46	1.57 ± 0.11	4.61 ± 0.56
57428	0.08 ± 0.03	1.36 ± 0.21	4758 ± 85	2.77 ± 0.25	6.10 ± 2.70	1.09 ± 0.16	6.89 ± 1.89
57820	0.00 ± 0.00	1.01 ± 0.09	4947 ± 80	3.40 ± 0.07	1.99 ± 0.37	1.64 ± 0.10	4.05 ± 0.44
58952	0.00 ± 0.00	1.73 ± 0.02	4662 ± 77	2.39 ± 0.03	5.61 ± 0.86	1.13 ± 0.05	10.85 ± 0.32
61740	0.17 ± 0.01	2.21 ± 0.03	4575 ± 79	2.35 ± 0.04	0.52 ± 0.11	2.75 ± 0.13	17.73 ± 0.76
74793	0.04 ± 0.04	2.38 ± 0.03	-	1.79 ± 0.06	1.77 ± 0.52	1.70 ± 0.20	26.47 ± 1.04
74961	0.13 ± 0.00	0.88 ± 0.05	5059 ± 84	3.47 ± 0.04	3.65 ± 0.46	1.32 ± 0.05	3.38 ± 0.19
75458	0.04 ± 0.00	1.77 ± 0.01	4581 ± 79	2.45 ± 0.05	2.60 ± 0.60	1.48 ± 0.13	11.59 ± 0.29
76311	0.13 ± 0.00	1.90 ± 0.03	4660 ± 78	2.48 ± 0.04	1.56 ± 0.33	1.87 ± 0.15	12.54 ± 0.04
77655	0.03 ± 0.00	1.10 ± 0.01	4900 ± 77	3.23 ± 0.02	2.36 ± 0.15	1.55 ± 0.03	4.79 ± 0.03
79219	0.05 ± 0.00	1.63 ± 0.05	4740 ± 77	2.45 ± 0.13	5.86 ± 4.05	1.06 ± 0.26	9.72 ± 0.60
80687	0.33 ± 0.14	0.93 ± 0.06	5227 ± 139	3.55 ± 0.03	2.92 ± 0.18	1.44 ± 0.03	3.19 ± 0.13
88048	0.16 ± 0.07	2.07 ± 0.03	5024 ± 124	2.60 ± 0.02	0.41 ± 0.04	2.94 ± 0.07	13.66 ± 0.28
89047	0.01 ± 0.00	1.02 ± 0.01	4986 ± 76	3.35 ± 0.01	2.04 ± 0.09	1.62 ± 0.03	4.27 ± 0.10
90344	0.02 ± 0.01	2.16 ± 0.02	4393 ± 80	2.03 ± 0.04	2.36 ± 0.52	1.45 ± 0.12	18.53 ± 0.48
91852	0.09 ± 0.00	1.95 ± 0.03	4781 ± 78	2.49 ± 0.06	1.33 ± 0.47	1.89 ± 0.26	12.48 ± 0.57
92895	0.32 ± 0.10	1.13 ± 0.11	5394 ± 132	3.43 ± 0.08	2.54 ± 0.56	1.48 ± 0.11	3.73 ± 0.46
94576	0.12 ± 0.00	1.64 ± 0.05	4995 ± 78	2.98 ± 0.04	0.60 ± 0.05	2.48 ± 0.08	8.10 ± 0.45
94951	0.25 ± 0.08	1.07 ± 0.09	5170 ± 107	3.42 ± 0.06	2.53 ± 0.40	1.49 ± 0.08	3.81 ± 0.37
95124	0.25 ± 0.08	1.17 ± 0.07	5039 ± 103	3.37 ± 0.04	1.57 ± 0.18	1.78 ± 0.07	4.39 ± 0.30
97938	0.09 ± 0.02	1.69 ± 0.02	4807 ± 132	2.39 ± 0.09	8.97 ± 4.60	0.91 ± 0.17	9.73 ± 0.24
99894	0.04 ± 0.01	1.08 ± 0.03	5125 ± 78	3.35 ± 0.03	2.04 ± 0.18	1.56 ± 0.49	4.19 ± 0.18
103527	0.05 ± 0.01	1.57 ± 0.02	5044 ± 78	3.05 ± 0.02	0.66 ± 0.03	2.38 ± 0.04	7.32 ± 0.23
104202	0.04 ± 0.01	1.09 ± 0.03	5101 ± 80	3.33 ± 0.03	2.10 ± 0.16	1.55 ± 0.04	4.28 ± 0.17
107251	0.15 ± 0.02	1.31 ± 0.16	5001 ± 91	3.28 ± 0.13	1.47 ± 0.45	1.82 ± 0.19	4.91 ± 0.94
109577	0.05 ± 0.03	1.13 ± 0.02	4993 ± 80	3.30 ± 0.02	1.66 ± 0.09	1.72 ± 0.03	4.70 ± 0.13
110813	0.16 ± 0.01	1.27 ± 0.09	5192 ± 83	3.26 ± 0.07	1.78 ± 0.34	1.63 ± 0.10	4.79 ± 0.53
HD 240210	0.46 ± 0.16	1.35 ± 0.33	-	2.03 ± 0.10	8.07 ± 2.96	1.09 ± 0.11	16.11 ± 2.28
114855	0.10 ± 0.02	1.75 ± 0.01	4688 ± 78	2.50 ± 0.06	2.80 ± 0.89	1.41 ± 0.17	10.64 ± 0.25
116076	0.13 ± 0.08	1.82 ± 0.04	4780 ± 95	2.44 ± 0.10	3.27 ± 1.93	1.30 ± 0.29	10.99 ± 0.30
Giants without planets							
729	0.12 ± 0.02	1.75 ± 0.03	4846 ± 79	2.70 ± 0.04	1.41 ± 0.22	1.90 ± 0.13	9.81 ± 0.32
873	0.10 ± 0.04	1.49 ± 0.03	4920 ± 81	2.95 ± 0.02	1.30 ± 0.12	1.88 ± 0.06	7.34 ± 0.25
6682	0.10 ± 0.03	1.15 ± 0.06	4887 ± 83	3.16 ± 0.01	3.42 ± 0.56	1.37 ± 0.07	4.90 ± 0.31
6999	0.09 ± 0.03	1.85 ± 0.03	4930 ± 80	2.74 ± 0.02	0.60 ± 0.08	2.56 ± 0.09	10.83 ± 0.33
7097	0.09 ± 0.06	2.66 ± 0.07	4922 ± 91	2.14 ± 0.06	0.22 ± 0.03	3.78 ± 0.16	26.48 ± 2.15
7607	0.08 ± 0.01	2.22 ± 0.02	4387 ± 79	2.07 ± 0.06	1.19 ± 0.32	1.98 ± 0.17	20.64 ± 0.73
7719	0.08 ± 0.03	1.80 ± 0.04	5135 ± 79	2.83 ± 0.04	0.56 ± 0.56	2.51 ± 0.08	9.65 ± 0.45
9222	0.11 ± 0.01	1.56 ± 0.02	4866 ± 77	2.80 ± 0.02	1.95 ± 0.16	1.60 ± 0.06	7.99 ± 0.21
13531	0.14 ± 0.03	2.28 ± 0.03	5507 ± 83	2.47 ± 0.03	0.39 ± 0.05	2.99 ± 0.10	16.08 ± 0.54
19038	0.08 ± 0.03	1.85 ± 0.02	4786 ± 82	2.66 ± 0.03	0.93 ± 0.19	2.28 ± 0.13	11.27 ± 0.27
42528	0.00 ± 0.00	1.15 ± 0.04	5077 ± 78	3.35 ± 0.03	1.37 ± 0.10	1.84 ± 0.05	4.57 ± 0.22
59285	0.01 ± 0.00	1.44 ± 0.02	4624 ± 83	2.77 ± 0.04	3.72 ± 0.72	1.41 ± 0.09	7.81 ± 0.27
59646	0.00 ± 0.00	0.87 ± 0.03	5092 ± 79	3.55 ± 0.02	2.27 ± 0.13	1.56 ± 0.03	3.34 ± 0.11
59847	0.05 ± 0.04	1.84 ± 0.03	4911 ± 83	2.55 ± 0.04	1.61 ± 0.33	1.72 ± 0.16	11.03 ± 0.31
59856	0.08 ± 0.06	2.11 ± 0.04	4563 ± 85	2.22 ± 0.05	1.34 ± 0.32	1.82 ± 0.16	16.58 ± 0.72
68904	0.10 ± 0.07	1.02 ± 0.06	4840 ± 95	3.26 ± 0.05	4.22 ± 0.82	1.29 ± 0.07	4.22 ± 0.28
69185	0.10 ± 0.07	1.04 ± 0.05	5224 ± 101	3.51 ± 0.03	5.40 ± 0.68	1.16 ± 0.04	3.00 ± 0.16
69427	0.09 ± 0.01	2.36 ± 0.02	-	1.58 ± 0.03	9.67 ± 0.97	1.46 ± 0.04	25.41 ± 0.74
69612	0.03 ± 0.01	1.76 ± 0.04	4824 ± 77	2.58 ± 0.05	1.83 ± 0.30	1.64 ± 0.12	10.42 ± 0.35

Table 3 Continued

HIP/ Other name (1)	A _V (mag) (2)	L _★ /L _⊙ (log) (3)	T _{eff} ^{phot} (K) (4)	log g _{evol} (cms ⁻²) (5)	Age (Gyr) (6)	Mass (M _⊙) (7)	Radius (R _⊙) (8)
70027	0.04 ± 0.04	1.70 ± 0.02	4502 ± 82	2.38 ± 0.05	4.66 ± 1.37	1.19 ± 0.13	11.12 ± 0.28
70038	0.12 ± 0.01	1.50 ± 0.04	5112 ± 79	3.10 ± 0.03	0.86 ± 0.07	2.15 ± 0.07	6.60 ± 0.34
80816	0.05 ± 0.05	2.18 ± 0.03	4973 ± 86	2.53 ± 0.02	0.36 ± 0.03	3.07 ± 0.06	15.21 ± 0.44
84975	0.30 ± 0.09	1.23 ± 0.05	5183 ± 107	3.21 ± 0.04	2.73 ± 0.33	1.42 ± 0.05	4.73 ± 0.22
88765	0.29 ± 0.12	2.10 ± 0.05	5171 ± 153	2.64 ± 0.02	0.44 ± 0.04	2.87 ± 0.07	12.97 ± 0.36
88836	0.05 ± 0.00	1.51 ± 0.02	4608 ± 79	2.78 ± 0.04	1.93 ± 0.35	1.67 ± 0.10	8.33 ± 0.26
89826	0.06 ± 0.00	2.15 ± 0.01	4586 ± 81	2.37 ± 0.03	0.54 ± 0.11	2.73 ± 0.12	17.16 ± 0.45
89918	0.28 ± 0.12	1.98 ± 0.05	5236 ± 124	2.74 ± 0.02	0.55 ± 0.06	2.60 ± 0.08	10.93 ± 0.33
89962	0.06 ± 0.03	1.28 ± 0.01	4951 ± 79	3.07 ± 0.02	2.31 ± 0.20	1.50 ± 0.04	5.71 ± 0.10
95822	0.12 ± 0.04	1.79 ± 0.04	4836 ± 82	2.69 ± 0.05	1.27 ± 0.27	2.01 ± 0.17	10.15 ± 0.39
95926	0.14 ± 0.07	0.88 ± 0.04	5117 ± 98	3.48 ± 0.03	3.29 ± 0.29	1.37 ± 0.04	3.38 ± 0.14
96016	0.11 ± 0.04	1.25 ± 0.03	5067 ± 82	3.16 ± 0.02	1.89 ± 0.13	1.60 ± 0.04	5.30 ± 0.15
96229	0.05 ± 0.01	1.39 ± 0.01	4567 ± 79	2.70 ± 0.06	6.71 ± 2.19	1.16 ± 0.10	7.66 ± 0.24
98210	0.29 ± 0.13	1.47 ± 0.07	4950 ± 128	2.88 ± 0.04	3.63 ± 0.69	1.32 ± 0.07	6.64 ± 0.33
98314	0.14 ± 0.03	1.23 ± 0.05	5060 ± 83	3.10 ± 0.03	3.53 ± 0.51	1.28 ± 0.05	5.06 ± 0.27
98845	0.19 ± 0.07	0.98 ± 0.05	5230 ± 98	3.45 ± 0.04	3.10 ± 0.41	1.35 ± 0.06	3.48 ± 0.19
98920	0.03 ± 0.00	1.41 ± 0.02	4770 ± 77	2.94 ± 0.04	1.69 ± 0.25	1.73 ± 0.09	7.08 ± 0.21
99171	0.03 ± 0.01	1.02 ± 0.02	4800 ± 77	3.17 ± 0.03	6.20 ± 1.18	1.17 ± 0.06	4.49 ± 0.13
99841	0.21 ± 0.08	1.80 ± 0.04	5138 ± 98	2.83 ± 0.03	0.79 ± 0.12	2.27 ± 0.10	9.19 ± 0.29
99913	0.13 ± 0.06	1.66 ± 0.04	4869 ± 87	2.78 ± 0.04	1.24 ± 0.13	1.93 ± 0.07	9.05 ± 0.38
100022	0.06 ± 0.02	0.86 ± 0.04	4887 ± 83	3.49 ± 0.03	2.71 ± 0.23	1.49 ± 0.05	3.49 ± 0.16
100503	0.18 ± 0.07	1.03 ± 0.05	5248 ± 96	3.44 ± 0.03	2.48 ± 0.19	1.45 ± 0.04	3.66 ± 0.17
100541	0.05 ± 0.01	1.67 ± 0.02	4892 ± 77	2.81 ± 0.04	1.18 ± 0.19	2.02 ± 0.11	8.95 ± 27.00
100587	0.17 ± 0.06	2.27 ± 0.03	4305 ± 85	1.82 ± 0.10	3.86 ± 1.89	1.29 ± 0.25	22.31 ± 0.84
101848	0.06 ± 0.01	0.86 ± 0.06	5047 ± 85	3.52 ± 0.04	3.43 ± 0.53	1.33 ± 0.06	3.20 ± 0.22
101936	0.04 ± 0.01	1.71 ± 0.04	4766 ± 83	2.71 ± 0.06	1.33 ± 0.29	1.95 ± 0.17	9.77 ± 0.47
102532	0.02 ± 0.01	1.52 ± 0.04	4804 ± 77	2.85 ± 0.03	1.81 ± 0.11	1.99 ± 0.06	8.43 ± 0.33
103004	0.08 ± 0.03	1.71 ± 0.04	5262 ± 81	2.99 ± 0.03	0.56 ± 0.03	2.49 ± 0.05	8.08 ± 0.33
103519	0.12 ± 0.05	1.62 ± 0.03	5026 ± 87	2.98 ± 0.02	0.63 ± 0.03	2.43 ± 0.04	8.05 ± 0.23
105390	0.09 ± 0.04	1.09 ± 0.04	5324 ± 85	3.33 ± 0.03	2.27 ± 0.20	1.50 ± 0.04	4.22 ± 0.18
105411	0.05 ± 0.01	1.67 ± 0.02	4707 ± 77	2.39 ± 0.09	8.40 ± 4.33	0.94 ± 0.18	9.81 ± 0.28
105502	0.03 ± 0.01	1.81 ± 0.01	4633 ± 76	2.45 ± 0.04	2.28 ± 0.52	1.53 ± 0.14	11.68 ± 0.27
106081	0.06 ± 0.01	1.37 ± 0.05	4729 ± 77	2.92 ± 0.05	2.77 ± 0.56	1.48 ± 0.09	6.75 ± 0.41
106093	0.16 ± 0.06	1.63 ± 0.03	5053 ± 88	2.90 ± 0.03	0.91 ± 0.13	2.16 ± 0.09	8.30 ± 0.19
110538	0.17 ± 0.06	1.79 ± 0.03	4841 ± 88	2.47 ± 0.09	3.83 ± 2.20	1.23 ± 0.26	10.34 ± 0.21
111944	0.17 ± 0.05	2.45 ± 0.03	4274 ± 82	1.80 ± 0.05	1.75 ± 0.49	1.65 ± 0.18	25.83 ± 0.95
112041	0.05 ± 0.03	1.62 ± 0.03	4751 ± 78	2.56 ± 0.03	5.33 ± 0.80	1.15 ± 0.47	8.98 ± 0.33
112067	0.07 ± 0.05	1.58 ± 0.03	4641 ± 84	2.71 ± 0.06	2.28 ± 0.60	1.55 ± 0.15	8.73 ± 0.36
112158	0.04 ± 0.02	2.48 ± 0.04	5155 ± 80	2.24 ± 0.04	0.28 ± 0.04	3.43 ± 0.15	22.30 ± 1.13
112242	0.05 ± 0.02	1.78 ± 0.02	4994 ± 78	2.88 ± 0.02	0.47 ± 0.02	2.70 ± 0.04	9.56 ± 0.24
115696	0.15 ± 0.09	1.28 ± 0.05	4936 ± 105	2.89 ± 0.04	9.78 ± 1.37	0.98 ± 0.04	5.68 ± 0.25
115830	0.06 ± 0.02	1.69 ± 0.01	4775 ± 118	2.70 ± 0.03	1.48 ± 0.12	1.84 ± 0.07	9.66 ± 0.23
115919	0.07 ± 0.02	1.68 ± 0.04	5041 ± 77	2.95 ± 0.03	0.59 ± 0.04	2.49 ± 0.06	8.44 ± 0.37
116584	0.05 ± 0.02	1.37 ± 0.01	4769 ± 80	2.77 ± 0.04	8.71 ± 1.87	1.01 ± 0.06	6.57 ± 0.13
116823	0.07 ± 0.02	1.16 ± 0.09	4590 ± 84	2.91 ± 0.08	8.57 ± 2.11	1.09 ± 0.07	5.86 ± 0.60
117375	0.10 ± 0.04	1.81 ± 0.03	5029 ± 82	2.78 ± 0.03	0.69 ± 0.11	2.42 ± 0.11	10.14 ± 0.31
117411	0.10 ± 0.02	1.02 ± 0.06	4787 ± 86	3.24 ± 0.05	4.24 ± 0.85	1.31 ± 0.08	4.37 ± 0.30
117541	0.10 ± 0.02	1.67 ± 0.03	4660 ± 78	2.50 ± 0.15	3.79 ± 3.14	1.28 ± 0.40	10.10 ± 0.48

Subgiants with planets

8159	0.00 ± 0.00	0.45 ± 0.01	5568 ± 80	3.98 ± 0.01	7.30 ± 0.24	1.09 ± 0.01	1.70 ± 0.04
12048	0.04 ± 0.03	0.41 ± 0.03	5755 ± 82	4.06 ± 0.02	7.19 ± 0.29	1.08 ± 0.01	1.54 ± 0.04
12191	0.05 ± 0.03	0.55 ± 0.04	5863 ± 94	4.05 ± 0.03	3.70 ± 0.59	1.26 ± 0.05	1.69 ± 0.07
27253	0.03 ± 0.01	0.77 ± 0.01	5516 ± 76	3.75 ± 0.01	3.41 ± 0.09	1.36 ± 0.01	2.47 ± 0.06
36795	0.02 ± 0.01	0.94 ± 0.01	6117 ± 88	3.70 ± 0.01	2.90 ± 0.05	1.34 ± 0.01	2.63 ± 0.02
42446	0.00 ± 0.00	0.52 ± 0.05	5016 ± 91	3.74 ± 0.04	4.95 ± 0.85	1.24 ± 0.06	2.38 ± 0.14
49813	0.04 ± 0.01	0.59 ± 0.06	5419 ± 86	3.85 ± 0.04	5.30 ± 0.98	1.20 ± 0.06	2.07 ± 0.14
54195	0.11 ± 0.01	0.61 ± 0.07	5697 ± 91	3.96 ± 0.05	5.13 ± 0.57	1.19 ± 0.04	1.82 ± 0.12
66192	0.00 ± 0.00	0.60 ± 0.05	5647 ± 84	3.92 ± 0.04	4.84 ± 0.49	1.21 ± 0.04	1.92 ± 0.11
93746	0.08 ± 0.03	0.73 ± 0.04	-	3.55 ± 0.04	3.81 ± 0.45	1.34 ± 0.05	3.09 ± 0.14
94256	0.12 ± 0.01	0.43 ± 0.04	5684 ± 86	4.10 ± 0.04	6.24 ± 0.70	1.11 ± 0.03	1.49 ± 0.08
HAT-P-7	0.24 ± 0.09	0.80 ± 6.18	6872 ± 143	4.11 ± 0.16	0.95 ± 0.58	1.46 ± 0.13	1.70 ± 0.40
96507	0.09 ± 0.03	0.68 ± 0.03	6023 ± 87	3.98 ± 0.03	3.12 ± 0.47	1.33 ± 0.05	1.87 ± 0.06
100970	0.05 ± 0.02	0.36 ± 0.03	5789 ± 82	4.12 ± 0.03	7.62 ± 0.89	1.05 ± 0.03	1.43 ± 0.06
115100	0.11 ± 0.02	0.47 ± 0.05	5883 ± 92	4.07 ± 0.04	6.21 ± 0.42	1.11 ± 0.02	1.55 ± 0.09
118319	0.10 ± 0.04	0.65 ± 0.08	5949 ± 100	4.01 ± 0.06	3.36 ± 0.56	1.30 ± 0.07	1.79 ± 0.16

Table 3 Continued

HIP/ Other name (1)	A _V (mag) (2)	L _★ /L _⊙ (log) (3)	T _{eff} ^{phot} (K) (4)	log g _{evol} (cms ⁻²) (5)	Age (Gyr) (6)	Mass (M _⊙) (7)	Radius (R _⊙) (8)
Subgiants without planets (this work)							
6512	0.06 ± 0.02	1.00 ± 0.02	5267 ± 78	3.49 ± 0.02	1.93 ± 0.08	1.61 ± 0.02	3.62 ± 0.10
60585	0.03 ± 0.01	0.29 ± 0.07	4716 ± 83	3.83 ± 0.03	10.06 ± 1.37	1.03 ± 0.04	1.97 ± 0.10
70616	0.07 ± 0.01	0.67 ± 0.03	4915 ± 81	3.67 ± 0.03	3.50 ± 0.22	1.36 ± 0.03	2.73 ± 0.12
98138	0.16 ± 0.06	1.21 ± 0.06	5929 ± 101	3.53 ± 0.04	1.91 ± 0.21	1.63 ± 0.06	3.51 ± 0.24
102531	0.02 ± 0.01	1.01 ± 0.04	6318 ± 83	3.78 ± 0.03	1.85 ± 0.17	1.61 ± 0.04	2.60 ± 0.12
Subgiants without planets (from the literature)							
2422	0.02 ± 0.00	0.71 ± 0.01	5100 ± 77	3.64 ± 0.03	3.55 ± 0.21	1.33 ± 0.03	2.80 ± 0.08
3185	0.10 ± 0.04	0.47 ± 0.02	5482 ± 89	3.78 ± 0.02	11.73 ± 0.07	0.91 ± 0.01	1.96 ± 0.04
4395	0.07 ± 0.01	0.43 ± 0.03	5407 ± 77	3.95 ± 0.03	8.33 ± 0.69	1.07 ± 0.02	1.74 ± 0.08
12350	0.07 ± 0.01	0.59 ± 0.03	5719 ± 78	3.94 ± 0.03	5.04 ± 0.39	1.20 ± 0.03	1.87 ± 0.07
14086	0.09 ± 0.04	0.71 ± 0.02	5258 ± 84	3.52 ± 0.02	10.81 ± 0.75	0.93 ± 0.02	2.67 ± 0.06
15776	0.05 ± 0.01	0.63 ± 0.02	5534 ± 77	3.76 ± 0.02	6.15 ± 0.41	1.08 ± 0.02	2.18 ± 0.07
16641	0.00 ± 0.00	0.76 ± 0.02	5011 ± 81	3.45 ± 0.05	6.78 ± 1.51	1.10 ± 0.07	3.16 ± 0.10
17027	0.00 ± 0.00	0.68 ± 0.01	5031 ± 77	3.65 ± 0.03	3.67 ± 0.21	1.33 ± 0.02	2.77 ± 0.09
17183	0.00 ± 0.00	0.60 ± 0.03	4944 ± 76	3.59 ± 0.05	6.71 ± 1.36	1.14 ± 0.06	2.71 ± 0.11
17378	0.01 ± 0.00	0.52 ± 0.01	5079 ± 87	3.77 ± 0.02	5.48 ± 0.24	1.19 ± 0.02	2.27 ± 0.06
18208	0.17 ± 0.07	0.90 ± 0.09	5294 ± 107	3.58 ± 0.06	3.44 ± 0.75	1.32 ± 0.08	2.98 ± 0.28
18309	0.18 ± 0.04	0.41 ± 0.05	5685 ± 96	3.81 ± 0.02	11.44 ± 0.40	0.92 ± 0.01	1.90 ± 0.05
18432	0.09 ± 0.01	0.47 ± 0.02	5460 ± 77	3.84 ± 0.02	10.39 ± 0.67	0.97 ± 0.02	1.88 ± 0.06
19070	0.01 ± 0.00	0.68 ± 0.03	5489 ± 87	3.82 ± 0.03	4.17 ± 0.35	1.27 ± 0.03	2.20 ± 0.10
21010	0.26 ± 0.13	0.62 ± 0.06	5764 ± 153	3.90 ± 0.02	7.42 ± 0.48	1.09 ± 0.02	1.87 ± 0.06
22319	0.08 ± 0.04	0.80 ± 0.02	5235 ± 83	3.61 ± 0.03	3.06 ± 0.14	1.38 ± 0.03	2.93 ± 0.10
26273	0.08 ± 0.01	0.53 ± 0.06	5531 ± 77	3.80 ± 0.04	2.29 ± 1.55	0.98 ± 0.04	1.97 ± 0.12
27641	0.04 ± 0.00	0.74 ± 0.03	5265 ± 80	3.68 ± 0.03	3.34 ± 0.27	1.35 ± 0.04	2.66 ± 0.86
40023	0.00 ± 0.00	0.91 ± 0.01	5261 ± 80	3.57 ± 0.02	2.26 ± 0.10	1.55 ± 0.03	3.25 ± 0.10
40506	0.05 ± 0.02	0.83 ± 0.04	5129 ± 82	3.60 ± 0.03	2.67 ± 0.19	1.47 ± 0.04	3.05 ± 0.15
41254	0.09 ± 0.02	0.76 ± 0.02	5733 ± 84	3.77 ± 0.02	4.12 ± 0.27	1.26 ± 0.02	2.33 ± 0.08
43634	0.09 ± 0.02	0.72 ± 0.03	6040 ± 85	3.95 ± 0.03	2.90 ± 0.40	1.38 ± 0.05	1.97 ± 0.08
62904	0.03 ± 0.00	0.70 ± 0.02	5392 ± 78	3.77 ± 0.02	3.28 ± 0.16	1.32 ± 0.02	2.37 ± 0.08
64408	0.04 ± 0.00	0.64 ± 0.01	5715 ± 92	3.90 ± 0.02	4.31 ± 0.30	1.25 ± 0.02	1.99 ± 0.05
68101	0.07 ± 0.03	0.78 ± 0.02	5315 ± 90	3.59 ± 0.03	4.15 ± 0.42	1.20 ± 0.03	2.82 ± 0.09
72830	0.09 ± 0.07	0.62 ± 0.05	5107 ± 97	3.69 ± 0.04	6.31 ± 1.05	1.15 ± 0.05	2.45 ± 0.14
75762	0.09 ± 0.02	0.48 ± 0.02	5341 ± 82	3.86 ± 0.02	8.06 ± 0.62	1.07 ± 0.02	1.94 ± 0.07
79214	0.21 ± 0.08	0.79 ± 0.06	6104 ± 126	3.83 ± 0.04	4.95 ± 0.68	1.19 ± 0.04	2.11 ± 0.14
81819	0.16 ± 0.06	0.54 ± 0.04	5518 ± 99	3.89 ± 0.03	7.66 ± 0.80	1.08 ± 0.03	1.88 ± 0.08
81991	0.06 ± 0.06	0.74 ± 0.03	5069 ± 91	3.54 ± 0.04	5.98 ± 1.11	1.15 ± 0.06	2.91 ± 0.11
82302	0.11 ± 0.05	0.70 ± 0.04	5136 ± 103	3.63 ± 0.04	4.80 ± 0.79	1.23 ± 0.05	2.71 ± 0.15
82636	0.07 ± 0.02	0.60 ± 0.02	5786 ± 82	3.85 ± 0.02	6.81 ± 0.33	1.07 ± 0.02	1.96 ± 0.06
84801	0.28 ± 0.12	0.97 ± 0.05	5387 ± 135	3.56 ± 0.03	2.60 ± 0.13	1.44 ± 0.03	3.16 ± 0.11
88217	0.05 ± 0.00	0.75 ± 0.02	5554 ± 77	3.78 ± 0.02	3.67 ± 0.13	1.32 ± 0.02	2.35 ± 0.07
90729	0.07 ± 0.02	0.48 ± 0.02	5422 ± 79	3.90 ± 0.02	7.83 ± 0.36	1.08 ± 0.02	1.87 ± 0.05
93518	0.28 ± 0.09	0.82 ± 0.15	5722 ± 116	3.82 ± 0.08	5.84 ± 2.24	1.16 ± 0.11	2.12 ± 0.31
98036	0.02 ± 0.01	0.79 ± 0.01	5158 ± 78	3.58 ± 0.03	3.09 ± 0.16	1.38 ± 0.03	3.04 ± 0.08
102642	0.18 ± 0.10	0.81 ± 0.04	5233 ± 113	3.62 ± 0.03	3.31 ± 0.20	1.36 ± 0.03	2.88 ± 0.09
103077	0.06 ± 0.01	0.69 ± 0.02	5775 ± 80	3.85 ± 0.02	4.38 ± 0.22	1.24 ± 0.02	2.12 ± 0.06
106527	0.04 ± 0.01	0.94 ± 0.02	6270 ± 78	3.84 ± 0.02	1.98 ± 0.15	1.55 ± 0.03	2.37 ± 0.08
109439	0.04 ± 0.01	1.03 ± 0.02	5628 ± 78	3.56 ± 0.02	2.23 ± 0.10	1.52 ± 0.03	3.27 ± 0.10
109572	0.12 ± 0.04	1.00 ± 0.02	6318 ± 92	3.81 ± 0.02	1.87 ± 0.14	1.59 ± 0.03	2.49 ± 0.05
109822	0.07 ± 0.00	0.57 ± 0.02	5073 ± 80	3.62 ± 0.03	10.21 ± 1.03	1.00 ± 0.03	2.46 ± 0.08
109836	0.12 ± 0.01	0.68 ± 0.05	5658 ± 92	3.95 ± 0.05	4.06 ± 0.68	1.26 ± 0.06	1.90 ± 0.12
110853	0.16 ± 0.03	0.74 ± 0.05	5455 ± 84	3.78 ± 0.04	4.08 ± 0.54	1.28 ± 0.05	2.31 ± 0.14
113386	0.10 ± 0.01	0.51 ± 0.05	5734 ± 91	3.96 ± 0.04	8.30 ± 1.05	1.06 ± 0.04	1.72 ± 0.12
113994	0.03 ± 0.02	0.54 ± 0.02	5173 ± 81	3.83 ± 0.02	5.59 ± 0.47	1.19 ± 0.03	2.11 ± 0.07
114699	0.05 ± 0.00	0.47 ± 0.01	5352 ± 77	3.86 ± 0.02	8.98 ± 0.38	1.05 ± 0.02	1.92 ± 0.05
116250	0.07 ± 0.02	0.62 ± 0.01	5813 ± 79	3.96 ± 0.03	3.97 ± 0.57	1.27 ± 0.05	1.88 ± 0.05
117668	0.10 ± 0.01	0.54 ± 0.04	5581 ± 78	3.86 ± 0.03	8.27 ± 1.15	1.06 ± 0.04	1.91 ± 0.10
Late main-sequence with planets							
GSC 02883-01687	1.12 ± 0.56	0.08 ± 0.23	5480 ± 77	4.47 ± 0.01	0.51 ± 0.38	1.03 ± 0.01	1.00 ± 0.00
20723	0.12 ± 0.01	0.11 ± 0.03	5628 ± 82	4.33 ± 0.04	6.14 ± 1.48	1.01 ± 0.01	1.09 ± 0.04
31246	0.04 ± 0.02	-0.10 ± 0.03	5282 ± 79	4.42 ± 0.02	10.64 ± 1.47	0.89 ± 0.01	1.00 ± 0.00
60081	0.02 ± 0.00	0.15 ± 0.03	5676 ± 85	4.31 ± 0.03	4.66 ± 1.14	1.06 ± 0.01	1.14 ± 0.05
80838	0.09 ± 0.03	0.48 ± 0.05	6081 ± 96	4.22 ± 0.04	1.82 ± 0.71	1.26 ± 0.02	1.38 ± 0.08

Table 3 Continued

HIP/ Other name (1)	A_V (mag) (2)	L_\star/L_\odot (log) (3)	$T_{\text{eff}}^{\text{phot}}$ (K) (4)	$\log g_{\text{evol}}$ (cm s^{-2}) (5)	Age (Gyr) (6)	Mass (M_\odot) (7)	Radius (R_\odot) (8)
TrES-4	0.11 ± 0.00	0.66 ± 0.05	-	4.19 ± 0.04	0.85 ± 0.46	1.40 ± 0.02	1.51 ± 0.08
95740	0.12 ± 0.06	0.30 ± 0.05	5894 ± 107	4.29 ± 0.04	3.01 ± 1.24	1.13 ± 0.02	1.22 ± 0.06
98767	0.03 ± 0.01	0.07 ± 0.01	5561 ± 76	4.31 ± 0.01	8.20 ± 0.58	0.98 ± 0.01	1.10 ± 0.01
109378	0.04 ± 0.00	-0.02 ± 0.01	5486 ± 78	4.39 ± 0.02	6.21 ± 1.11	0.97 ± 0.01	1.00 ± 0.01
113357	0.03 ± 0.01	0.13 ± 0.01	5782 ± 79	4.35 ± 0.01	3.69 ± 0.59	1.06 ± 0.01	1.10 ± 0.01
113421	0.03 ± 0.01	0.08 ± 0.01	5606 ± 79	4.33 ± 0.02	6.34 ± 0.81	1.01 ± 0.01	1.09 ± 0.01

Table 5 Derived abundances of Na, Mg, Al, Si, Ca, Sc, Ti I, Ti II, V, Cr I, Cr II, Mn, Co, Ni, and Zn.

HIP/Other	[Na/H]	[Mg/H]	[Al/H]	[Si/H]	[Ca/H]	[Sc/H]	[Ti I/H]	[Ti II/H]	[V/H]	[Cr I/H]	[Cr II/H]	[Mn/H]	[Co/H]	[Ni/H]	[Zn/H]
Giants with planets															
1692	-0.12 ± 0.11	-0.17 ± 0.06	0.10 ± 0.04	0.07 ± 0.12	-0.34 ± 0.12	-0.11 ± 0.27	0.12 ± 0.15	0.12 ± 0.22	0.23 ± 0.24	-0.30 ± 0.10	-0.20 ± 0.13	0.05 ± 0.18	-0.20 ± 0.17	-0.12 ± 0.09	-0.22 ± 0.29
4297	0.13 ± 0.06	0.05 ± 0.06	0.24 ± 0.03	0.15 ± 0.06	-0.01 ± 0.10	-0.05 ± 0.13	0.15 ± 0.04	0.09 ± 0.09	0.32 ± 0.15	-0.02 ± 0.04	0.01 ± 0.08	0.33 ± 0.14	0.02 ± 0.11	0.12 ± 0.04	0.12 ± 0.20
10085	-0.11 ± 0.09	-0.21 ± 0.10	-0.07 ± 0.12	-0.01 ± 0.09	-0.36 ± 0.12	-0.09 ± 0.27	0.15 ± 0.16	-0.17 ± 0.16	0.35 ± 0.24	-0.20 ± 0.12	-0.40 ± 0.14	-0.05 ± 0.23	-0.29 ± 0.16	-0.19 ± 0.09	-0.56 ± 0.21
12247	0.16 ± 0.06	0.05 ± 0.11	0.11 ± 0.03	0.13 ± 0.06	-0.04 ± 0.10	-0.23 ± 0.12	0.06 ± 0.12	0.04 ± 0.04	0.08 ± 0.10	-0.08 ± 0.10	-0.15 ± 0.04	0.22 ± 0.12	-0.16 ± 0.11	-0.01 ± 0.04	0.02 ± 0.06
HD 17092	0.42 ± 0.22	0.11 ± 0.06	0.33 ± 0.04	0.34 ± 0.08	0.08 ± 0.10	0.14 ± 0.20	0.15 ± 0.09	0.43 ± 0.19	0.43 ± 0.18	0.05 ± 0.06	0.05 ± 0.09	0.46 ± 0.22	0.11 ± 0.14	0.25 ± 0.06	0.69 ± 0.13
20889	0.46 ± 0.11	0.12 ± 0.09	0.27 ± 0.02	0.32 ± 0.07	0.09 ± 0.09	-0.07 ± 0.13	0.19 ± 0.05	0.23 ± 0.12	0.23 ± 0.12	0.07 ± 0.04	0.15 ± 0.05	0.38 ± 0.12	0.05 ± 0.10	0.22 ± 0.04	0.17 ± 0.20
36616	0.28 ± 0.09	0.09 ± 0.10	0.30 ± 0.05	0.35 ± 0.09	0.07 ± 0.11	0.15 ± 0.19	0.18 ± 0.09	0.39 ± 0.19	0.39 ± 0.18	0.04 ± 0.06	-0.01 ± 0.21	0.44 ± 0.19	0.13 ± 0.14	0.24 ± 0.05	0.05 ± 0.39
37826	0.24 ± 0.07	0.09 ± 0.08	0.20 ± 0.03	0.24 ± 0.05	-0.03 ± 0.11	-0.16 ± 0.11	0.10 ± 0.08	0.23 ± 0.12	0.23 ± 0.13	0.02 ± 0.04	0.00 ± 0.14	0.25 ± 0.12	0.00 ± 0.11	0.12 ± 0.04	0.11 ± 0.16
42527	0.04 ± 0.15	-0.08 ± 0.09	0.08 ± 0.04	-0.17 ± 0.09	-0.18 ± 0.18	-0.18 ± 0.09	0.02 ± 0.16	0.19 ± 0.18	-0.22 ± 0.05	-0.24 ± 0.14	0.00 ± 0.16	-0.19 ± 0.14	-0.08 ± 0.14	-0.26 ± 0.05	-0.26 ± 0.20
46471	-0.26 ± 0.06	-0.15 ± 0.09	-0.09 ± 0.05	-0.14 ± 0.06	-0.31 ± 0.11	-0.55 ± 0.11	-0.23 ± 0.08	-0.21 ± 0.08	-0.29 ± 0.11	-0.46 ± 0.06	-0.51 ± 0.17	-0.29 ± 0.13	-0.46 ± 0.11	-0.29 ± 0.06	-0.27 ± 0.12
BD+20 2457	-0.79 ± 0.11	-0.54 ± 0.07	-0.62 ± 0.05	-0.50 ± 0.13	-0.70 ± 0.20	-0.86 ± 0.15	-0.38 ± 0.12	-0.45 ± 0.13	-0.52 ± 0.14	-0.78 ± 0.12	-0.84 ± 0.11	-0.98 ± 0.11	-0.87 ± 0.11	-0.79 ± 0.09	-0.80 ± 0.15
γ^1 Leo	-0.21 ± 0.10	-0.23 ± 0.13	-0.16 ± 0.08	-0.15 ± 0.09	-0.41 ± 0.12	-0.53 ± 0.19	-0.24 ± 0.15	-0.24 ± 0.20	-0.49 ± 0.24	-0.49 ± 0.10	-0.51 ± 0.12	-0.32 ± 0.17	-0.53 ± 0.16	-0.36 ± 0.09	0.00 ± 0.32
50887	-0.03 ± 0.04	-0.03 ± 0.10	0.05 ± 0.06	0.02 ± 0.05	-0.08 ± 0.08	-0.25 ± 0.10	0.03 ± 0.04	0.00 ± 0.07	-0.10 ± 0.09	-0.13 ± 0.03	0.00 ± 0.08	-0.18 ± 0.12	-0.04 ± 0.09	-0.07 ± 0.03	-0.07 ± 0.07
53666	0.04 ± 0.07	0.04 ± 0.17	0.14 ± 0.06	0.12 ± 0.05	0.00 ± 0.19	-0.12 ± 0.12	0.09 ± 0.05	0.10 ± 0.09	0.22 ± 0.19	-0.05 ± 0.11	-0.07 ± 0.24	0.16 ± 0.24	-0.02 ± 0.10	0.06 ± 0.08	0.03 ± 0.31
57428	-0.18 ± 0.04	-0.01 ± 0.03	0.04 ± 0.09	-0.08 ± 0.06	-0.23 ± 0.09	-0.43 ± 0.08	-0.05 ± 0.04	-0.06 ± 0.09	-0.43 ± 0.12	-0.48 ± 0.04	-0.33 ± 0.04	-0.30 ± 0.10	-0.29 ± 0.04	-0.16 ± 0.10	-0.16 ± 0.10
57820	0.13 ± 0.08	0.12 ± 0.10	0.25 ± 0.06	0.32 ± 0.05	0.03 ± 0.08	-0.04 ± 0.10	0.16 ± 0.04	0.29 ± 0.07	0.33 ± 0.09	0.11 ± 0.03	0.24 ± 0.08	0.42 ± 0.13	0.04 ± 0.12	0.25 ± 0.07	0.22 ± 0.07
58952	-0.21 ± 0.06	-0.06 ± 0.07	0.03 ± 0.07	-0.05 ± 0.06	-0.30 ± 0.10	-0.48 ± 0.11	-0.13 ± 0.08	-0.13 ± 0.11	-0.46 ± 0.13	-0.46 ± 0.04	-0.40 ± 0.06	-0.42 ± 0.11	-0.38 ± 0.11	-0.28 ± 0.05	-0.15 ± 0.10
61740	0.75 ± 0.24	0.22 ± 0.04	0.65 ± 0.06	0.63 ± 0.10	0.27 ± 0.11	0.51 ± 0.29	0.50 ± 0.10	0.31 ± 0.24	0.85 ± 0.22	0.24 ± 0.06	0.21 ± 0.14	0.93 ± 0.29	0.44 ± 0.15	0.51 ± 0.06	0.38 ± 0.57
74793	0.13 ± 0.11	-0.02 ± 0.09	0.21 ± 0.06	0.28 ± 0.12	-0.18 ± 0.30	0.13 ± 0.15	0.27 ± 0.19	0.54 ± 0.25	-0.02 ± 0.10	-0.07 ± 0.14	-0.36 ± 0.20	-0.00 ± 0.14	0.10 ± 0.16	0.00 ± 0.04	0.91 ± 0.03
74961	-0.04 ± 0.04	-0.09 ± 0.07	0.06 ± 0.04	-0.01 ± 0.05	-0.13 ± 0.09	-0.25 ± 0.09	-0.01 ± 0.04	-0.06 ± 0.08	0.11 ± 0.09	-0.17 ± 0.04	-0.18 ± 0.04	-0.01 ± 0.11	-0.15 ± 0.11	-0.06 ± 0.03	-0.03 ± 0.08
75458	0.31 ± 0.11	0.10 ± 0.08	0.37 ± 0.05	0.43 ± 0.10	0.08 ± 0.23	0.19 ± 0.09	0.25 ± 0.20	0.55 ± 0.21	0.09 ± 0.10	0.14 ± 0.06	0.54 ± 0.10	0.21 ± 0.22	0.31 ± 0.14	0.81 ± 0.06	0.81 ± 0.19
76311	0.51 ± 0.11	0.25 ± 0.09	0.53 ± 0.03	0.70 ± 0.16	0.25 ± 0.11	0.37 ± 0.26	0.42 ± 0.10	0.36 ± 0.22	0.73 ± 0.20	0.27 ± 0.05	0.22 ± 0.16	0.82 ± 0.26	0.42 ± 0.15	0.48 ± 0.06	0.38 ± 0.26
77655	0.17 ± 0.06	0.11 ± 0.08	0.28 ± 0.05	0.24 ± 0.06	0.04 ± 0.09	0.13 ± 0.14	0.15 ± 0.05	0.38 ± 0.11	0.38 ± 0.14	0.03 ± 0.04	0.37 ± 0.12	0.20 ± 0.11	0.20 ± 0.04	0.09 ± 0.21	0.09 ± 0.10
79219	-0.07 ± 0.06	-0.08 ± 0.11	0.00 ± 0.04	0.01 ± 0.05	-0.16 ± 0.11	-0.40 ± 0.29	-0.08 ± 0.10	-0.17 ± 0.13	-0.07 ± 0.14	-0.25 ± 0.06	-0.29 ± 0.12	-0.01 ± 0.11	-0.29 ± 0.11	-0.11 ± 0.24	-0.24 ± 0.16
80687	0.17 ± 0.03	0.07 ± 0.11	0.21 ± 0.03	0.16 ± 0.07	0.02 ± 0.10	-0.10 ± 0.13	0.17 ± 0.05	0.22 ± 0.08	0.32 ± 0.09	0.05 ± 0.04	0.01 ± 0.09	0.30 ± 0.24	0.00 ± 0.10	0.16 ± 0.04	0.15 ± 0.12
88048	0.50 ± 0.10	0.14 ± 0.11	0.25 ± 0.01	0.30 ± 0.06	0.06 -0.09	-0.09 ± 0.17	0.20 ± 0.17	0.21 ± 0.20	0.21 ± 0.21	0.05 ± 0.05	0.20 ± 0.20	0.48 ± 0.21	0.03 ± 0.03	0.20 ± 0.26	0.26 ± 0.07
89047	0.06 ± 0.06	0.04 ± 0.06	0.15 ± 0.03	0.16 ± 0.05	-0.02 ± 0.10	-0.14 ± 0.10	0.11 ± 0.04	0.23 ± 0.09	-0.03 ± 0.14	-0.06 ± 0.04	-0.25 ± 0.06	-0.01 ± 0.15	0.10 ± 0.14	0.06 ± 0.04	0.08 ± 0.10
90344	-0.20 ± 0.06	-0.23 ± 0.08	-0.04 ± 0.04	-0.10 ± 0.09	-0.37 ± 0.15	-0.31 ± 0.09	-0.09 ± 0.09	-0.08 ± 0.10	0.06 ± 0.15	-0.39 ± 0.05	-0.44 ± 0.08	-0.18 ± 0.11	-0.32 ± 0.15	-0.25 ± 0.05	-0.26 ± 0.18
91852	0.03 ± 0.06	0.04 ± 0.08	0.00 ± 0.05	0.05 ± 0.07	-0.09 ± 0.11	-0.35 ± 0.11	-0.01 ± 0.05	0.03 ± 0.11	0.10 ± 0.14	-0.13 ± 0.06	-0.13 ± 0.14	0.13 ± 0.17	-0.25 ± 0.11	-0.04 ± 0.05	-0.09 ± 0.11
92895	-0.07 ± 0.03	0.02 ± 0.07	0.09 ± 0.02	0.03 ± 0.06	-0.04 ± 0.11	-0.25 ± 0.03	0.05 ± 0.05	0.05 ± 0.09	0.10 ± 0.15	-0.10 ± 0.04	-0.10 ± 0.03	0.00 ± 0.10	-0.08 ± 0.08	0.00 ± 0.04	-0.02 ± 0.08
94576	0.70 ± 0.24	0.27 ± 0.06	0.45 ± 0.06	0.35 ± 0.07	0.22 ± 0.09	0.38 ± 0.16	0.27 ± 0.06	0.54 ± 0.12	0.54 ± 0.11	0.25 ± 0.08	0.24 ± 0.12	0.71 ± 0.10	0.22 ± 0.10	0.30 ± 0.20	0.36 ± 0.22
94951	0.06 ± 0.05	-0.05 ± 0.11	0.13 ± 0.03	0.11 ± 0.04	-0.05 ± 0.09	-0.22 ± 0.05	0.05 ± 0.04	0.21 ± 0.06	0.21 ± 0.07	-0.07 ± 0.04	-0.03 ± 0.04	0.19 ± 0.13	-0.06 ± 0.13	0.06 ± 0.09	0.06 ± 0.17
95124	0.31 ± 0.05	-0.04 ± 0.18	0.35 ± 0.01	0.35 ± 0.05	0.15 ± 0.10	0.11 ± 0.12	0.31 ± 0.05	0.30 ± 0.09	0.50 ± 0.14	0.15 ± 0.04	0.52 ± 0.05	0.52 ± 0.16	0.20 ± 0.10	0.29 ± 0.04	0.25 ± 0.22
97938	0.02 ± 0.04	0.10 ± 0.08	0.18 ± 0.05	0.09 ± 0.07	-0.06 ± 0.11	-0.19 ± 0.11	0.16 ± 0.05	0.14 ± 0.11	0.27 ± 0.09	-0.22 ± 0.04	-0.30 ± 0.04	0.08 ± 0.13	-0.11 ± 0.15	-0.06 ± 0.03	0.00 ± 0.30
99894	-0.14 ± 0.03	-0.14 ± 0.04	-0.06 ± 0.07	-0.14 ± 0.05	-0.16 ± 0.10	-0.38 ± 0.09	-0.09 ± 0.04	-0.10 ± 0.08	-0.24 ± 0.10	-0.18 ± 0.04	-0.20 ± 0.04	-0.08 ± 0.16	-0.33 ± 0.07	-0.18 ± 0.04	-0.20 ± 0.04
103527	0.19 ± 0.05	0.05 ± 0.14	0.13 ± 0.02	0.10 ± 0.05	0.03 ± 0.09	-0.15 ± 0.08	0.16 ± 0.04	0.13 ± 0.07	0.14 ± 0.07	0.02 ± 0.04	0.15 ± 0.04	0.14 ± 0.15	0.11 ± 0.11	0.03 ± 0.03	0.10 ± 0.10
104202	-0.13 ± 0.03	-0.11 ± 0.08	-0.06 ± 0.04	-0.11 ± 0.06	-0.14 ± 0.12	-0.31 ± 0.03	-0.03 ± 0.04	-0.06 ± 0.08	-0.21 ± 0.11	-0.26 ± 0.04	-0.08 ± 0.10	-0.30 ± 0.15	-0.14 ± 0.11	-0.16 ± 0.05	-0.16 ± 0.05
107251	0.20 ± 0.02	0.18 ± 0.09	0.30 ± 0.05	0.27 ± 0.05	0.06 ± 0.08	0.25 ± 0.16	0.41 ± 0.06	0.36 ± 0.11	0.56 ± 0.12	0.10 ± 0.07	0.15 ± 0.12	0.34 ± 0.27	0.28 ± 0.12	0.33 ± 0.04	0.11 ± 0.40
109577	0.08 ± 0.02	0.03 ± 0.08	0.19 ± 0.08	0.13 ± 0.04	0.01 ± 0.12	-0.13 ± 0.28	0.13 ± 0.15	0.14 ± 0.24	0.23 ± 0.26	0.02 ± 0.10	0.24 ± 0.				

Table 5 Continued

HIP/Other	[Na/H]	[Mg/H]	[Al/H]	[Si/H]	[Ca/H]	[Sc/H]	[Ti I/H]	[Ti II/H]	[V/H]	[Cr I/H]	[Cr II/H]	[Mn/H]	[Co/H]	[Ni/H]	[Zn/H]
116076	-0.14 ± 0.06	0.00 ± 0.06	0.08 ± 0.04	0.02 ± 0.06	-0.23 ± 0.10	-0.43 ± 0.11	0.00 ± 0.08	0.05 ± 0.12	-0.01 ± 0.14	-0.37 ± 0.05	-0.38 ± 0.07	-0.21 ± 0.07	-0.22 ± 0.09	-0.17 ± 0.12	-0.19 ± 0.04
Giants without planets															
729	0.21 ± 0.06	0.05 ± 0.10	0.21 ± 0.01	0.20 ± 0.07	0.03 ± 0.10	-0.14 ± 0.12	0.12 ± 0.05	0.13 ± 0.11	0.22 ± 0.12	-0.02 ± 0.04	0.02 ± 0.06	0.36 ± 0.16	-0.07 ± 0.12	0.09 ± 0.04	-0.03 ± 0.20
873	0.08 ± 0.05	0.03 ± 0.12	0.14 ± 0.05	0.16 ± 0.07	0.01 ± 0.10	-0.15 ± 0.12	0.12 ± 0.05	0.15 ± 0.09	0.21 ± 0.12	-0.03 ± 0.04	0.02 ± 0.10	0.29 ± 0.17	-0.06 ± 0.11	0.08 ± 0.04	0.02 ± 0.12
6682	0.03 ± 0.05	0.02 ± 0.09	0.17 ± 0.05	0.14 ± 0.06	-0.04 ± 0.10	-0.08 ± 0.13	0.12 ± 0.05	0.12 ± 0.10	0.28 ± 0.14	-0.06 ± 0.04	-0.09 ± 0.09	-0.10 ± 0.09	-0.04 ± 0.48	0.06 ± 0.12	-0.01 ± 0.04
6999	0.38 ± 0.13	0.07 ± 0.13	0.23 ± 0.02	0.23 ± 0.07	0.04 ± 0.10	-0.15 ± 0.13	0.14 ± 0.05	0.19 ± 0.10	0.18 ± 0.14	0.00 ± 0.04	0.02 ± 0.09	0.37 ± 0.15	-0.02 ± 0.12	0.13 ± 0.04	0.06 ± 0.08
7097	0.18 ± 0.08	-0.07 ± 0.06	-0.01 ± 0.02	0.07 ± 0.07	-0.18 ± 0.10	-0.44 ± 0.13	-0.09 ± 0.05	-0.13 ± 0.11	-0.09 ± 0.09	-0.17 ± 0.04	-0.19 ± 0.18	-0.13 ± 0.04	-0.44 ± 0.18	-0.12 ± 0.03	0.17 ± 0.28
7607	0.45 ± 0.25	-0.02 ± 0.05	0.35 ± 0.04	0.44 ± 0.14	-0.07 ± 0.13	0.14 ± 0.30	0.24 ± 0.15	0.34 ± 0.23	0.48 ± 0.25	-0.04 ± 0.10	0.05 ± 0.15	0.73 ± 0.15	0.15 ± 0.24	0.25 ± 0.17	0.30 ± 0.09
7719	0.12 ± 0.06	-0.08 ± 0.07	-0.03 ± 0.03	-0.01 ± 0.05	-0.10 ± 0.09	-0.41 ± 0.13	-0.07 ± 0.04	-0.07 ± 0.10	-0.14 ± 0.09	-0.15 ± 0.04	0.02 ± 0.07	-0.03 ± 0.22	-0.35 ± 0.10	-0.12 ± 0.03	-0.26 ± 0.11
9222	-0.05 ± 0.03	-0.08 ± 0.12	0.05 ± 0.07	0.04 ± 0.05	-0.13 ± 0.09	-0.26 ± 0.11	0.01 ± 0.04	0.06 ± 0.09	0.10 ± 0.10	-0.19 ± 0.04	-0.22 ± 0.06	-0.01 ± 0.14	-0.18 ± 0.12	-0.09 ± 0.04	-0.23 ± 0.14
13531	0.06 ± 0.05	-0.23 ± 0.02	-0.08 ± 0.03	-0.06 ± 0.06	-0.22 ± 0.09	-0.56 ± 0.13	-0.21 ± 0.04	-0.21 ± 0.08	-0.25 ± 0.05	-0.30 ± 0.04	-0.22 ± 0.15	-0.25 ± 0.15	-0.44 ± 0.10	-0.21 ± 0.03	-0.32 ± 0.11
19038	0.30 ± 0.06	0.12 ± 0.10	0.24 ± 0.01	0.26 ± 0.08	0.03 ± 0.09	-0.06 ± 0.15	0.20 ± 0.05	0.21 ± 0.13	0.26 ± 0.12	0.01 ± 0.04	0.05 ± 0.07	0.49 ± 0.29	0.02 ± 0.12	0.16 ± 0.04	0.12 ± 0.28
42528	0.25 ± 0.03	0.06 ± 0.12	0.11 ± 0.02	0.10 ± 0.05	-0.01 ± 0.09	-0.16 ± 0.10	0.10 ± 0.04	0.11 ± 0.09	0.00 ± 0.06	-0.05 ± 0.04	-0.03 ± 0.10	-0.09 ± 0.13	0.07 ± 0.10	-0.02 ± 0.04	-0.02 ± 0.14
59285	0.32 ± 0.21	0.07 ± 0.04	0.34 ± 0.06	0.27 ± 0.09	0.15 ± 0.12	0.24 ± 0.20	0.27 ± 0.09	0.47 ± 0.15	0.17 ± 0.21	-0.03 ± 0.06	0.04 ± 0.07	0.56 ± 0.29	0.16 ± 0.12	0.17 ± 0.06	0.28 ± 0.33
59646	0.16 ± 0.06	0.10 ± 0.08	0.16 ± 0.01	0.19 ± 0.05	0.06 ± 0.10	-0.11 ± 0.11	0.19 ± 0.04	0.19 ± 0.08	0.19 ± 0.10	0.09 ± 0.03	0.09 ± 0.22	0.41 ± 0.12	0.01 ± 0.07	0.14 ± 0.04	0.18 ± 0.07
59847	-0.03 ± 0.06	-0.18 ± 0.14	-0.02 ± 0.01	-0.05 ± 0.06	-0.18 ± 0.10	-0.52 ± 0.07	-0.17 ± 0.04	-0.15 ± 0.09	-0.29 ± 0.07	-0.24 ± 0.04	-0.05 ± 0.27	-0.10 ± 0.10	-0.40 ± 0.08	-0.22 ± 0.04	-0.27 ± 0.14
59856	0.03 ± 0.07	-0.03 ± 0.07	0.08 ± 0.03	0.07 ± 0.08	-0.24 ± 0.11	-0.26 ± 0.09	-0.03 ± 0.13	0.12 ± 0.10	-0.23 ± 0.10	-0.01 ± 0.23	0.15 ± 0.01	-0.21 ± 0.15	-0.08 ± 0.12	-0.08 ± 0.06	0.10 ± 0.07
68904	0.21 ± 0.11	-0.07 ± 0.04	0.24 ± 0.01	0.12 ± 0.07	0.05 ± 0.08	-0.02 ± 0.13	0.14 ± 0.05	0.27 ± 0.09	0.08 ± 0.08	0.04 ± 0.04	0.05 ± 0.07	0.27 ± 0.12	-0.16 ± 0.09	0.07 ± 0.04	0.03 ± 0.21
69185	-0.23 ± 0.03	-0.18 ± 0.07	-0.16 ± 0.05	-0.17 ± 0.05	-0.26 ± 0.09	-0.53 ± 0.10	-0.23 ± 0.04	-0.21 ± 0.06	-0.28 ± 0.03	-0.33 ± 0.04	-0.24 ± 0.04	-0.28 ± 0.10	-0.41 ± 0.08	-0.26 ± 0.03	-0.27 ± 0.04
69427	-0.33 ± 0.09	-0.21 ± 0.04	-0.05 ± 0.07	-0.12 ± 0.09	-0.45 ± 0.12	-0.22 ± 0.25	-0.02 ± 0.15	-0.04 ± 0.21	-0.08 ± 0.25	-0.42 ± 0.09	-0.46 ± 0.16	-0.24 ± 0.23	-0.41 ± 0.17	-0.29 ± 0.09	-0.47 ± 0.28
69612	0.05 ± 0.05	-0.02 ± 0.09	0.09 ± 0.01	0.09 ± 0.05	-0.09 ± 0.13	-0.31 ± 0.02	0.02 ± 0.05	0.06 ± 0.11	-0.16 ± 0.11	-0.18 ± 0.04	-0.19 ± 0.11	0.16 ± 0.12	-0.19 ± 0.08	-0.03 ± 0.04	0.03 ± 0.17
70027	0.36 ± 0.11	0.14 ± 0.04	0.49 ± 0.04	0.53 ± 0.11	0.12 ± 0.09	0.35 ± 0.27	0.39 ± 0.10	0.54 ± 0.22	0.72 ± 0.21	0.16 ± 0.06	0.18 ± 0.06	0.87 ± 0.24	0.35 ± 0.15	0.38 ± 0.06	0.45 ± 0.40
70038	0.17 ± 0.07	-0.03 ± 0.10	0.05 ± 0.01	0.06 ± 0.06	-0.05 ± 0.09	-0.28 ± 0.11	0.01 ± 0.04	0.02 ± 0.08	0.03 ± 0.05	-0.05 ± 0.04	-0.04 ± 0.15	0.20 ± 0.10	-0.21 ± 0.04	-0.03 ± 0.04	-0.11 ± 0.07
80816	0.19 ± 0.09	-0.13 ± 0.20	0.01 ± 0.06	0.05 ± 0.08	-0.04 ± 0.13	-0.34 ± 0.17	0.00 ± 0.06	0.03 ± 0.11	-0.12 ± 0.09	-0.12 ± 0.04	-0.02 ± 0.04	0.07 ± 0.11	-0.33 ± 0.15	-0.05 ± 0.04	-0.06 ± 0.09
84975	-0.10 ± 0.03	-0.07 ± 0.07	-0.04 ± 0.03	-0.07 ± 0.05	-0.19 ± 0.09	-0.39 ± 0.08	-0.09 ± 0.04	-0.07 ± 0.07	-0.02 ± 0.07	-0.24 ± 0.03	-0.25 ± 0.06	-0.12 ± 0.14	-0.30 ± 0.17	-0.16 ± 0.09	-0.23 ± 0.03
88765	0.26 ± 0.07	0.08 ± 0.16	0.11 ± 0.04	0.15 ± 0.06	0.01 ± 0.13	-0.23 ± 0.05	0.07 ± 0.09	0.09 ± 0.17	0.02 ± 0.11	-0.04 ± 0.26	0.24 ± 0.26	0.23 ± 0.11	-0.17 ± 0.09	0.02 ± 0.31	-0.10 ± 0.31
88836	0.60 ± 0.28	0.18 ± 0.04	0.49 ± 0.02	0.42 ± 0.09	0.17 ± 0.13	0.34 ± 0.24	0.33 ± 0.09	0.32 ± 0.18	0.63 ± 0.20	0.13 ± 0.06	0.18 ± 0.11	0.72 ± 0.21	0.28 ± 0.15	0.34 ± 0.06	0.39 ± 0.37
89826	0.50 ± 0.21	0.07 ± 0.08	0.28 ± 0.02	0.37 ± 0.09	0.04 ± 0.10	0.01 ± 0.19	0.23 ± 0.09	0.28 ± 0.18	0.34 ± 0.17	0.03 ± 0.06	0.06 ± 0.09	0.60 ± 0.18	0.06 ± 0.15	0.22 ± 0.06	0.15 ± 0.36
89918	0.16 ± 0.06	-0.01 ± 0.09	0.00 ± 0.01	0.02 ± 0.05	-0.06 ± 0.09	-0.37 ± 0.10	-0.04 ± 0.04	-0.03 ± 0.08	-0.06 ± 0.05	-0.12 ± 0.03	0.00 ± 0.04	0.04 ± 0.09	-0.31 ± 0.10	-0.06 ± 0.03	-0.12 ± 0.05
89962	-0.12 ± 0.03	-0.11 ± 0.08	-0.03 ± 0.01	-0.09 ± 0.05	-0.18 ± 0.09	-0.35 ± 0.09	-0.09 ± 0.04	-0.08 ± 0.08	-0.01 ± 0.08	-0.26 ± 0.04	-0.30 ± 0.06	-0.08 ± 0.11	-0.30 ± 0.12	-0.18 ± 0.04	-0.21 ± 0.08
95822	0.18 ± 0.05	0.08 ± 0.10	0.19 ± 0.03	0.21 ± 0.07	0.06 ± 0.10	-0.11 ± 0.11	0.20 ± 0.05	0.19 ± 0.12	0.30 ± 0.11	0.02 ± 0.04	0.02 ± 0.08	0.42 ± 0.16	-0.02 ± 0.12	0.11 ± 0.04	0.54 ± 0.40
95926	-0.03 ± 0.04	-0.06 ± 0.12	0.08 ± 0.05	0.04 ± 0.05	-0.11 ± 0.10	-0.25 ± 0.09	0.01 ± 0.04	0.00 ± 0.08	0.13 ± 0.11	-0.12 ± 0.04	-0.05 ± 0.04	0.05 ± 0.11	-0.14 ± 0.09	-0.01 ± 0.04	-0.04 ± 0.04
96016	-0.11 ± 0.04	-0.07 ± 0.09	-0.03 ± 0.03	-0.03 ± 0.05	-0.15 ± 0.09	-0.37 ± 0.09	-0.05 ± 0.04	-0.01 ± 0.06	-0.06 ± 0.05	-0.20 ± 0.03	-0.09 ± 0.04	-0.04 ± 0.09	-0.25 ± 0.12	-0.11 ± 0.04	-0.13 ± 0.06
96229	0.40 ± 0.25	0.20 ± 0.25	0.47 ± 0.03	0.40 ± 0.10	0.00 ± 0.09	0.37 ± 0.26	0.35 ± 0.09	0.40 ± 0.20	0.61 ± 0.22	0.04 ± 0.06	0.04 ± 0.10	0.42 ± 0.22	0.26 ± 0.14	0.27 ± 0.06	0.45 ± 0.39
98210	-0.12 ± 0.04	-0.08 ± 0.08	0.03 ± 0.03	-0.03 ± 0.07	-0.20 ± 0.09	-0.32 ± 0.07	-0.07 ± 0.02	0.00 ± 0.04	-0.24 ± 0.04	-0.24 ± 0.03	-0.07 ± 0.04	-0.07 ± 0.24	-0.15 ± 0.14	-0.07 ± 0.07	-0.07 ± 0.07
98314	-0.25 ± 0.03	-0.26 ± 0.03	-0.21 ± 0.03	-0.24 ± 0.05	-0.33 ± 0.10	-0.53 ± 0.09	-0.27 ± 0.04	-0.24 ± 0.08	-0.29 ± 0.08	-0.44 ± 0.04	-0.43 ± 0.04	-0.39 ± 0.15	-0.50 ± 0.15	-0.33 ± 0.06	-0.37 ± 0.05
98845	-0.09 ± 0.05	-0.06 ± 0.08	-0.11 ± 0.03	-0.18 ± 0.05	-0.22 ± 0.09	-0.48 ± 0.04	-0.08 ± 0.03	-0.19 ± 0.08	-0.13 ± 0.05	-0.25 ± 0.04	-0.31 ± 0.04	-0.14 ± 0.09	-0.35 ± 0.11	-0.22 ± 0.04	-0.12 ± 0.05
98920	0.24 ± 0.08	0.12 ± 0.12	0.28 ± 0.10	0.22 ± 0.06	0.08 ± 0.10	0.04 ± 0.10	0.29 ± 0.04	0.24 ± 0.08	0.44 ± 0.10	0.06 ± 0.04	0.06 ± 0.05	0.49 ± 0.10	0.13 ± 0.04	0.19 ± 0.04	0.26 ± 0.19
99171	0.07 ± 0.09	0.08 ± 0.06	0.28 ± 0.03	0.16 ± 0.06	-0.06 ± 0.08	0.07 ± 0.16	0.17 ± 0.05	0.35 ± 0.09	0.13 ± 0.17	-0.09 ± 0.04	-0.01 ± 0.04	0.18 ± 0.13	0.04 ± 0.11	0.07 ± 0.04	0.17 ± 0.14
99841	0.08 ± 0.04	-0.08 ± 0.12	0.03 ± 0.02	0.02 ± 0.05	-0.08 ± 0.10	-0.34 ± 0.04	-0.03 ± 0.01	-0.06 ± 0.06	-0.15 ± 0.05	-0.17 ± 0.04	0.05 ± 0.10	-0.27 ± 0.05	-0.07 ± 0.11	-0.15 ± 0.04	

Table 5 Continued

HIP/Other	[Na/H]	[Mg/H]	[Al/H]	[Si/H]	[Ca/H]	[Sc/H]	[Ti I/H]	[Ti II/H]	[V/H]	[Cr I/H]	[Cr II/H]	[Mn/H]	[Co/H]	[Ni/H]	[Zn/H]
100541	0.12	-0.05	0.05	0.13	-0.08	-0.33	-0.04	0.07	-0.02	-0.13	-0.11	0.13	-0.21	-0.01	-0.04
	± 0.05	± 0.12	± 0.03	± 0.06	± 0.09	± 0.11	± 0.05	± 0.09	± 0.09	± 0.04	± 0.03	± 0.13	± 0.10	± 0.04	± 0.12
100587	0.22	-0.07	0.17	0.30	-0.23	0.07	0.20	0.25	0.40	-0.09	-0.08	0.55	-0.04	0.14	0.79
	± 0.21	± 0.14	± 0.06	± 0.10	± 0.17	± 0.28	± 0.06	± 0.23	± 0.23	± 0.12	± 0.24	± 0.33	± 0.14	± 0.09	± 0.56
101848	-0.11	-0.12	-0.03	-0.07	-0.17	-0.34	-0.08	-0.06	-0.05	-0.21	-0.19	-0.05	-0.27	-0.15	-0.18
	± 0.02	± 0.08	± 0.04	± 0.05	± 0.09	± 0.12	± 0.04	± 0.05	± 0.07	± 0.03	± 0.06	± 0.12	± 0.09	± 0.04	± 0.03
101936	0.22	0.06	0.18	0.25	0.02	-0.13	0.15	0.19	0.22	-0.02	0.00	0.42	-0.03	0.12	0.03
	± 0.07	± 0.12	± 0.01	± 0.07	± 0.10	± 0.15	± 0.05	± 0.12	± 0.12	± 0.04	± 0.05	± 0.18	± 0.12	± 0.04	± 0.16
102532	0.26	0.10	0.31	0.27	0.09	0.07	0.23	0.26	0.39	0.05	0.08	0.49	0.13	0.22	0.02
	± 0.10	± 0.10	± 0.06	± 0.07	± 0.11	± 0.15	± 0.05	± 0.13	± 0.15	± 0.04	± 0.12	± 0.19	± 0.11	± 0.04	± 0.26
103004	0.15	-0.08	-0.02	0.02	-0.07	-0.34	-0.05	-0.04	-0.09	-0.11	-0.04	0.04	-0.34	-0.08	-0.05
	± 0.07	± 0.06	± 0.03	± 0.05	± 0.09	± 0.12	± 0.04	± 0.07	± 0.06	± 0.04	± 0.16	± 0.07	± 0.10	± 0.03	± 0.09
103519	0.35	0.11	0.25	0.26	0.07	-0.06	0.20	0.20	0.28	0.07	0.11	0.48	0.06	0.20	0.06
	± 0.09	± 0.09	± 0.01	± 0.06	± 0.10	± 0.12	± 0.04	± 0.10	± 0.10	± 0.04	± 0.09	± 0.17	± 0.11	± 0.04	± 0.20
105390	-0.13	-0.14	-0.09	-0.10	-0.19	-0.42	-0.14	-0.12	-0.12	-0.25	-0.21	-0.17	-0.35	-0.19	-0.22
	± 0.04	± 0.08	± 0.04	± 0.05	± 0.09	± 0.09	± 0.04	± 0.06	± 0.06	± 0.04	± 0.02	± 0.12	± 0.08	± 0.04	± 0.03
105411	0.00	0.08	0.22	0.12	-0.10	-0.17	0.15	0.17	0.21	-0.23	-0.27	0.11	-0.09	-0.03	0.05
	± 0.06	± 0.06	± 0.03	± 0.07	± 0.09	± 0.13	± 0.05	± 0.11	± 0.13	± 0.04	± 0.02	± 0.07	± 0.12	± 0.04	± 0.13
105502	0.13	0.02	0.19	0.20	-0.03	-0.14	0.12	0.16	0.17	-0.10	-0.03	0.32	-0.08	0.03	0.52
	± 0.16	± 0.17	± 0.05	± 0.07	± 0.19	± 0.15	± 0.06	± 0.14	± 0.21	± 0.11	± 0.22	± 0.26	± 0.12	± 0.09	± 0.38
106081	0.18	0.10	0.32	0.26	0.01	0.07	0.19	0.23	0.42	0.03	0.09	0.50	0.13	0.21	0.07
	± 0.09	± 0.07	± 0.02	± 0.08	± 0.09	± 0.19	± 0.09	± 0.14	± 0.20	± 0.05	± 0.09	± 0.19	± 0.13	± 0.06	± 0.36
106093	0.25	0.07	0.17	0.20	0.04	-0.18	0.11	0.15	0.16	-0.01	-0.05	0.35	-0.06	0.09	0.45
	± 0.06	± 0.10	± 0.02	± 0.06	± 0.09	± 0.11	± 0.04	± 0.09	± 0.09	± 0.04	± 0.03	± 0.14	± 0.10	± 0.04	± 0.24
110538	-0.18	-0.19	-0.10	-0.13	-0.28	-0.46	-0.15	-0.17	-0.10	-0.35	-0.28	-0.19	-0.36	-0.24	-0.26
	± 0.06	± 0.10	± 0.06	± 0.06	± 0.11	± 0.11	± 0.08	± 0.07	± 0.13	± 0.04	± 0.09	± 0.12	± 0.13	± 0.05	± 0.09
111944	0.11	-0.15	0.01	0.14	-0.30	-0.23	0.02	-0.07	0.10	-0.19	-0.28	0.14	-0.29	-0.14	-0.38
	± 0.17	± 0.07	± 0.05	± 0.13	± 0.13	± 0.22	± 0.15	± 0.16	± 0.24	± 0.10	± 0.17	± 0.24	± 0.17	± 0.09	± 0.36
112041	-0.28	-0.31	-0.20	-0.26	-0.39	-0.59	-0.31	-0.25	-0.29	-0.51	-0.49	-0.42	-0.50	-0.37	-0.37
	± 0.04	± 0.09	± 0.04	± 0.05	± 0.10	± 0.09	± 0.04	± 0.07	± 0.06	± 0.03	± 0.05	± 0.09	± 0.10	± 0.03	± 0.09
112067	0.12	-0.07	0.16	0.17	-0.05	-0.13	0.12	0.13	0.31	-0.11	0.11	0.47	-0.11	0.08	0.09
	± 0.11	± 0.09	± 0.03	± 0.09	± 0.10	± 0.15	± 0.08	± 0.18	± 0.11	± 0.06	± 0.32	± 0.12	± 0.15	± 0.05	± 0.04
112158	0.13	-0.16	-0.07	-0.06	-0.17	-0.51	-0.19	-0.17	-0.26	-0.21	-0.21	-0.44	-0.21	-0.15	-0.15
	± 0.06	± 0.04	± 0.01	± 0.05	± 0.09	± 0.12	± 0.04	± 0.09	± 0.05	± 0.04	± 0.14	± 0.09	± 0.09	± 0.03	± 0.13
112242	0.50	0.12	0.23	0.29	0.09	-0.10	0.15	0.20	0.16	0.07	0.23	0.46	-0.01	0.20	0.10
	± 0.10	± 0.10	± 0.02	± 0.06	± 0.10	± 0.12	± 0.04	± 0.09	± 0.09	± 0.03	± 0.22	± 0.14	± 0.10	± 0.03	± 0.10
115696	-0.29	-0.29	-0.21	-0.25	-0.40	-0.58	-0.32	-0.26	-0.33	-0.49	-0.46	-0.40	-0.51	-0.38	-0.31
	± 0.03	± 0.09	± 0.05	± 0.05	± 0.09	± 0.09	± 0.04	± 0.06	± 0.07	± 0.03	± 0.06	± 0.09	± 0.09	± 0.04	± 0.09
115830	0.36	0.06	0.22	0.24	0.03	-0.09	0.18	0.20	0.23	-0.01	0.04	0.43	0.02	0.16	0.16
	± 0.19	± 0.11	± 0.04	± 0.08	± 0.10	± 0.16	± 0.08	± 0.14	± 0.17	± 0.05	± 0.11	± 0.18	± 0.13	± 0.06	± 0.12
115919	0.28	0.07	0.16	0.18	0.04	-0.21	0.11	0.10	0.10	0.00	0.18	0.31	-0.11	0.07	0.04
	± 0.07	± 0.10	± 0.03	± 0.07	± 0.10	± 0.12	± 0.04	± 0.09	± 0.08	± 0.04	± 0.26	± 0.13	± 0.10	± 0.04	± 0.10
116584	-0.26	-0.32	0.11	-0.24	-0.29	-0.33	-0.11	-0.12	-0.05	-0.43	-0.65	-0.52	-0.49	-0.40	-0.09
	± 0.08	± 0.08	± 0.17	± 0.06	± 0.09	± 0.10	± 0.04	± 0.09	± 0.07	± 0.04	± 0.06	± 0.12	± 0.03	± 0.24	± 0.24
116823	0.12	0.11	0.46	0.42	0.01	0.36	0.35	0.38	0.61	0.06	0.10	0.69	0.26	0.29	0.30
	± 0.10	± 0.04	± 0.04	± 0.10	± 0.09	± 0.27	± 0.09	± 0.19	± 0.21	± 0.06	± 0.09	± 0.25	± 0.14	± 0.06	± 0.29
117375	0.08	0.01	0.11	0.10	-0.02	-0.33	0.01	-0.01	-0.05	-0.12	0.03	0.15	-0.25	-0.01	-0.04
	± 0.06	± 0.11	± 0.01	± 0.06	± 0.10	± 0.13	± 0.04	± 0.09	± 0.07	± 0.04	± 0.15	± 0.11	± 0.09	± 0.03	± 0.22
117411	0.42	0.18	0.37	0.36	0.07	0.26	0.28	0.30	0.54	0.10	0.17	0.64	0.29	0.31	0.32
	± 0.20	± 0.06	± 0.01	± 0.08	± 0.08	± 0.21	± 0.06	± 0.13	± 0.17	± 0.04	± 0.08	± 0.24	± 0.12	± 0.04	± 0.27
117541	0.26	0.11	0.31	0.29	0.02	0.03	0.31	0.32	0.43	-0.02	0.03	0.52	0.10	0.17	0.19
	± 0.17	± 0.08	± 0.02	± 0.09	± 0.10	± 0.21	± 0.09	± 0.17	± 0.19	± 0.06	± 0.09	± 0.18	± 0.16	± 0.06	± 0.25

Subgiants with planets															
8159	0.16	0.11	0.22	0.17	0.08	-0.06	0.15	0.13	0.09	0.08	0.04	0.22	0.00	0.17	0.12
	± 0.06	± 0.16	± 0.04	± 0.05	± 0.18	± 0.15	± 0.04	± 0.06	± 0.15	± 0.11	± 0.20	± 0.22	± 0.07	± 0.08	± 0.29
12048	0.11	0.13	0.17	0.16	0.07	-0.08	0.16	0.14	0.10	0.09	0.19	0.17	-0.07	0.15	0.11
	± 0.05	± 0.15	± 0.05	± 0.05	± 0.19	± 0.14	± 0.05	± 0.06	± 0.15	± 0.11	± 0.22	± 0.23	± 0.09	± 0.08	± 0.29
12191	0.44	0.25	0.36	0.37	0.24	0.11	0.30	0.31	0.26	0.25	0.36	0.42	0.20	0.37	0.28
	± 0.06	± 0.16	± 0.05	± 0.06	± 0.18	± 0.20	± 0.04	± 0.06	± 0.16	± 0.12	± 0.23	± 0.24	± 0.08	± 0.08	± 0.29
27253	0.45	0.29	0.40	0.38	0.25	0.17	0.33	0.35	0.37	0.32	0.30	0.57	0.27	0.39	0.26
	± 0.08	± 0.17	± 0.04	± 0.05	± 0.18	± 0.14	± 0.05	± 0.08	± 0.16	± 0.13	± 0.20	± 0.27	± 0.08	± 0.09	± 0.29
36795	-0.12	-0.20	-0.43	-0.15	-0.23	-0.14	-0.18	-0.23	-0.48	-0.30	-0.30	-0.37	-0.44	-0.28	-0.33
	± 0.09	± 0.14	± 0.03	± 0.06	± 0.19	± 0.05	± 0.06	± 0.15	± 0.11	± 0.21	± 0.22	± 0.09	± 0.09	± 0.09	± 0.29
42446	0.26	0.25	0.38	0.35	0.15	0.34	0.45	0.39	0.75	0.21	0.48	0.63	0.43	0.39	0.13
	± 0.14	± 0.09	± 0.01	± 0.06	± 0.0										

Table 5 Continued

HIP/Other	[Na/H]	[Mg/H]	[Al/H]	[Si/H]	[Ca/H]	[Sc/H]	[Ti I/H]	[Ti II/H]	[V/H]	[Cr I/H]	[Cr II/H]	[Mn/H]	[Co/H]	[Ni/H]	[Zn/H]	
Subgiants without planets																
6512	0.02 ± 0.03	0.07 ± 0.08	0.18 ± 0.05	0.07 ± 0.05	-0.07 ± 0.09	-0.15 ± 0.11	0.10 ± 0.04	0.09 ± 0.08	0.10 ± 0.06	-0.09 ± 0.04	-0.12 ± 0.05	-0.02 ± 0.08	-0.10 ± 0.08	-0.01 ± 0.03	0.03 ± 0.03	
60585	-0.10 ± 0.08	-0.14 ± 0.08	-0.07 ± 0.13	0.26 ± 0.05	-0.30 ± 0.10	-0.52 ± 0.17	-0.57 ± 0.05	0.11 ± 0.06	-0.60 ± 0.20	-0.38 ± 0.08	0.55 ± 0.10	-0.27 ± 0.09	-0.19 ± 0.08	-0.08 ± 0.04	0.32 ± 0.38	
70616	0.59 ± 0.22	0.25 ± 0.06	0.58 ± 0.02	0.46 ± 0.07	0.25 ± 0.10	0.54 ± 0.17	0.45 ± 0.05	0.33 ± 0.06	0.86 ± 0.20	0.31 ± 0.08	0.42 ± 0.10	0.81 ± 0.09	0.55 ± 0.08	0.52 ± 0.04	0.57 ± 0.21	
98138	0.11 ± 0.09	0.00 ± 0.15	0.10 ± 0.06	0.12 ± 0.05	0.02 ± 0.18	-0.28 ± 0.23	0.03 ± 0.06	0.07 ± 0.06	-0.03 ± 0.17	-0.02 ± 0.11	0.08 ± 0.21	-0.01 ± 0.22	-0.23 ± 0.22	0.05 ± 0.11	-0.11 ± 0.08	0.05 ± 0.33
102531	0.14 ± 0.06	0.04 ± 0.15	0.11 ± 0.10	0.19 ± 0.05	0.09 ± 0.18	-0.23 ± 0.27	0.07 ± 0.06	0.07 ± 0.06	0.12 ± 0.15	0.05 ± 0.11	0.15 ± 0.20	0.02 ± 0.22	-0.13 ± 0.11	0.13 ± 0.08	0.08 ± 0.29	
Late main-sequence with planets																
GSC02	0.35 ± 0.07	0.26 ± 0.15	0.40 ± 0.04	0.32 ± 0.06	0.18 ± 0.18	0.33 ± 0.16	0.44 ± 0.06	0.29 ± 0.10	0.33 ± 0.16	0.28 ± 0.11	0.32 ± 0.41	0.33 ± 0.26	0.26 ± 0.12	0.42 ± 0.09	0.45 ± 0.29	
20723	0.32 ± 0.07	0.17 ± 0.16	0.29 ± 0.06	0.27 ± 0.05	0.13 ± 0.19	0.09 ± 0.13	0.23 ± 0.05	0.24 ± 0.07	0.29 ± 0.16	0.19 ± 0.11	0.25 ± 0.20	0.36 ± 0.26	0.21 ± 0.09	0.31 ± 0.09	0.26 ± 0.29	
31246	0.34 ± 0.05	0.17 ± 0.10	0.38 ± 0.02	0.31 ± 0.05	0.17 ± 0.10	0.22 ± 0.09	0.30 ± 0.04	0.32 ± 0.06	0.54 ± 0.10	0.21 ± 0.04	0.26 ± 0.04	0.41 ± 0.17	0.32 ± 0.08	0.37 ± 0.04	0.33 ± 0.12	
60081	0.37 ± 0.06	0.23 ± 0.16	0.37 ± 0.04	0.33 ± 0.06	0.20 ± 0.19	0.16 ± 0.15	0.30 ± 0.05	0.30 ± 0.06	0.33 ± 0.10	0.25 ± 0.04	0.29 ± 0.04	0.39 ± 0.17	0.24 ± 0.08	0.37 ± 0.04	0.30 ± 0.29	
80838	0.50 ± 0.06	0.02 ± 0.25	0.45 ± 0.16	0.41 ± 0.06	0.26 ± 0.18	0.63 ± 0.16	0.46 ± 0.06	0.46 ± 0.06	0.40 ± 0.17	0.71 ± 0.13	0.54 ± 0.24	0.47 ± 0.29	0.49 ± 0.10	0.49 ± 0.09	0.55 ± 0.31	
TrES-4	0.48 ± 0.06	0.40 ± 0.18	0.07 ± 0.39	0.37 ± 0.06	0.35 ± 0.21	0.51 ± 0.05	0.53 ± 0.06	0.50 ± 0.06	0.09 ± 0.15	0.49 ± 0.12	0.38 ± 0.24	0.32 ± 0.23	0.62 ± 0.23	0.50 ± 0.35	0.35 ± 0.09	0.35 ± 0.29
95740	0.41 ± 0.11	0.36 ± 0.18	0.41 ± 0.10	0.42 ± 0.06	0.32 ± 0.17	0.37 ± 0.28	0.45 ± 0.05	0.26 ± 0.06	0.62 ± 0.23	0.40 ± 0.11	0.54 ± 0.27	0.54 ± 0.27	0.49 ± 0.08	0.36 ± 0.09	0.50 ± 0.29	
98767	0.29 ± 0.11	0.25 ± 0.18	0.38 ± 0.06	0.32 ± 0.07	0.19 ± 0.21	0.20 ± 0.18	0.35 ± 0.06	0.37 ± 0.06	0.40 ± 0.17	0.23 ± 0.13	0.28 ± 0.24	0.40 ± 0.29	0.25 ± 0.10	0.34 ± 0.09	0.45 ± 0.31	
109378	0.24 ± 0.07	0.18 ± 0.15	0.35 ± 0.04	0.27 ± 0.05	0.11 ± 0.19	0.12 ± 0.12	0.30 ± 0.04	0.27 ± 0.08	0.33 ± 0.16	0.17 ± 0.11	0.21 ± 0.20	0.31 ± 0.28	0.18 ± 0.09	0.27 ± 0.08	0.37 ± 0.30	
113357	0.18 ± 0.13	0.15 ± 0.16	0.25 ± 0.04	0.24 ± 0.05	0.11 ± 0.19	0.04 ± 0.17	0.21 ± 0.05	0.21 ± 0.06	0.16 ± 0.15	0.16 ± 0.11	0.16 ± 0.21	0.31 ± 0.24	0.10 ± 0.08	0.28 ± 0.08	0.21 ± 0.29	
113421	0.39 ± 0.09	0.29 ± 0.16	0.40 ± 0.05	0.37 ± 0.05	0.18 ± 0.18	0.21 ± 0.13	0.37 ± 0.05	0.36 ± 0.07	0.45 ± 0.16	0.30 ± 0.11	0.36 ± 0.20	0.53 ± 0.29	0.32 ± 0.09	0.43 ± 0.08	0.34 ± 0.29	

Table 7 Radial velocities and Galactic spatial-velocity components.

HIP/ Other (1)	V_r^* (kms $^{-1}$) (2)	U_{LSR} (kms $^{-1}$) (3)	V_{LSR} (kms $^{-1}$) (4)	W_{LSR} (kms $^{-1}$) (5)	C † (6)
Giants with planets					
1692	17.58 ± 0.25	-8.80 ± 8.15	3.94 ± 3.75	-10.75 ± 0.94	D
4297	-0.21 ± 0.31	25.28 ± 1.68	-13.56 ± 2.00	-5.40 ± 1.33	D
10085	25.36 ± 0.46	-13.81 ± 3.55	22.85 ± 3.10	8.97 ± 6.33	D
12247	8.60 ± 0.31	3.65 ± 0.49	-20.57 ± 1.33	-0.63 ± 0.41	D
HD17092	5.56 ± 0.31	-7.50 ± 6.73	-7.26 ± 8.17	8.42 ± 1.49	D
20889	38.21 ± 0.23	-31.04 ± 0.23	-13.42 ± 0.27	6.02 ± 0.19	D
36616	-36.17 ± 0.35	57.99 ± 0.56	-18.66 ± 1.07	0.29 ± 0.32	D
37826	3.20 ± 0.30	-6.12 ± 0.27	10.03 ± 0.07	-18.84 ± 0.16	D
42527	13.62 ± 0.49	-8.81 ± 0.53	21.29 ± 0.56	-2.98 ± 0.61	D
46471	37.55 ± 0.63	-18.24 ± 0.55	-44.62 ± 1.82	37.08 ± 0.57	R
BD+20 2457	145.08 ± 0.18	-77.33 ± 159.56	-78.88 ± 215.25	99.18 ± 149.85	TD
γ^1 Leo	-36.98 ± 0.46	82.23 ± 21.54	2.91 ± 9.60	2.00 ± 11.69	D
50887	7.03 ± 0.35	33.96 ± 0.91	-3.86 ± 0.40	19.02 ± 0.44	D
53666	7.98 ± 0.16	3.01 ± 0.89	-29.64 ± 3.58	-9.48 ± 2.73	D
57428	-11.86 ± 0.65	-0.30 ± 3.26	13.10 ± 1.78	-4.03 ± 0.80	D
57820	-26.08 ± 0.88	16.99 ± 0.68	-15.89 ± 1.41	-11.45 ± 0.88	D
58952	-20.83 ± 0.46	86.08 ± 1.65	-4.01 ± 0.37	37.49 ± 1.13	R
61740	-18.74 ± 0.41	-18.40 ± 0.69	-9.46 ± 0.73	-15.66 ± 0.41	D
74793	-18.82 ± 0.70	12.51 ± 0.76	-4.80 ± 0.69	-9.64 ± 0.74	D
74961	-35.20 ± 0.85	67.76 ± 3.75	-65.54 ± 3.09	-5.51 ± 1.23	R
75458	-11.34 ± 0.51	7.86 ± 0.12	-2.17 ± 0.35	-1.54 ± 0.39	D
76311	-9.46 ± 0.59	2.95 ± 0.81	-7.35 ± 0.72	5.80 ± 0.68	D
77655	-25.95 ± 0.31	42.81 ± 0.33	-36.39 ± 0.28	-12.40 ± 0.26	D
79219	-4.14 ± 0.46	-13.35 ± 1.35	9.44 ± 0.70	14.71 ± 0.81	D
80687	-35.00 ± 0.40	-25.25 ± 0.42	-2.12 ± 0.45	1.07 ± 0.49	D
88048	12.66 ± 0.50	30.34 ± 0.48	-12.31 ± 0.31	-1.73 ± 0.16	D
89047	-18.29 ± 0.41	-52.77 ± 0.88	4.69 ± 0.44	-15.71 ± 0.36	D
90344	31.68 ± 1.15	12.08 ± 0.53	56.28 ± 1.14	-22.14 ± 1.09	R
91852	-61.84 ± 0.47	-51.14 ± 1.76	-32.46 ± 0.94	-9.72 ± 0.95	D
92895	19.42 ± 0.49	56.29 ± 3.86	-23.01 ± 4.99	-13.08 ± 2.70	D
94576	-73.87 ± 0.20	-42.68 ± 1.45	-46.24 ± 0.92	-26.11 ± 1.53	R
94951	-4.29 ± 1.00	0.91 ± 1.07	0.18 ± 0.69	-11.92 ± 2.02	D
95124	-0.90 ± 1.50	19.70 ± 1.62	-17.90 ± 1.82	22.26 ± 1.45	D
97938	-42.07 ± 0.42	-17.87 ± 0.37	-33.39 ± 0.42	-19.55 ± 0.74	D
99894	12.51 ± 0.48	33.55 ± 0.73	0.90 ± 0.66	6.46 ± 0.31	D
103527	3.72 ± 0.43	30.65 ± 0.61	-0.13 ± 0.45	12.44 ± 0.43	D
104202	-72.19 ± 0.48	-58.90 ± 1.26	-33.77 ± 0.64	24.71 ± 0.77	R
107251	-18.91 ± 0.28	-2.57 ± 1.03	-3.64 ± 0.77	18.73 ± 0.73	D
109577	15.98 ± 0.46	16.44 ± 0.32	16.05 ± 0.42	-3.77 ± 0.36	D
110813	14.28 ± 0.20	84.67 ± 7.47	-35.42 ± 5.02	9.58 ± 1.74	R
HD240210	8.63 ± 0.35	-5.45 ± 115.43	8.94 ± 38.90	7.01 ± 34.02	D
114855	-26.44 ± 0.39	-63.14 ± 0.96	-37.07 ± 0.47	0.14 ± 0.55	D
116076	-60.15 ± 0.51	-55.61 ± 1.89	-96.91 ± 1.19	-31.83 ± 1.49	TD
Giants without planets					
729	-19.83 ± 0.36	-31.77 ± 1.42	-41.72 ± 1.06	3.51 ± 0.65	D
873	8.14 ± 0.54	-29.25 ± 1.13	-28.40 ± 1.04	-12.39 ± 0.62	D
6682	-3.95 ± 0.39	-39.03 ± 3.30	-38.87 ± 2.66	10.49 ± 0.49	D
6999	-11.77 ± 0.42	17.77 ± 0.46	-9.04 ± 0.50	-6.51 ± 0.68	D
7097	13.60 ± 0.42	-6.73 ± 0.83	3.35 ± 0.72	-1.19 ± 0.35	D
7607	16.21 ± 0.11	-12.11 ± 0.20	-0.91 ± 0.25	-21.46 ± 0.36	D
7719	6.91	12.03	16.95	7.49	D
9222	-0.63 ± 0.67	9.26 ± 0.61	8.17 ± 0.63	22.21 ± 0.68	D
13531	2.20	8.22	6.27	5.31	D
19038	8.88 ± 0.22	-5.02 ± 0.23	-21.63 ± 0.38	10.08 ± 0.16	D
42528	24.02 ± 0.85	-16.02 ± 0.80	4.79 ± 0.88	20.20 ± 0.55	D
59285	1.53 ± 0.84	53.18 ± 1.03	-36.11 ± 1.05	-15.69 ± 0.95	D
59646	-4.42 ± 1.22	-12.23 ± 0.75	-11.02 ± 0.84	-3.49 ± 1.12	D
59847	-28.16 ± 1.94	5.26 ± 0.39	2.59 ± 0.40	-22.05 ± 1.92	D
59856	-40.40	18.99	-53.30	-31.03	R
68904	-10.92 ± 0.45	59.85 ± 3.50	-35.42 ± 2.63	-4.45 ± 0.46	D
69185	-30.59 ± 0.62	-21.24 ± 1.46	32.45 ± 1.89	-25.42 ± 0.63	D
69427	-4.24 ± 0.58	-10.78 ± 0.52	45.05 ± 0.81	34.51 ± 0.76	R
69612	32.07 ± 0.38	53.22 ± 1.65	-50.11 ± 2.80	19.94 ± 0.94	R
70027	-8.29 ± 0.22	-29.95 ± 0.57	-7.41 ± 0.34	15.89 ± 0.32	D

Table 7 Continued

HIP/ Other (1)	V_r^* (kms $^{-1}$) (2)	U_{LSR} (kms $^{-1}$) (3)	V_{LSR} (kms $^{-1}$) (4)	W_{LSR} (kms $^{-1}$) (5)	C † (6)
70038	-45.27 ± 0.53	-42.56 ± 1.34	-20.32 ± 1.85	-18.77 ± 0.66	D
80816	-25.91	-8.70	-21.68	4.27	D
84975	-1.20 ± 0.50	23.49 ± 0.82	-7.78 ± 0.74	-10.99 ± 0.93	D
88765	-3.76 ± 0.40	-0.73 ± 0.50	13.08 ± 0.57	8.17 ± 0.50	D
88836	-8.43 ± 0.24	59.09 ± 0.95	-33.49 ± 0.63	14.12 ± 0.48	D
89826	-24.65 ± 0.16	-13.09 ± 0.38	-13.13 ± 0.24	7.80 ± 0.36	D
89918	7.34 ± 0.51	14.23 ± 0.46	11.68 ± 0.39	9.86 ± 0.32	D
89962	8.87 ± 0.40	51.49 ± 0.37	-59.93 ± 0.30	22.07 ± 0.07	R
95822	-42.02 ± 0.49	-18.20 ± 0.47	-26.76 ± 0.47	-15.41 ± 1.04	D
95926	-5.20 ± 0.55	25.53 ± 0.89	-14.38 ± 0.79	21.63 ± 0.70	D
96016	5.45 ± 0.50	6.10 ± 0.45	13.53 ± 0.48	8.83 ± 0.39	D
96229	-24.81 ± 0.08	-6.81 ± 0.08	-18.97 ± 0.10	-30.91 ± 0.34	D
98210	27.29 ± 0.37	53.21 ± 1.17	-31.53 ± 2.56	-36.03 ± 1.80	R
98314	56.51 ± 0.53	38.38 ± 0.78	53.29 ± 0.69	-7.73 ± 0.64	R
98845	37.08 ± 0.60	28.26 ± 0.59	38.41 ± 0.59	-5.55 ± 0.86	D
98920	-41.13 ± 0.24	-27.47 ± 0.39	-19.54 ± 0.30	15.24 ± 0.21	D
99171	-3.64 ± 0.39	1.30 ± 0.34	-3.66 ± 0.33	-20.47 ± 0.68	D
99841	-9.22 ± 0.59	58.38 ± 1.78	-20.40 ± 0.81	-10.81 ± 0.89	D
99913	-5.62 ± 0.21	14.00 ± 0.49	-4.59 ± 0.35	-1.37 ± 0.60	D
100022	-18.12 ± 0.26	-22.72 ± 1.46	-6.16 ± 0.38	-26.31 ± 1.39	D
100503	-20.16 ± 0.63	-22.80 ± 1.36	-6.16 ± 0.72	-15.15 ± 1.25	D
100541	-11.99 ± 0.37	15.28 ± 0.52	-14.04 ± 0.47	12.04 ± 0.33	D
100587	-12.01	-1.68	-4.22	-4.81	D
101848	-33.39 ± 0.56	-63.65 ± 4.21	6.62 ± 2.16	-3.44 ± 1.61	D
101936	-40.15 ± 0.31	-33.24 ± 0.98	-22.52 ± 0.32	-6.81 ± 1.55	D
102532	-6.33 ± 0.35	33.75 ± 1.39	-19.95 ± 1.07	-6.95 ± 0.85	D
103004	4.40 ± 0.85	35.18 ± 1.02	2.05 ± 0.85	10.04 ± 0.39	D
103519	-22.60	-36.47	-13.97	-3.96	D
105390	-27.69 ± 0.60	3.02 ± 0.61	-25.61 ± 0.62	-8.05 ± 1.11	D
105411	-88.98 ± 0.50	-51.61 ± 1.07	-97.62 ± 0.76	-62.58 ± 2.58	TD
105502	-76.80	-40.51	-56.09	26.34	R
106081	13.89 ± 0.26	67.36 ± 3.22	-3.31 ± 1.27	-30.56 ± 2.07	R
106093	22.24 ± 0.44	-22.30 ± 0.66	-16.56 ± 0.44	23.02 ± 0.37	D
110538	-11.59 ± 0.49	39.67 ± 0.33	-3.46 ± 0.49	-28.85 ± 0.39	D
111944	-10.89 ± 0.37	-29.09 ± 1.23	-16.02 ± 0.48	-7.71 ± 0.72	D
112041	-14.01 ± 0.58	-52.65 ± 2.22	-19.74 ± 0.69	3.02 ± 0.51	D
112067	-28.77 ± 0.36	-20.70 ± 1.03	-31.66 ± 0.64	1.46 ± 0.90	D
112158	4.17	10.20	5.05	-3.16	D
112242	12.80 ± 0.31	10.35 ± 0.25	18.42 ± 0.30	6.08 ± 0.27	D
115696	8.50 ± 0.51	44.88 ± 1.70	0.89 ± 0.74	-56.56 ± 2.72	R
115830	5.73 ± 0.12	37.98 ± 0.36	12.36 ± 0.14	6.04 ± 0.14	D
115919	-16.88 ± 0.43	-6.21 ± 0.76	-8.64 ± 0.34	18.25 ± 0.33	D
116584	6.84	9.09	-3.06	-49.03	R
116823	-3.84 ± 0.30	47.10 ± 4.06	11.19 ± 1.00	16.15 ± 0.74	D
117375	-15.63 ± 0.11	-30.29 ± 1.10	-18.91 ± 0.50	11.10 ± 0.30	D
117411	-0.93 ± 0.17	2.51 ± 0.75	2.57 ± 0.52	6.45 ± 0.28	D
117541	-17.39 ± 0.17	-59.79 ± 2.38	1.26 ± 0.33	19.34 ± 0.25	D

Subgiants with planets

8159	-46.70 ± 0.30	47.03 ± 0.26	-23.44 ± 0.22	24.54 ± 0.30	D
12048	-51.54 ± 0.17	99.27 ± 1.66	-39.81 ± 1.21	5.89 ± 1.20	R
12191	21.01 ± 0.68	0.23 ± 0.60	19.05 ± 0.47	-12.31 ± 0.71	D
27253	30.14 ± 0.57	-4.52 ± 0.55	-18.91 ± 0.35	-24.72 ± 0.46	D
36795	60.72 ± 1.64	12.12 ± 0.26	-51.44 ± 1.52	-15.70 ± 0.56	R
42446	9.65 ± 1.06	-11.97 ± 1.26	-26.28 ± 1.76	-35.77 ± 3.00	R
49813	-4.47 ± 1.04	44.40 ± 2.43	-87.01 ± 6.79	-21.55 ± 2.03	TD
54195	11.89 ± 0.71	-6.98 ± 1.47	-12.14 ± 1.00	4.98 ± 1.10	D
66192	-29.47 ± 1.99	7.18 ± 0.80	-51.44 ± 2.96	1.50 ± 2.21	D
93746	-72.42 ± 0.14	-13.64 ± 0.68	-65.20 ± 0.47	0.09 ± 0.45	R
94256	19.16 ± 0.58	51.99 ± 1.44	-20.23 ± 1.90	29.81 ± 1.35	R
HAT-P-7	-10.80 ± 0.51	4.75	-10.84	29.77	D
96507	-17.86 ± 0.63	20.54 ± 0.72	-19.84 ± 0.66	3.61 ± 0.36	D
100970	-92.01 ± 0.67	-62.82 ± 1.19	-70.97 ± 0.60	-32.28 ± 2.23	R
115100	-24.43 ± 0.45	11.51 ± 0.42	-12.42 ± 0.44	24.08 ± 0.44	D
118319	0.98 ± 1.20	-56.76 ± 6.18	-14.19 ± 2.01	-6.44 ± 1.66	D

Subgiants without planets (this work)

Table 7 Continued

HIP/ Other (1)	V_r^* (kms $^{-1}$) (2)	U_{LSR} (kms $^{-1}$) (3)	V_{LSR} (kms $^{-1}$) (4)	W_{LSR} (kms $^{-1}$) (5)	C † (6)
6512	8.18 \pm 0.59	-50.57 \pm 1.32	-11.90 \pm 0.70	38.93 \pm 0.91	R
60585	-19.15 \pm 0.44	27.96 \pm 1.40	-12.36 \pm 1.61	-13.29 \pm 0.45	D
70616	13.66 \pm 0.36	30.57 \pm 0.69	-15.91 \pm 0.90	9.51 \pm 0.53	D
98138	-23.69 \pm 1.12	-9.41 \pm 1.08	-12.69 \pm 1.11	22.63 \pm 1.37	D
102531	-7.25 \pm 0.44	30.12 \pm 1.05	-20.44 \pm 0.91	-10.99 \pm 0.92	D
Subgiants without planets (from the literature)					
2422	13.98 \pm 0.22	-51.04 \pm 0.74	-13.24 \pm 0.45	-0.63 \pm 0.27	D
3185	-48.21 \pm 1.27	-38.10 \pm 0.69	-85.07 \pm 1.19	48.74 \pm 1.27	TD
4395	-65.30	-83.05	23.39	40.27	R
12350	9.80	-28.76	-46.28	20.51	R
14086	37.98 \pm 6.85	21.47 \pm 2.46	-80.46 \pm 2.41	-9.01 \pm 6.01	R
15776	41.30 \pm 0.92	5.77 \pm 0.75	-28.70 \pm 0.61	-37.82 \pm 0.76	R
16641	11.10 \pm 0.20	5.93 \pm 0.22	-48.32 \pm 1.08	-25.92 \pm 0.57	R
17027	40.30 \pm 0.10	1.47 \pm 0.28	-23.74 \pm 0.33	-35.45 \pm 0.22	D
17183	46.60 \pm 3.00	-36.67 \pm 2.23	-93.87 \pm 2.74	5.16 \pm 2.22	TD
17378	-6.00 \pm 0.70	-3.50 \pm 0.46	32.11 \pm 0.16	19.85 \pm 0.50	D
18208	18.81 \pm 1.25	-26.63 \pm 2.25	-25.40 \pm 3.60	27.96 \pm 2.84	D
18309	143.27 \pm 2.07	-137.56 \pm 2.20	37.56 \pm 2.43	-8.29 \pm 0.78	TD
18432	45.00 \pm 0.10	20.55 \pm 0.82	-61.02 \pm 1.13	-21.48 \pm 0.22	R
19070	24.80	-6.51	-9.08	-8.67	D
21010	20.95 \pm 0.86	-17.64 \pm 0.85	-0.98 \pm 0.34	26.36 \pm 0.66	D
22319	38.40 \pm 0.20	-32.11 \pm 0.30	10.39 \pm 0.44	0.30 \pm 0.36	D
26273	11.90 \pm 0.20	73.72 \pm 5.31	-48.84 \pm 3.51	-13.26 \pm 1.30	R
27641	-4.51 \pm 0.39	13.30 \pm 0.39	9.68 \pm 0.40	8.42 \pm 0.38	D
40023	-44.00 \pm 0.40	49.04 \pm 0.35	-45.88 \pm 0.94	-44.39 \pm 0.52	R
40506	25.80	-5.31	-17.24	16.53	D
41254	44.60 \pm 0.10	16.94 \pm 0.42	-41.23 \pm 0.27	3.79 \pm 0.49	D
43634	8.90 \pm 0.30	-14.97 \pm 0.75	-37.44 \pm 1.53	-14.33 \pm 1.05	D
62904	-0.10 \pm 0.30	3.61 \pm 0.29	-43.27 \pm 1.16	2.34 \pm 0.32	D
64408	-15.00	-29.51	-3.70	7.96	D
68101	6.16 \pm 1.27	3.92 \pm 0.89	-14.84 \pm 1.00	-30.05 \pm 0.78	D
72830	-44.94 \pm 0.28	-48.25 \pm 2.29	-9.34 \pm 0.47	-16.58 \pm 0.89	D
75762	-45.00	-34.71	10.88	-6.05	D
79214	-53.20 \pm 0.20	-38.17 \pm 0.27	10.17 \pm 0.86	-26.48 \pm 1.53	D
81819	-8.10	-0.78	-9.66	-7.16	D
81991	-5.70 \pm 0.60	26.75 \pm 0.79	-65.41 \pm 1.97	17.17 \pm 0.52	R
82302	29.40	28.35	-29.54	21.95	D
82636	4.61 \pm 1.25	86.05 \pm 1.46	-1.16 \pm 0.93	-13.97 \pm 0.92	R
84801	-33.07 \pm 0.22	-1.50 \pm 0.54	-33.00 \pm 0.84	-33.57 \pm 0.87	R
88217	3.80	27.87	-10.22	9.36	D
90729	-59.00	5.21	-59.67	-26.51	R
93518	-7.43 \pm 0.99	40.37 \pm 6.38	-55.27 \pm 9.77	-7.72 \pm 2.73	R
98036	-39.60 \pm 2.30	-0.71 \pm 1.57	-43.14 \pm 1.63	-2.78 \pm 0.45	D
102642	-43.03 \pm 0.23	26.17 \pm 0.40	-34.14 \pm 0.24	-30.59 \pm 0.68	R
103077	-3.50 \pm 2.05	-1.07 \pm 1.42	11.79 \pm 1.05	5.67 \pm 1.11	D
106527	16.51 \pm 0.51	21.92 \pm 0.36	12.93 \pm 0.51	-11.26 \pm 0.45	D
109439	20.01 \pm 1.34	8.19 \pm 0.42	5.09 \pm 1.22	-34.87 \pm 1.00	D
109572	-20.78 \pm 0.65	-32.11 \pm 0.42	-25.23 \pm 0.64	1.97 \pm 0.21	D
109822	11.90	40.15	-47.10	-17.82	R
109836	7.60 \pm 0.20	26.45 \pm 1.00	-27.02 \pm 2.39	-19.20 \pm 1.38	D
110853	-8.60 \pm 0.20	3.34 \pm 0.51	-8.55 \pm 1.01	10.99 \pm 0.39	D
113386	0.00 \pm 0.20	-1.71 \pm 0.88	-84.06 \pm 5.51	-18.04 \pm 1.58	R
113994	-27.40	54.93	-25.46	13.58	D
114699	-31.19 \pm 0.79	-55.98 \pm 0.70	-55.10 \pm 0.88	37.28 \pm 0.63	R
116250	26.00 \pm 0.86	20.44 \pm 0.42	-11.34 \pm 0.53	-10.08 \pm 0.55	D
117668	1.60 \pm 0.20	5.96 \pm 0.45	27.70 \pm 1.24	4.80 \pm 0.22	D
Late main-sequence with planets					
GSC 02883-01687	31.21 \pm 0.33	-22.55 \pm 55.04	3.64 \pm 175.13	-1.68 \pm 171.95	D
20723	50.20 \pm 0.58	-23.55 \pm 0.47	-30.88 \pm 0.78	-15.36 \pm 0.51	D
31246	-1.29 \pm 0.35	21.21 \pm 0.48	-15.40 \pm 0.77	17.35 \pm 0.49	D
60081	25.21 \pm 0.70	7.79 \pm 0.49	-21.88 \pm 0.79	21.30 \pm 0.70	D
80838	-18.54 \pm 0.56	-22.70 \pm 1.61	-16.03 \pm 0.80	16.62 \pm 1.39	D
TrES-4	-16.51 \pm 1.96	72.63 \pm 274.67	-42.41 \pm 264.26	-1.56 \pm 211.42	R
95740	-50.55 \pm 0.73	-19.14 \pm 0.76	-36.97 \pm 0.76	11.06 \pm 0.49	D
98767	-45.76 \pm 0.40	-2.35 \pm 0.17	-39.99 \pm 0.37	-56.78 \pm 0.36	R

Table 7 Continued

HIP/ Other (1)	V_r^* (km s^{-1}) (2)	U_{LSR} (km s^{-1}) (3)	V_{LSR} (km s^{-1}) (4)	W_{LSR} (km s^{-1}) (5)	C [†] (6)
109378	-21.38 ± 0.12	14.17 ± 0.18	-45.72 ± 0.42	1.12 ± 0.26	D
113357	-33.71 ± 0.46	-5.42 ± 0.12	-24.84 ± 0.38	22.96 ± 0.26	D
113421	-13.72 ± 0.21	8.40 ± 0.08	-3.41 ± 0.14	17.80 ± 0.18	D

* For those stars in binary systems we have considered the radial velocity of the centre of mass of the system.

† Thin/thick disc classification, D: Thin disc, TD: Thick disc, R: Transition